CHARACTERIZATION OF STRUCTURAL RELAXATION IN INORGANIC GLASSES USING LENGTH DILATOMETRY

A Dissertation

Presented To

the Graduate School of

Clemson University

In Partial Fulfillment

of the Requirements for the Degree

Doctor of Philosophy

Materials Science and Engineering

---

by

Erick Koontz

May 2015

Accepted by:

Dr. Igor Luzinov, Committee Chair

Dr. Kathleen Richardson, Adviser, Co-Chair

Dr. O. Thompson Mefford

Dr. Vincent Blouin

Dr. J. David Musgraves

ABSTRACT

Structural relaxation in inorganic glasses is a phenomenon of much study in the glass community. The processes that govern how a glass relaxes towards its thermodynamic quasi-equilibrium state are major factors in understanding glass behavior near the glass transition region, as characterized by the glass transition temperature (T_g). Study of the glass transition has been going for as long as glass science has been a field and much of the cutting edge literature published in glass science today relates to it in some way. Intrinsic glass properties such as specific volume, enthalpy, entropy, density, etc. are used to map the behavior of the glass network below in and near the transition region. The question of whether a true thermodynamic second order phase transition takes place in the glass transition region is another pending question in the glass community. Linking viscosity behavior to entropy as Adam and Gibbs did, or viewing the glass configuration as an energy landscape are just a couple of the most prevalent methods used for attempting to understand the glass transition.[1,2]

The structural relaxation behavior of inorganic glasses is important for more than scientific reasons, many commercial glass processing operations including glass melting and certain forms of optical fabrication include significant time spent in the glass transition region. For this reason knowledge of structural relaxation processes can, at a minimum, provide information for annealing duration of melt-quenched glasses. The development of a predictive model for annealing time prescription has the potential to save glass manufacturers significant time and money as well as increasing volume throughput. In

optical hot forming processes such as precision glass molding, molded optical components can significantly change in shape upon cooling through the glass transition. This change in shape is not scientifically predictable as of yet though manufacturers typically use empirical rules developed in house. The classification of glass behavior in the glass transition region would allow molds to be accurately designed and save money for the producers.

The work discussed in this dissertation is comprised of the development of a dilatometric measurement and characterization method of structural relaxation. The measurement and characterization technique is comprised of three main components: experimental measurements, fitting of configurational length change, and description of glass behavior by analysis of fitting parameters. N-BK7 optical glass from Schott was used as the proof of concept glass but the main scientific interest was in three chalcogenide glasses: $As_{40}Se_{60}$, $As_{20}Se_{80}$, and $Ge_{17.9}As_{19.7}Se_{62.4}$.

The dilatometric experiments were carried out using a thermomechanical analyzer (TMA) on glass sample that were synthesized by the author, in all cases except N-BK7. Isothermal structural relaxation measurements were done on (12 mm tall x 3 mm x 3 mm) beams placed vertically in the TMA. The samples were equilibrated at a starting temperature (T_0) until structural equilibrium was reached then a temperature down step was initiated to the final temperature (T_1) and held isothermally until relaxation concluded. The configurational aspect of length relaxation, and therefore volume relaxation was extracted and fit with a Prony series. The Prony series parameters indicated a number of relaxation

events occurring within the glass on timescales typically an order of magnitude apart in time. The data analysis showed as many as 4 discrete relaxation times at lower temperatures. The number of discrete relaxation decreased as the temperature increased until just one single relaxation was left in the temperature range just at or above T_g. In the case of N-BK7 these trends were utilized to construct a simple model that could be applied to glass manufacturing in the areas of annealing or PGM. A future development of a rather simple finite element model (FEM) would easily be able to use this model to predict the exponential-like, temperature and time dependent relaxation behaviors of the glass. The predictive model was not extended to the chalcogenide glass studied here, but could easily be applied to them in the future.

The relaxation time trends versus temperature showed a definite region of transition between a low temperature state with many relaxations to a high temperature state with only a single relaxation. Evidence was found for the existence of a definitive transition of some kind in the range of T_g possibly relating the idea of a percolation temperature (T*) as defined by Carmi.[3] The results of the measurements showed substantial support for both the Adam-Gibbs interpretation of decreasing entropy towards the Kauzmann temperature, while also displaying trends compatible with energy landscape theory and the idea of broken ergodicity of glass configuration below T_g.[4] In addition effective relaxation energies were calculated and the energy needed for relaxation showed a definite upward trend with decreasing temperature also supporting the idea of reduced entropy and configurational freedom at lower temperatures. The effective relaxation energies are not

purely thermodynamic in nature because they also characterize the effects of viscosity and the kinetics of the material that was relaxing.

The experimentation, characterization, and analysis of structural relaxation behavior presented in this dissertation is one of the few instances of thermodynamic change in volume being measured for inorganic glass. The results point towards the validity of many common structural and configurational models and show features which suggest the necessity of a transition in the glass network and hint at a possible discontinuity in entropy changes between temperatures in the glass transition region.

DEDICATION

I dedicate this dissertation first to my Lord and Savior Jesus Christ by whose grace I live every day. To my wonderful wife Gerrilyn without whose love and constant support none of this would have been possible. And to my parents Don and Angie Koontz who taught me how to work hard and be excellent and on whose shoulders I stand.

ACKNOWLEDGEMENTS

The author would like to acknowledge the people who helped mold and shape the discussion laid out in the dissertation. I would like to thank my family for their constant support, my wife Gerrilyn, my parents Don and Angie Koontz, my brothers Brian and Adam as well as my sister Jacki Guthrie. I would like to thank my father and mother in-law Ron and Marilyn Mele.

I would like to thank Dr. Kathleen Richardson for her unwavering support and confidence in my scientific ability, and her mentorship and friendship. I would like to thank Pete Wachtel and Dr. Dave Musgraves who were pivotal in discussing and refining the ideas embodied in this work.

I would like to thank my entire PhD committee, Dr. Luzinov, Dr. Richardson, Dr. Blouin, Dr. Mefford, and Dr. Musgraves who were always available to help make sense of things. Definitely not least of all, I would like to thank my GPCL research colleagues, Benn Gleason, Spencer Novak, James Marro, Laura Sisken, Andy Buff, Guillaume Guery, and Rebecca Whitsitt. Finally our technical staff Dr. Charmayne Smith, Dr. Jason Lonegan, Karima Chamma, and Devon McClane.

TABLE OF CONTENTS

Page

Table of Contents (Continued)

Page

Table of Contents (Continued)

Page

Table of Contents (Continued)

Page

LIST OF TABLES

Table Page

LIST OF FIGURES

Figure Page

Figure Page

List of Figures (Continued)

Figure Page

INTRODUCTION

Optical systems are continually being pushed to the limits of their capabilities. Advances in microelectronics and sensor technology, have challenged optical components to keep pace in modern optical systems. This challenge of increased functionality is being met through the pioneering efforts of optical designers who create more and more complex optical systems, relying on increasingly unconventional lens shapes and form factors. Two of the most significant bottlenecks to increasing lens complexity and therefore lens design are lens fabrication methods and lens materials. While the field of optical materials is being advanced in terms of number of materials and types of materials available for optical components, little is being done to address the need for improvement in optical manufacturing techniques. Most advances in this area are simply newer versions of old technology. Techniques such as diamond turning, grinding, and polishing can produce very high quality optical elements, but have limitations as far as the rotational symmetry and overall shape of the optic they produce. Production of optical elements must account for micro-roughness and scratch density which can severely affect optical system performance particularly in laser applications.[5]

These issues are exacerbated when considering infrared glasses for near, mid, and far infrared systems. These glasses have mechanical and thermal properties that make traditional lens shaping more difficult and less deterministic.[6,7] A technology that has risen to meet these challenges is precision glass molding also known as PGM. PGM is essentially hot forming of glassy material, one subset of the many types of optical

materials. The materials most commonly associated with infrared optics are crystalline silicon and germanium, however in recent years these expensive materials have been being replaced or used in concert with chalcogenide (IR) transparent glasses. Chalcogenides (ChG) are the most common example of these IR glasses. The continuous viscosity versus temperature behavior of glass enables it to be hot formed without reaching its molten state. This allows for various degrees of hot forming ranging from casting at high temperatures, near melting, to drawing at slightly lower temperatures, and forming under significant load as in forging, at temperatures only slightly above the glass transition temperature (T_g). PGM uses a glass's viscoelastic behavior in the temperature range just above T_g in order to form the glass into the shape of the molds.

In PGM an upper and lower mold are mounted in a temperature controlled chamber, and a glass gob of specific volume is loaded into the mold chamber. The system is heated to a predetermined temperature and after soaking to reach an isothermal condition, force is exerted on the glass via the molds. The glass flows and conforms to the mold shape and the system is then cooled and force removed. The super-cooled liquid is now a glass in the shape of the desired mold. In a perfect world, the lens could be directly mounted in an optical system. However, the material behavior of the glass is not linear and at temperatures near T_g, the glass may change shape in a temperature and time dependent way. This process is typically referred to as annealing. This annealing is caused by a phenomenon called structural relaxation.

Structural relaxation occurs when the material is in a state of thermodynamic disequilibrium. Figure 3.1 shows an example of a typical volume versus temperature curve

for a standard glass forming material. This disequilibrium is most observable in the glass transition region. When a molten glass is cooled, the thermodynamic state of that glass, which can be observed by measuring properties like volume and enthalpy, are kept at equilibrium by rearrangement of the atoms comprising the glass. As the temperature decreases the kinetics of the glass slows, causing the rearrangement or relaxation time of the atoms to increase. Eventually it begins to take more time for the atoms to rearrange themselves to achieve thermodynamic equilibrium than it takes for the glass to change its thermodynamic state. When this happens the intrinsic properties of the glass such as volume, enthalpy, and entropy, deviate from their equilibrium thermodynamic state as dictated by temperature. This phenomenon occurs in the glass transition region. The deviation from the liquid equilibrium line increases as the temperature is dropped farther below T_g. The faster the glass is cooled the more severe and sudden this departure from equilibrium will occur. The higher the quench rate of the glass, the farther above T_g the glass will depart from the equilibrium line and the greater the stress on the glass network will be. In conventional glass processing this stress is relieved through annealing, during which, the glass is heated to a temperature approximately 40 °C below T_g and held isothermally for a long period of time varying from hours to days, even to weeks in some cases. During this process the equilibrium thermodynamic state of the glass is fixed and enough time is allowed for the kinetics to relax the glass network back to the liquid equilibrium state.

During annealing, structural relaxation leads to a change in the glass network configuration which relieves stress in the glass and reduces unwanted optical effects such

as stress birefringence. The same phenomenon of structural disequilibrium upon cooling can be seen in the PGM process. In bulk glass-making the change in volume and shape during structural relaxation is often acceptable, however, when manufacturing a lens with tight optical tolerances a deviation in shape from the mold profile such as can occur when the structure relaxes is unacceptable. One remedy is to leave the glass in a stressed, disequilibrium state, but issues such as stress birefringence and increased internal stress are sometimes prohibitive. Even when an annealing step is not done, the glass still structurally relaxes during the time it spends in the temperature range near T_g. This leads to previously unpredictable volume and shape change, further leading to potentially unacceptable optical variation from the designed lens.

Although structural relaxation has been studied in glasses for many years, the majority of studies have occurred in the realm of heat capacity changes resulting from structural relaxation. As this dissertation will show, the trends and behaviors seen in heat capacity relaxation are not of precisely the same nature as those determined directly from a measurement of volume change caused by structural relaxation. Glasses are by their nature amorphous, and this typically leads to isotropic behavior. Given that fact, glasses experience length change due to temperature equally in every direction; this means that a measurement of bulk length change during structural relaxation can be accurately considered as 1/3 of the volume relaxation.[8] The relationship between volume and length change can be seen in Equation 1, where ΔV is the change in volume and Δl is the change in length.

Equation 1

$$\Delta V = 3 * \Delta l$$

In addition to the need for an understanding of structural relaxation as it pertains to PGM, there is an ongoing effort in the glass community to accurately characterize structural relaxation and gain insight into its atomistic origins.

The true nature of the glass transition has been debated for some time. The work of Kauzmann suggested a need for a true thermodynamic transition somewhere between T_g and the "zero-point entropy" of the glass network.[4] A glass has excess entropy above the crystalline state because of its amorphous nature, all glass would achieve lower internal energies as a crystal, however the kinetics of the glass can be made to interfere with such crystallization. This leaves the material in a metastable state in which it adheres as much as possible to a "liquid equilibrium". This excess entropy decreased with temperature below T_g, but the speed at which it decreases suggests an approach of the glassy state to the crystalline state at some temperature well above absolute zero. The idea of the glass being more entropically favorable than the crystal is of course paradoxical; hence it is termed the Kauzmann Paradox. Differing theories have been put forth as to whether a second order transition occurs within the glass as it approaches the Kauzmann temperature, also restyled as T_2 by Gibbs and DiMarzio.[9] Theories further developed by Adam and Gibbs described the state of the material with decreasing temperature as losing configurational freedom as T_2 is approached.[1] More recent work using the idea of the glass configuration as defined by an energy landscape describes a transition occurring

closer to T_g with a break down in ergodicity of the glass network.[3] Which of these descriptions is more accurate is a subject of current, ongoing study and debate in the glass community. This dissertation seeks to shine some light on the issue and determine which argument is most reasonable based on a configuration volume approach.

This dissertation aims to test some of some of the theoretical models detailed above. Experimental verification of or modification of these theories would constitute a significant contribution to glass science.

CHAPTER 1

INFRARED OPTICAL MATERIALS AND OPTICS FABRICATION

The need for complex IR optical systems is driven primarily by the military apparatus in large, developed nations. The U.S. is foremost in that category and thus represents the largest market for infrared optics. These optics are used in a wide range of applications, from sensing chemicals and scanning terrain, to guiding missiles and smart bombs, much of the capabilities of the U.S. military rely heavily on IR imaging. The infrared region of the electromagnetic spectrum is typically split into multiple bands of interest, for the military there are 5 bands. The near-infrared (NIR), short-wavelength infrared (SWIR), mid-wavelength infrared (MWIR), long-wavelength infrared (LWIR), and far-infrared (FIR). A representation of the relevant IR bands is shown in Figure 1.1. The wavelength divisions defining these various regions are dependent on the conventions of various organizations and therefore differ somewhat. However for the sake of this dissertation, the convention described above and represented in Figure 1.1 will be used.

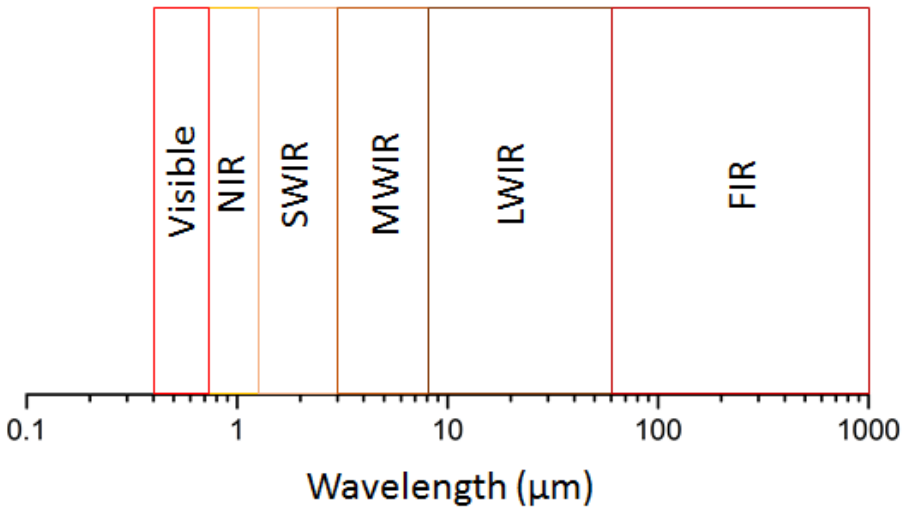

Figure 1.1: Representation of the visible and infrared electromagnetic spectrum as a function of wavelength

The divisions of the IR spectrum are a result of bands of transmittance found in IR optical materials as well as bands of absorption found in the atmosphere. Fiber optic telecommunication can be achieved in the NIR due to the transparency of Silica (SiO_2) in this region. The NIR is also the range of operation for active optical systems such as night vision where it is necessary to amplify the IR signal that is observed and convert it to a visible light scale, in order to create an image that humans can see. The main use for SWIR wavelengths is long distance telecommunications, and this range can be limited due to significant CO_2 and H_2O absorptions from the atmosphere. MWIR is used utilized in many military applications, as most heat-guided weapons operate in this range. Objects at temperatures only slightly above room temperature can be detected in this wavelength regime. The LWIR is the range of thermal imaging. At these wavelengths it is possible to discern considerable variation in thermal energy without any active signal amplification. Satellite imaging for defense as well as meteorological applications primarily make use of

this range. The final range, FIR, can observe bodies at temperatures from near absolute zero to around room temperature. For this reason it is used in astronomy to look at gaseous matter in the universe. There is also wide application of FIR systems in ballistic missile defense sectors.[10] The broad range of wavelengths that comprise the infrared section of the electromagnetic spectrum requires materials that can transmit this radiation low attenuation.

1 Infrared Optical Materials

Utilizing a specific wavelength of the electromagnetic spectrum requires the ability to image and sense those wavelengths. In most cases this cannot be done without optical components. Transparency in the visible wavelengths is an easy concept to experience, however being able to "see" in wavelengths beyond what our unaided eyes can see becomes more difficult. In the IR wavelength of light, materials must be used which can transmit and perform some optical function on that light. The materials suitable for IR optical use tend to vary from those used in the visible although there is some overlap.

Materials used more commonly in visible light applications such as SiO_2 do transmit into the NIR and SWIR. For this reason most of the telecommunications technologies use NIR and SWIR wavelengths. Other oxide and fluoride glasses can be doped with rare earth elements for uses out to the MIR.[11] Figure 1.2 demonstrates the transmission spectra of SiO_2 along with other common glasses.

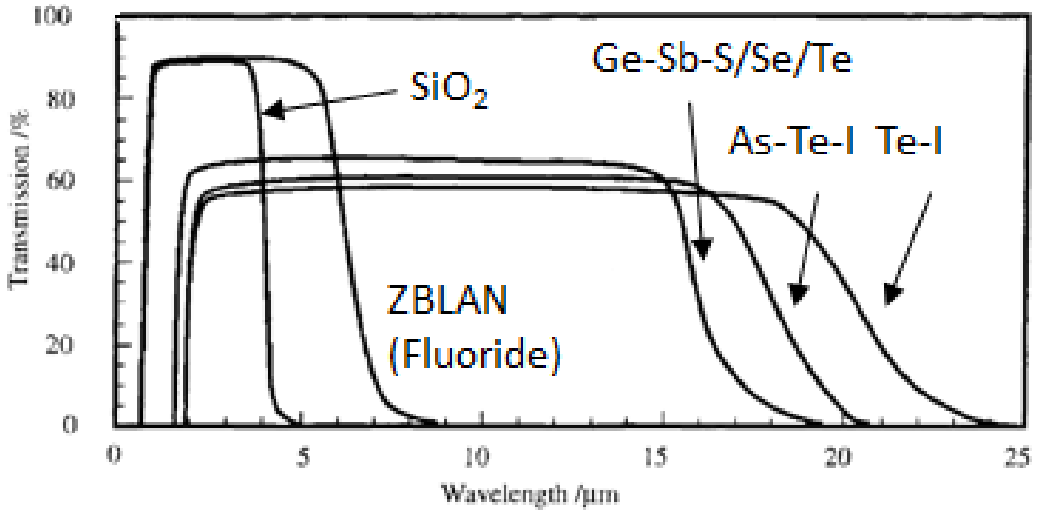

Figure 1.2: Infrared transmission spectra of some common optical materials

Although a variety of doped oxide glasses as well as doped and undoped transparent glass-ceramics transmit in the infrared, a large part of the current consumer infrared optics market is comprised of optical elements made of crystalline materials such as germanium, silicon, and zinc selenide/sulfide.[12] The main drawback with regards to these crystalline optics is the expense of the materials. Crystalline germanium in particular is expensive with raw material cost pushing the price of germanium IR optics upwards.

These crystalline materials have more recently seen competition from chalcogenide glasses (ChG). ChGs are glasses comprised of elements from the chalcogen group (group XI) of the periodic table, most commonly sulfur, selenium, and tellurium. While the chalcogen elements are necessary for a glass to be called a chalcogenide, they are typically alloyed with metalloids such as germanium, arsenic and antimony. Though less common, metals such as gallium, lead, tin, and indium can be alloyed with chalcogens or added to a chalcogen-metalloid mix to form glass.

1.1 Infrared Optical Glasses

1.1.1 Arsenic and antimony selenide/sulfide

The most commonly used and studied IR glasses are arsenic selenide and arsenic sulfide. These glasses form one of the simplest, most stable broadly IR transmissive glassy material systems in the chalcogenide family. A simpler glass of amorphous selenium or sulfur can be formed, however the T_g of pure Se/S glass is ~40°C, a temperature that can be reached by holding a bulk Se/S glass in human hands. In addition, pure Se/S glasses are very sensitive to radiation including sunlight so proper handling and storage is crucial. The binary mixture of arsenic and selenium forms a glass network through bonding that is almost entirely covalent.[13] The stoichiometric composition of arsenic selenide is $As_{40}Se_{60}$; due to its stoichiometry and small number of chemical constituents it is a glass used in many fundamental scientific studies on glass material properties.[14-17] The glassy As-Se network is a 2-D network composed of $As_2Se_{3/2}$ pyramids. One 3-coordinated arsenic bonds to three 2-coordinated selenium which each in turn bond to another arsenic. This bonding scheme is strictly followed at the $As_{40}Se_{60}$ composition, while at higher selenium content, the number of selenium between each arsenic increases, creating pyramids separated by Se chains. The As-Se pyramids form sheets of 2-dimensional structure, those sheets are weakly bonded to one another through van Der Waal's forces. $As_{40}Se_{60}$ is stoichiometric and considered to be ideally coordinated. This concept refers to the average coordination number, $<r>$ or CN, which is the average number of bonds per atom. Arsenic is 3-coordinated while selenium is 2-coordinated. When mixed in a 40/60% ratio this leads to $<r>= 2.4$. Phillips was the first in the glass community to theorize and

confirm this fact, he also postulated that glasses with <r> values closer to ideal would be superior glass formers as compared to glasses that were farther from the ideal average coordination.[18] Antimony can be isostructurally substituted in for arsenic in Se/S glasses especially where the use of arsenic poses price barriers due to regulation of arsenic disposal. Structurally, antimony causes minimal structural change from an arsenic containing composition.

Selenium and sulfur are isostructural to one another in chalcogenide glasses and in systems with additional constituents, substitution of one for the other can lead to a change in dominant bonding schemes.[19] Arsenic selenide and arsenic sulfide, which are both stoichiometric in the 40/60 atomic % composition ratio, exhibit nearly identical thermal properties. For instance T_g, which serves as perhaps the most common and widely used thermal property in glasses, is essentially the same for both glasses ($As_{40}Se_{60}$ T_g = 193°C [17], $As_{40}S_{60}$ T_g = 188°C [20]). The main operative difference between As_xSe_{100-x} and As_xS_{100-x} is the transmission window for a given value of 'x'. (Transmission window data for As-Se and As-S glass.) Arsenic selenide glasses can transmit from ~1 μm – 20μm, while arsenic sulfide glasses do not reach as high in the spectrum in terms of wavelength. Higher sulfur glasses can transmit down as far as 580 nm, just into the yellow part of the visible spectrum. Substitution of selenium for sulfur or vice versa is sometimes done as a way to shift either the electronic band gap or the the multi-phonon edge one way or the other.

$As_{40}Se_{60}$ glass is commercially available in bulk form from suppliers like Schott AG (IRG26), Amorphous Materials Inc. (AMTIR-2), Vitron (IG6), and IRradiance glass

(IRRADIANCE™CLASSIC-6). Glass can be purchased from the above suppliers in blank form (disks, rods, sheets) or preforms for optics (spheres, hemispheres, near net shape lenses).

1.1.2 Germanium-containing glasses

Beyond binary arsenic selenide or sulfide glasses, those that contain germanium also see wide use. Figure 1.3 shows the common ternary representation of the Ge-As-Se system. Although there is only one unrestricted, widely commercially available binary arsenic selenide glasses ($As_{40}Se_{60}$), there are 4 commercial glasses containing germanium. The addition of germanium adds two main desirable traits to the glass network.

First, germanium has a higher refractive index than the chalcogens and their typical metalloid alloying elements (with the exception of lead). The refractive index *(n)* of germanium is 4.10, while $n = 2.79$ for $As_{40}Se_{60}$ and $n = 2.41$ for $As_{40}S_{60}$.[21] For this reason, germanium is added to typical binary chalcogenide glasses in order to modify optical properties to boost the refractive index. Second, the addition of germanium, which is 4-coordinated, raises the coordination number of the glass. In the case of $As_{40}Se_{60}$ $\langle r \rangle = 2.4$, adding an element in germanium where $\langle r \rangle = 4$, the average coordination number is increased. This increase in the average number of bonds per atom raises the connectivity and dimensionality of the network as well. The results of this on physical properties include, higher T_g, higher hardness, improved chemical durability, among other things. In applications where binary chalcogenide glasses are not suitable due to the mechanical rigors of operation or processing conditions, germanium addition is a possible solution.

The only main drawback to the use of germanium is cost. However, a transition from pure germanium optics to chalcogenide glasses in which germanium makes up only 10-35 atomic percent is a transition in the direction of reduced raw material cost.

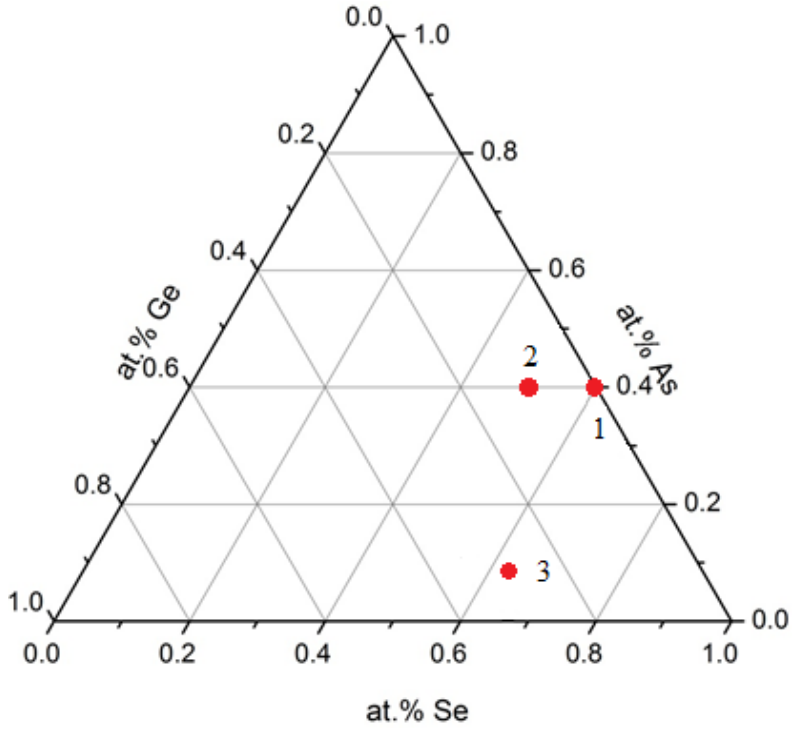

Figure 1.3: Ternary diagram of Ge-As-Se in atomic %, dots mark the commercially available Ge-As-Se compositions. Numbers 1, 2, and 3 correspond to $As_{40}Se_{60}$ (IG6), $Ge_{10}As_{40}Se_{50}$ (IG4), and $Ge_{33}As_{12}Se_{55}$ (IG2) respectively

2 Infrared Optics Fabrication

In order for any homogeneous, single phase material to be used as a lens, it must be shaped in order to focus the wavelength of light desired. Without shaping of any kind, the material is only a window. Certain defense applications need windows to allow sensors and cameras to look out of housings on aircraft for instance. However the properties

required of windows are often somewhat different than those of lenses from a mechanical and thermal standpoint. Windows, which still fall under the heading of optical elements are often subjected to constant thermal and mechanical strain. A thermal imaging device on an Airforce drone, fighter plane, or support aircraft cannot be hanging off of the aircraft into the wind. The device must be enclosed, however, it must retain its ability to let infrared light through to the camera or other sensing device. Now put this thermal imaging capability on an F-18 flying low over Iraq, from the temperature near the desert floor to the temperature at 30,000 feet, the change in temperature could be over 100 °F, the window must withstand that but the lens inside the camera does not. Additionally the abrasion of sand at Mach 1.5 requires a high hardness window material, the lens inside the system does not need to withstand that abrasion. This serves to demonstrate the range of mechanical and thermal properties that are needed to create just one optical system.

The shaping of lenses can be done in a number of ways and to a number of degrees. The first step is the blanking step, where a preform of an optic is cut out of a glass sheet or boule. This is often done by the glass manufacturer. Glass is supplied in various preform shapes and sizes as detailed in Section 1.1. These processing steps are applicable to most glasses, this dissertation will focus on chalcogenides. Following receipt of the preform the glass can follow one of 3 main paths. The traditional path is one of grinding and polishing in recurring steps to produce an optic of a particular size, shape, and finish. Another is single point diamond turning (SPDT) to the final shape or a near net shape which needs fine polishing to complete. The final mainstream possibility is that the preform will be subject to a PGM process after which it may be in final form or may need a final

grinding/polishing step. In addition to traditional polishing which typically employs an abrasive impregnated, shaped polishing tool that removes material to reduce roughness and correct shape, magnetorheological finishing (MRF) can be employed to make minute adjustments to the shape of an optic. The material, overall form of the optic, and nature of the final tolerances combine to dictate the proscribed fabrication method.

1.1 Traditional Grinding and polishing

Traditional grinding and polishing of optics involves very complex material interactions. These interactions are often difficult to model and explain scientifically, although there has been no shortage of research on the issue.[22-26] In industrial optics manufacturing the processes used to shape glass into lenses and other optical elements are very empirical in nature. There are a number of variations on the grinding and polishing of optics. The common theme in all grinding and polishing operations is abrasive. This abrasive can be in the form of a slurry or "loose abrasive", this is most common in polishing of flat surfaces such as the planar side of a plano-convex lens.[27,28] More common for shaped grinding tools used to form more complex geometries such as spherical and aspherical profiles is bound abrasive.[29,30]

Grinding and polishing are based on the principle of abrasion. As two materials rub against one another with some amount of normal force, friction is created. This friction breaks pieces of the materials off the bulk. The materials most common in grinding and polishing of optical glasses are diamond and cerium oxide.[31,32] The smaller the abrasive particles, the smaller the pieces of glass that are removed. Grinding begins with larger

diameter particles and works down in grit size to very small often < 100 nm size polishing particles. Conventional grinding and polishing can achieve adequately low surface roughness in most cases. Typical root-mean-square (RMS) roughness values are below 1 nm. However, when manufacturing lenses, the deviation from the designed shape of the lens is of great importance. Although grinding and polishing sometimes achieves the specified roughness and form factor, another step is sometimes required.

1.1.1 Magnetorheological finishing

Magnetorheological finishing or MRF is a process by which small height deviations on the surface of the lens can be corrected without the need to re-polish an entire surface. MRF is a strictly computer controlled process. After a part has been ground and polished, it is evaluated to determine if any aspects of the shape are out of specification. Once the surface has been evaluated, that data is fed into the computer and finishing begins. The fluid used in MRF contains a high concentration of magnetic particles. The viscosity of the fluid can be controlled by altering the magnetic field under which the fluid is placed. This technique allows a fluid to be pumped, sprayed and collected with the ease of managing water, but while the fluid is in the workspace, it becomes much stiffer and therefore is more efficient at material removal. In addition to fluid viscosity, the shape of the stream can be altered to treat larger or smaller areas or correct certain error very specifically. In the optics and optical material science community, developing MRF into a deterministic process where the effects of flow rates, particle sizes and fluid viscosities on material removal rate can be reliably predicted, has received a lot of scientific study.[33-

35] MRF is now a crucial technology used for material removal from complex shapes during final polishing.

1.2 Single point diamond turning

Single point diamond turning or SPDT for short, is an optical fabrication process that involves removal of material in a manner much like traditional metal turning. The glass work piece is mounted on a rotating spindle, essentially a lathe, with the optical axis of rotational symmetry matching the rotational axis of the spindle. Then a diamond or diamond coated tool is moved into contact with the glass work piece. As the two come into contact, the diamond tool removes material from the work piece, shaping it into an optical element of some kind. The smaller the point of contact between the diamond tool and the work piece, the smaller the removal pattern. The smaller the grooves made when removing material, the lower the final surface roughness that can be achieved. The process is called “single point” because rather than contacting an entire edge of the tool with the part as in wood or metal working, only the very tip or point of the tool touches the work piece. This is important for two reasons. First, it allows the final finish to be as fine as the single point of the tool. Second, it allows a higher stress to be imparted to the material for a given tool force. The feed rate determines how much load is put on the tool, and the area of the contact between the tool and work piece determine the pressure exerted on the glass.[36] The higher the stress, the higher the removal rate but the faster the tool wears. At high enough pressures, the glass behaves in a ductile way which allows for smooth material removal and low roughness.[37] This ductile material behavior is necessary to achieve a smooth finish, a brittle material response would lead to chipping.

SPDT has a couple of limitations. For one, it requires the desired profile of the optic to be rotationally symmetric. The second limitation which applies to certain chalcogenides, occurs when too much heat builds up in areas of the work piece, this can cause cracking due to thermal stresses from non-uniform material expansion.

1.3 Precision glass molding

Precision glass molding or PGM, is a thermoforming process designed to hot-form a glass or plastic lens preform to a desired lens shape. The optical fabrication techniques listed above are all room temperature material removal processes. PGM can be a material shaping process with no material removal necessary. A schematic of a typical PGM process can be seen in

Figure 1.4. The process involves heating of a glass preform from room temperature, to the molding temperature, soaking at that temperature to ensure an isothermal condition throughout the glass, molding the glass under force, cooling while maintaining force, and finally release of force and cooling to below T_g.

Hot-forming a glass into a lens has benefits that are not obtainable in the shaping and finishing methods detailed in the previous sections. PGM is a faster process than grinding and polishing per unit volume change. A glass preform can be molded from a spherical or cylindrical shape in 30 minutes for a typical glass material and lens geometry, whereas grinding a spherical lens and finishing it with polishing and/or MRF would take significantly longer than that. Additionally the PGM process should yield no waste material, and if the mold tooling is sufficiently smooth can yield a product with final

surface finish to meet specifications. When grinding and polishing chalcogenide glasses, the resulting slurry contains toxic elements and regulatory compliance costs associated with waste disposal.

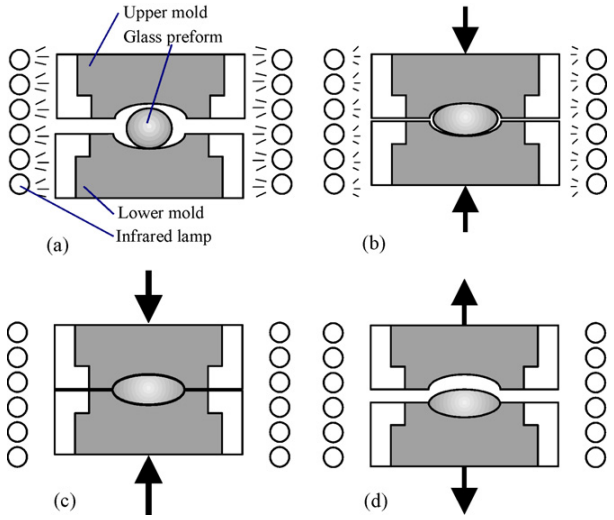

Figure 1.4: Schematics of four stages of a glass lens molding process: (a) heating (b) pressing, (c) annealing, and (d) cooling [8]

SPDT is a process that is capable of yielding lenses at a rate similar to PGM and it does so without intentionally heating the material. If, however, a finishing step using either traditional polishing or MRF is needed after SPDT, that advantage is no longer significant. In the case of chalcogenide glasses, where local heating can cause detrimental stresses in the glass and lead to fracture, PGM has a definite advantage. The heating of glass during PGM is reasonably uniform across the entire glass preform and does not cause non-uniform stresses due to spatially differing temperatures.

PGM has some limitations, one of which became an inspiration for the work in this dissertation. In industry the main gauge of any process or procedure is cost. Time is money,

money is money, almost everything relates to cost in some way. The manufacture of mold tools in PGM is an area of deep concern in the optics manufacturing community. This represents itself in two ways. The first is related to structural relaxation of glasses. Since glass is a viscoelastic material, its deformation under load and recovery or "spring back" after load is released is time and temperature dependent and nonlinear. As a glass is quenched from the molding temperature the glass structure relaxes toward equilibrium at discreet temperature or thermodynamic state. If the glass is quenched quickly it will retain stresses that can affect the optical properties and cause unacceptable optical effects. To alleviate these effects, the glass may be annealed which will change its shape, so when designing glass molds for PGM, the process is more complicated than simply taking the elastic thermal expansion into consideration. There are time and temperature dependent properties that can make designing a lens mold based on calculations alone very difficult. Current industry technique is to design a mold based on prior experience and test that mold by making lens. The lens is then measured and the mold must be machined again to account for any error in lens shape or form factor. This process is not trivial because glass molds are most commonly made of tungsten carbide (WC) which is expensive and time consuming to machine. Each mold redesign iteration can consume 4-8 weeks and up to many thousand dollars for each mold pair. Accurate mold, and preform design leading to lower prefabrication costs as well as conservation of raw materials is key in reducing the price per unit for PGM and increasing its viability in the market place.

Therefore, work is being done on modeling of viscoelastic and structural relaxation effects in an attempt to be able to predict glass behavior and increase the accuracy of mold

design.[8,38,39] The work presented in the experimental and theoretical sections of this dissertation advances the fundamental scientific understanding of structural relaxation and paves the way for that understanding to apply to the modeling of shape change during molding or post process annealing. The second cost center as relates to PGM is glass interaction with mold tooling. The glass and mold tools interact with one another at relatively high temperatures. The Arrhenius equation predicts an exponential relationship between chemical reaction and mobility of species with regards to temperature. The high temperatures and low viscosities ($\eta \approx 9$ log (Pa*s) [40]) that the glass experiences during molding can cause significant wear on the mold tools.[41,42] Reducing the chemical interaction and physical abrasion of the mold tooling increases mold lifetime and reduces cost per unit of production. This is the second area of active study in the realm of PGM and is often combined with research on protective, release coatings for mold tools.[43-45]

The production of high quality, low deviation, and low roughness optics depends on solving the problems stated above. Work on coatings and longer lifetime mold materials is the most common approach because it deals with principles that can be borrowed from and applied to other high temperature processes where chemical interaction and wear cause degradation. The less studied aspect is the characterization of the structural relaxation of glasses in an effort to accurately predict final lens shape after molding and annealing. This dissertation addresses the fundamental science behind the basic need to understand and characterize structural relaxation. It provides the experimental method and modeling starting point for this problem to be solved.

CHAPTER 2

SYNTHESIS AND FABRICATION OF CHALCOGENIDE GLASSES FOR USE IN EXPERIMENTATION

Chapter 1 introduced infrared optical materials and optical fabrication methods, specifically PGM, as it relates to structural relaxation in glasses. Infrared optical glasses are commercially available in the compositions discussed in the last chapter. Those glasses which are available through companies like Schott, Vitron, and IRradiance Glass were originally chosen due to their optical properties like index of refraction (n), dispersion, change in index with temperature$\left(\frac{dn}{dT}\right)$, and transmission window. When considering a glass for PGM, other factors are important such as the fragility of the glass, which is defined as the slope of the viscosity vs. temperature curve at a viscosity of 12 log (Pa*s) and the corresponding temperature which is known as T_{12}.[17] The higher the glass fragility, the more sensitive the viscosity is to changes in temperature, for this reason it can be difficult to keep the viscosity of some glasses constant during the molding cycle in PGM if there are temperature fluctuations. Additionally, some glassed exhibit greater thermal expansion and structural relaxation magnitudes over a given temperature, these are factors that can affect the accuracy with which PGM can form a lens. From an engineering standpoint, it is entirely possible that one of the glasses commercially available may meet the index requirements of a design but be entirely suboptimal in properties that dictate ease of manufacture. This is one of the primary reasons that a company like IRradiance Glass has recently come into the marketplace. They offer custom designed glasses that can be ordered to match as closely as possible, both traditionally considered optical properties as

well as those related to manufacturing, mounting, and field use. In a similar way, IR glasses that are commercially available often do not contain the level of material property evaluation necessary to answer specific scientific questions related to glass structure and resulting structural relaxation characteristics. The IR glasses used in this study were synthesized from elemental raw materials.

2 Germanium-arsenic-selenium glasses

The IR material system of study in this dissertation is the germanium, arsenic, and selenium ternary system ($Ge_xAs_ySe_{100-x-y}$). The three glasses chosen for study were selected based on their contrasting glass network characteristics. The defining characteristics of interest were dimensionality, coordination number $<r>$, and stoichiometry. The first glass that was chosen was $As_{40}Se_{60}$ where x = 0 and y = 40 in the $Ge_xAs_ySe_{100-x-y}$ convention. This glass is the most commonly studied glass in the Ge-As-Se system, it is the stoichiometric composition on the As-Se binary. This is the composition at which all of the arsenic bonds can be satisfied by selenium bonds, and a negligible number of homopolar bonds are thought to exist. Glasses in this system with x = 0 and y < 40 or y >40 will have homopolar bonding of Se-Se or As-As respectively. Some authors theorize that at a ratio of 40/60 atomic %, the glass still contains homopolar bonds but that is disputed by other reputable authors and the debate is ongoing.[46] The author of this dissertation takes the view that an insignificantly small amount of homopolar bonding occurs in $As_{40}Se_{60}$ glass. This glass is composed of As_2Se_3 pyramids forming a puckered layer, 2-D structure. The puckered layers act, in the bulk, like a crumpled sheet of paper, so that layers are forced near one another and are attracted via weak van Der

Waal's forces.[47] This glass has a 2-D structure with an average coordination number $<r>$ = 2.4 as stated in the previous chapter.[18]

The second composition chosen also contains no germanium (x = 0). That composition is $As_{20}Se_{80}$ (x = 0, and y = 20). The structure of non-stoichiometric and non-ideally coordinated As-Se glasses are less clear. The average coordination number which can be calculated using Equation 2, where *A* is the coordination number (CN) of germanium (4), *B* is the CN of arsenic (3) and *C* is the CN of selenium (2) and *x* and *y* are the percentages of germanium and arsenic as stated above.

Equation 2

$$< r >= A * x + B * y + C * (1 - x - y)$$

In the case of $As_{20}Se_{80}$, $<r>$ = 2.2. This demonstrates a coordination lower than the ideal average coordination number of 2.4, which puts the glass in a structural mode known as "floppy" because the number of bonds are less than the number of degrees of freedom.[48] Coordination can give you an idea of the nature of the glass structure, but its actual structure deserved more attention. X-ray Photoelectron Spectroscopy (XPS) was done on a number of As-Se glasses to determine the bonding scheme at higher selenium levels. Since $As_{40}Se_{60}$ shows pyramidal As_2Se_3 units, it would follow that a higher selenium glass would separate those units with extra selenium atoms. This is in fact the case with a thorough study showing that $As_{20}Se_{80}$ is made up of 72% Se-**Se**-As fragments which represents two selenium between each arsenic and 28% Se-**Se**-Se fragments which

represent three selenium between each arsenic.[49] This composition represents a non-stoichiometric, under-coordinated glass with a dimensionality between 1-D and 2-D.

The third ChG chosen for study, contained germanium. This glass is stoichiometric, with a composition where x = 17.9 and y = 19.7. It is located on the stoichiometric tie line that runs between $As_{40}Se_{60}$ and $Ge_{33.3}Se_{66.6}$ ($GeSe_2$) on the Ge-As-Se ternary as shown in Figure 2.1. Equation 2 was used to calculate the CN, $\langle r \rangle = 2.56$. This glass resembles $As_{40}Se_{60}$ in that, theoretically, all of the bonds are heteropolar. The result is a glass network made up Ge-Se and As-Se bonds, there should be an insignificant number of homopolar Se-Se bonds. Understanding the Ge-As-Se network is best approached by starting with $As_{40}Se_{60}$, which as previously stated contains stacked layers of As-Se pyramids, also denoted $AsSe_{3/2}$. The addition of germanium serves primarily to cross link the stacked-layered structure found in $As_{40}Se_{60}$.[50] Germanium and selenium have a larger electronegativity difference than arsenic and selenium, this causes selenium to bond preferentially to germanium. However, for this stoichiometric composition there is enough selenium to fully bond with all available arsenic and germanium. Germanium is 4-coordinated and bonds to 4 selenium, in a $GeSe_{4/2}$ manner.[51] Each selenium is bonded to an arsenic or germanium, and since the percentage of arsenic and germanium are nearly the same it is assumed that most of the selenium atoms are bonded to one of each in the homogenous glass. If any selenium are bonded to the same element on both sides it is statistically probable that arsenic would be the element, due to the slightly higher concentration of arsenic.

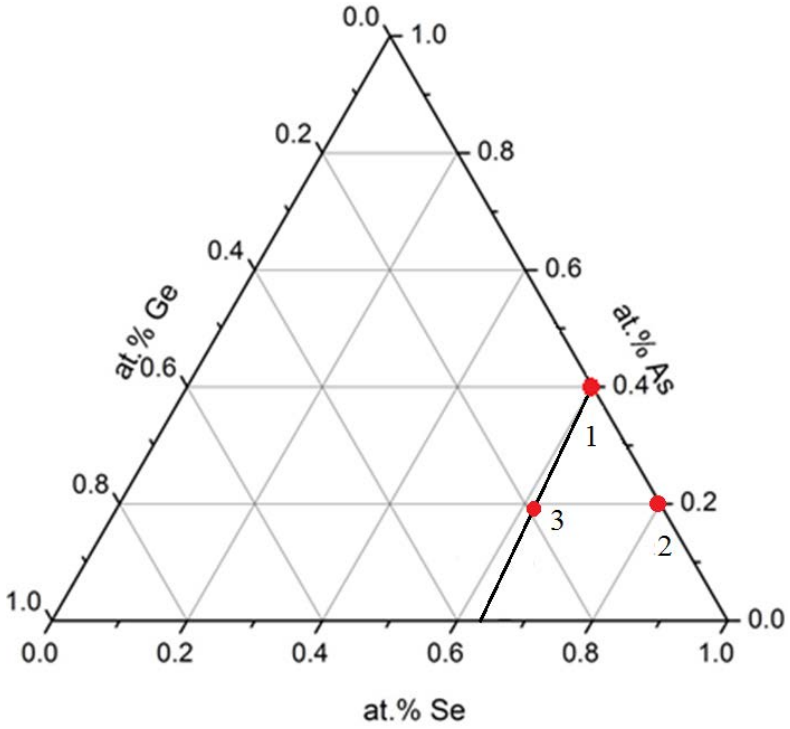

Figure 2.1: Ternary diagram of Ge-As-Se in atomic %, dots mark custom made Ge-As-Se compositions. Numbers 1, 2, and 3 correspond to $As_{40}Se_{60}$, $As_{20}Se_{80}$, and $Ge_{17.9}As_{19.7}Se_{62.4}$ respectively

The crosslinking of germanium in this composition serves to interconnect the puckered layer structure observed in $As_{40}Se_{60}$ and increases connectivity along with dimensionality. This germanium containing composition is between $GeSe_2$ which is 3-D and As_2Se_3 which is closer to 2-D.[52] This set of glasses was chosen in order to judge the evolution of structural relaxation behavior with varying composition, stoichiometry, coordination, and dimensionality.

2 Synthesis of Ge-As-Se glasses

Synthesis of the three ChG compositions detailed in Section 1 of this chapter was done as follows. The raw materials were batched in an Ultra-High Purity (UHP) nitrogen atmosphere glove box. This was done to eliminate oxygen from the final glass network. Elemental arsenic, germanium, and selenium of 99.999% purity were used in the synthesis of this glass. From the desired atomic % composition, the appropriate mass of each component was calculated, that mass was weight out on a balance with a resolution of 0.0001 grams. The elements were added into a quartz tube beginning with the lowest melting temperature element and increasing to the highest melting temperature. The order for Ge-As-Se glasses was first selenium, then arsenic, then germanium. This was done so that as the bottom elements melt, the higher elements sink into the melt and are then "fluxed" in. "Fluxing" elements refers to their dissolution in the liquid of a different element, leading to a decrease in apparent melting temperature. This allows elements like germanium which has a melting point of 938.2 °C to melt at 750 °C when fluxed by molten selenium and arsenic.

These elements were weighed and batched into a cylindrical quartz ampoule having and inner diameter (ID) of 25.4 mm as seen in Figure 2.2. Each composition was synthesized with a 150 gram total batch size. Once the elements were batched in the silica ampoule or tube, ~150 mm of empty, "head space" remained above the elements. While still in the nitrogen glovebox, a vacuum fitting was placed on top of the ampoule which flanges down to 10 mm ID. The entire assembly was removed from the glovebox, and the vacuum fitting was attached to a vacuum pump. The ampoule was placed in a tube furnace

held at 90°C while under vacuum to drive off any surface water. After 15 min the ampoule was removed from the furnace and the ampoule fitting was closed, leaving the inside of the ampoule under vacuum.

Figure 2.2: Quartz ampoule 25.4 mm ID

The ampoule was then sealed with a methane and oxygen fueled torch at the top where the ID was smallest. The sealing process created a seal that held the contents under vacuum as well as separated the upper most part of the tube containing the fitting from the rest of the sealed ampoule. Once sealed, the ampoule was placed in a rocking tube furnace. The furnace was set to rock at an angular velocity of approximately 6°/second and the temperature was ramped at 2 °C/minute up to the melting temperature. The melting temperature was 650 °C for the binary As-Se compositions and 750 °C for the Ge containing glass. After melting overnight for ~18 hrs, the rocking was stopped so that the ampoule was oriented vertically. The temperature was ramped down at a rate of 2 °C/minute to the quench temperature of 570 °C for the binary As-Se compositions and 600 °C for the Ge containing glass. Once the quench temperature was reached the ampoule containing the molten glass was removed from the furnace and cooled using forced nitrogen cooling. During cooling, the glass contracts. When the forces causing adhesion to the ampoule wall were exceeded by the force of the glass contracting, the glass released from the ampoule in dramatic fashion. This typically coincides with cooling through T_g.

The ampoule and glass, having solidified, were placed in an annealing furnace. The annealing temperature is set at 40 °C below T_g (the method of T_g measurement is detailed in a following section). The annealing temperatures were 70, 155, and 230 °C for $As_{20}Se_{80}$, $As_{40}Se_{60}$, and $Ge_{17.9}As_{19.7}Se_{62.4}$, respectively. After annealing for ~18 hours, the tube was removed from the furnace and carefully broken open to extract the glass. The resulting piece of glass in all cases was a ~125 mm long cylinder with a meniscus at one end from cooling and a hemisphere at the other. This glass was used, first for characterization, then for fabrication of relaxation samples.

3 Characterization of Ge-As-Se glasses

In order to understand the basic properties of the custom glasses that were synthesized, full thermal characterization was done. This also ensured that the material was handled, processed, and tested in a safe manner. The structural relaxation experiments detailed in the upcoming sections relied on an understanding of the thermal and thermo-mechanical properties of the materials in question. Some of the key properties of interest included the glass transition temperature (T_g), dilatometric softening point (T_d), coefficient of thermal expansion (CTE) of both liquid (α_L) and glass (α_g), and the temperature at which the glass has a viscosity of 12 log (Pa*s) (T_{12}).

3.1 Characterization Tools

3.1.1 Differential Scanning Calorimetry (DSC)

A differential scanning calorimeter (DSC) is an instrument that measures heat flow in and out of a sample, thereby allowing phase transitions and other thermal events to be detected. This technique was developed in 1962 by Michael O'Neil and Emmett Watson who worked for Perkin Elmer and served as a breakthrough in the ability to measure enthalpy and specific heats in materials as a function of temperature.[53] A typical DSC contains a cell with two sample pads. One pad is for the experimental sample and one pad is for a reference. A DSC works by comparing the amount of heat flow needed to keep both pads at the same temperature during a temperature ramp. The difference in heat flow between the sample and the reference represents the temperature dependent thermal signature of the material in question. One of the most commonly sough material properties is T_g. In addition to the glass transition temperature, a DSC can also reveal the crystallization temperature(s) (T_x), the melting temperature (T_m), and can also be used to calculate the temperature dependent heat capacity (C_p) of the material.

The value of most interest in these glasses was T_g, the glass transition region is indicated by the shaded box in Figure 2.3. There are several ways to classify the glass transition temperature, for this dissertation the inflection point T_g is used. This temperature value is determined by finding the inflection point of the heat flow curve within the glass transition region. This can be done using software or the derivative of the heat flow can

be taken and the minimum value in the glass transition region corresponds to the inflection point as seen in Figure 2.3.

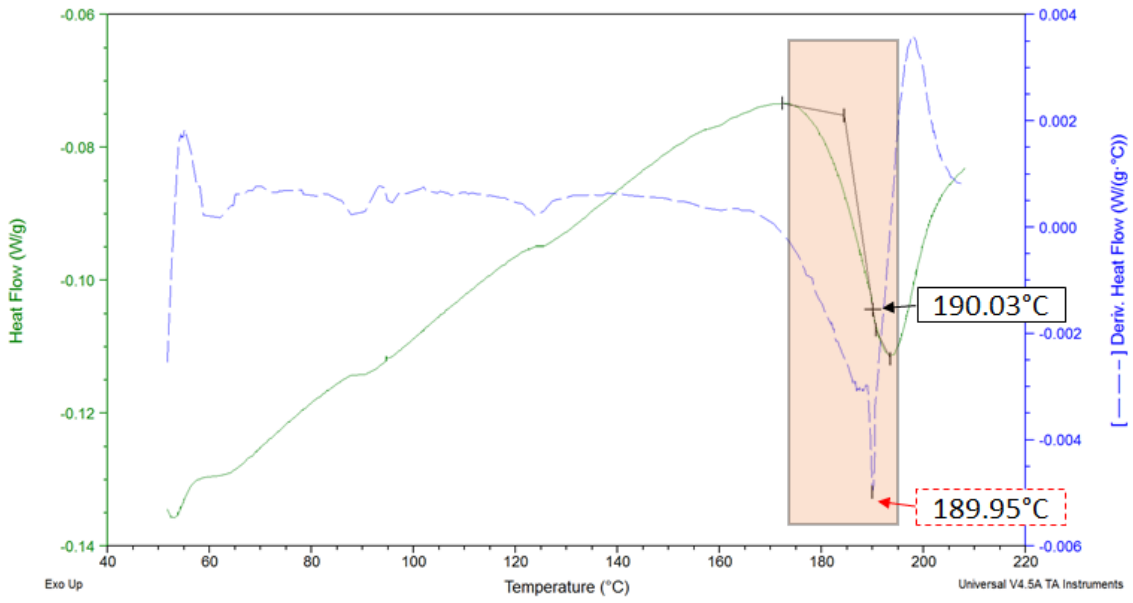

Figure 2.3: DSC signal of $As_{40}Se_{60}$ for heat flow (solid) and the derivative of heat flow (dashed); inflection point T_g as calculated from the heat flow and derivative heat flow are indicated by the solid box and dashed box respectively

The T_g of each glass synthesized was measured as well as that of N-BK7 an oxide optical glass that was included in the relaxation studies.[38] The DSC used in this study utilizes aluminum pans which limit the normal operating temperature of the instrument to 600 °C. The ramp rate used for all DSC studies was 10 °C/min. Each run included a ramp to ~25 °C above T_g to ensure the glass was fully annealed. Following this step, the temperature was equilibrated at 50 °C and a final 10 °C ramp to ~25 °C above T_g was done and the T_g signal observed during this final section was used to calculate the T_g referred to in this study as the DSC T_g. Two different methods for T_g measurement were used in this

work, the first is described in this section and the second is called the dilatometric T_g ($T_{g,d}$) and described in Section 3.1.2 below. The DSC that was used for this research was a DSC 2920 from TA Instruments, it has a temperature uncertainty of ± 2 °C, so the discrepancy seen in Figure 2.3 is not significant.

3.1.2 Thermomechanical Analysis (TMA)

Thermomechanical analysis is done on materials to characterize their change in length or volume with changing temperature. In analysis of crystalline materials the main information that can be extracted is thermal expansion behavior, described by the coefficient of thermal expansion (CTE). In glassy or amorphous materials, a TMA can be used to identify the glass transition region as well as the dilatometric softening point (T_d) of a glass. A typical TMA curve can be seen in Figure 2.4. The important values shown in Figure 2.4 are first the solid or glass CTE (black) which is calculated from the slope of the curve, $\frac{dL}{dT}$, between two selected points below T_g using Equation 3, where α_g is the CTE of the glass, L_i is the initial length of the sample.

Equation 3

$$\alpha_{g,l} = \frac{1}{L_i}\frac{dL}{dT}$$

The liquid CTE (α_L), (green), is calculated the same way, with the exception that $\frac{dL}{dT}$ is taken as the tangent between two points just above T_g. Thermal expansion in materials is driven by the temperature dependent equilibrium spacing between atoms. The higher the temperature, the greater the equilibrium atomic distance, this phenomenon leads to an

overall expansion of the material upon heating. A majority of materials behave this way including all of the materials discussed in this dissertation.

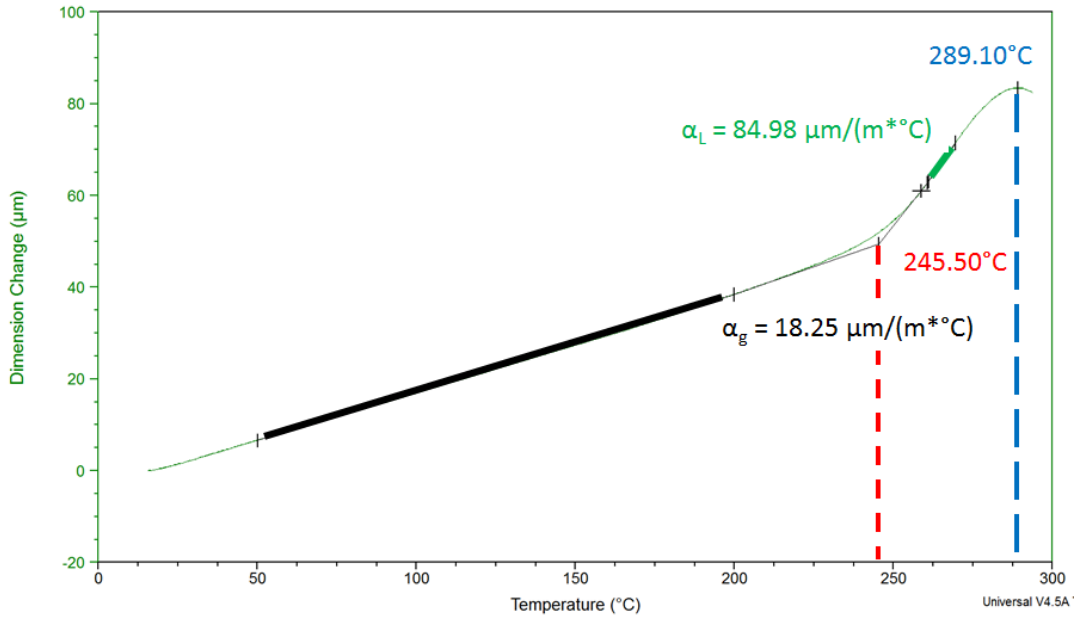

Figure 2.4: TMA plot of dimension change (µm) versus temperature (°C) for $Ge_{17.9}As_{19.7}Se_{62.4}$; glass CTE ($\alpha_g$, black), dilatometric T_g (red), liquid CTE (α_L, green), and T_d (blue) are shown

The dilatometric glass transition temperature is equal to the temperature at which the glass and liquid CTE slopes intersect. The glass transition temperature has been studied as much as any other topic in the field of glass science.[54-59] $T_{g,d}$ is the temperature at which the change of the glass network from that of a super-cooled liquid to that of an equilibrium liquid can be observed by the measurement system in question.

The final material property that can be obtained from a plot like Figure 2.4 is the dilatometric softening point (T_d). The softening point is defined as the temperature at which the plot reaches its maximum change in height. This behavior is related to what is

known as “slumping” in glass. It is the temperature at which the glass viscosity becomes low enough that the sample can no longer support its own weight. Just after T_d, evidence can be seen of the glass “sagging” under its own weight and the decrease in height due to viscous flow is greater than the expansion of the material due to thermal expansion. CTE testing was done with the same samples that would be used in relaxation testing, therefore this measurement occurred after sample fabrication which is detailed in later in Section 4 of this chapter.

Thermomechanical analysis of the glasses used in this study was done using a TMA 2940 from TA Instruments. Figure 2.5 demonstrates the sample orientation in the testing cell. The sample sat on a fused silica stage, while the top of the sample was held by a fused silica probe rod. Fused silica was used in this instrument due to its extremely low expansion coefficient 0.55 $\frac{10^{-6}}{^{\circ}C}$ over the test temperature range, which reduces expansion of the system and ensures that the expansion of the material in question comprises the majority of the expansion behavior. The measured CTE values are reported in section 3.2, but for contrast the CTE of fused silica is anywhere from 36 – 50 times smaller than that of the ChGs measured in this study and approximately 16 times less than N-BK7. The fused silica probe is a “shepherd’s hook”, the long leg of the hook extends down into the center of the instrument and is attached to a magnet that runs through a linear variable differential transformer commonly known as an LVDT. An LVDT measures vertical change in position of the hook and therefore height change of the sample. The entire stage-hook-sample assembly is encased in a furnace that has an upper temperature limit of ~600 °C in the current configuration. The TMA described in this section was used throughout

the structural relaxation testing that is the focus of this dissertation with an identical sample setup.

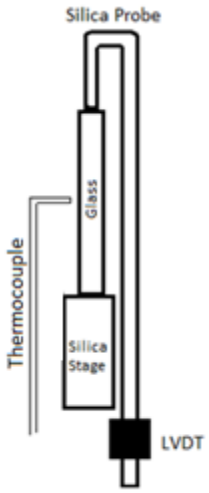

Figure 2.5: Schematic of sample setup in the TMA

3.1.3 Beam bending viscometer (BBV)

Viscosity is an important material property for PGM, it is also important to analyze and understand the role viscosity plays in structural relaxation behavior. Full characterization of a glass viscosity versus temperature is typically done with at least two measurement methods. Each method has limitations to the temperature range it can cover. In the case of this present work, a beam bending viscometer (BBV) was used because it has the ability to quantify glass viscosity in the temperature range near T_g. Since this covers the range of temperature studied in this research only this viscometry method was deemed necessary. In addition to the viscosities near T_g, BBV measurements allow the fragility of the glass to be calculated. The fragility is the slope of the viscosity curve at T_{12} which is

the temperature at which the viscosity is 12 log(Pa*s). The fragility is designated by the parameter "*m*" and is listed in Table 2.1.

Figure 2.6 is a picture of sample fixturing in the BBV. The tube seen in the picture is made of fused silica for its low expansion properties, following a similar design principle to the TMA. The glass sample must be a beam of at least 25 or 55 mm in length, depending on the sample holder, and have a rectangular cross section no larger than 3 x 3 mm. This beam spans the holding tube and rests in square notches on each side of the tube. As seen in Figure 2.6, a fused silica shepherd's hook is suspended from the beam. This shepherd's hook has a long leg which extends through an LVDT below the sample chamber and ends with a mass basket.

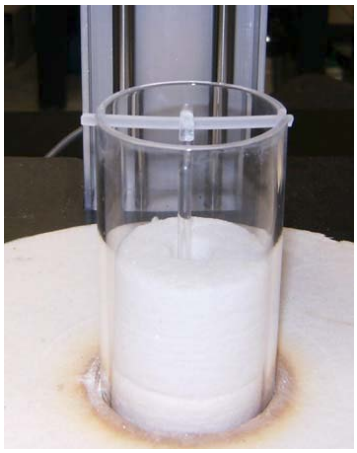

Figure 2.6: Picture of BBV sample fixturing [60]

The experimental procedure for all samples was as follows. Basic material property data such as sample dimensions and CTE were input to the BBV program on a computer.

The sample was set it place and the shepherd's hook was suspended from it. A mass was added to the mass basket connected to the base of the shepherd's hook and that mass was input to the computer. The temperature was then ramped to the testing temperature. Once that temperature was reached the instrument began collecting deflection data. Data continued to be collected until the sample reached its maximum deflection distance which was set at 10 mm. The only variation in procedure for different samples was that measurement above T_g had the additional step of keeping the shepherd's hook and mass from being suspended on the sample beam until after the target temperature was reached. This was to prevent rapid deformation under non-isothermal conditions which would not return accurate viscosity data.

The deflection data was then analyzed using the ASTM standard for beam bending viscometry measurements.[61] The computer's automatic calculation of viscosity was confirmed by hand calculation using Equation 4, where η is the viscosity in (Pa*s), g is the constant acceleration due to gravity (9.81 m/s^2), L is the span length of the sample beam in cm, M is the mass of the shepherd's hook plus the added mass in grams, ρ is the density in grams/cm^3, A is the cross sectional area of the sample in cm^2, I_c is the moment of inertia of the sample beam along the long axis, and $\frac{dh}{dt}$ is the change in height with respect to time in cm/s. The standard contains additional terms to account for the CTE of the glass sample

and the stage where α_s and α_g are the CTE of the stage and sample glass respectively, and T is temperature in °C.

Equation 4

$$\eta = \frac{gL^3}{1440 I_c \left[\frac{dh}{dt}\right]}\left[M + \frac{\rho AL}{1.6}\right]\left[\frac{(1+\alpha_s T)^3}{(1+\alpha_g T)^4}\right]$$

The viscosity versus temperature behavior of ChG glasses over the relatively small range of temperatures in question is essentially linear as will be shown in the following section. This linear behavior allowed three measurements of glass viscosity to be made for each composition in question, all within or just outside the glass transition temperature. One measurement below, one above and one at T_g were made for each composition synthesized as well as N-BK7.

Sources of error in BBV measurement include sample fabrication error such as inconsistent cross section extending the length of the sample, temperature uncertainty within the furnace during the test, and stability of temperature during the test. The uncertainty regarding the sample cross section can be minimized by proper fabrication of a glass sample. The cross section of the samples used in this test were (3.000 x 1.955 mm ± 0.05). The temperature within the furnace was calibrated using a separate thermocouple dedicated to the sample. The difference between measured furnace temperature and actual sample temperature was characterized and used to adjust the temperature data gathered. Experimentally the temperature had a standard error of ± 0.095 °C from isothermal and the viscosities varied ± 0.095 log(Pa*s).

3.2 Results of thermal characterization

Thermal characterization was carried out on the three custom chalcogenide glasses that were synthesized, as well as the commercial material, N-BK7 optical glass from SCHOTT. The results are shown in Table 2.1 and Table 2.2. The gaps in knowledge are due to instrumental limitations. The DSC used in this study was limited to 600 °C so it was impossible to experimentally determine the T_g by DSC for N-BK7. Ramping to a high enough temperature above T_g to anneal the glass and rescan was not possible. In addition, the TMA was limited in temperature by the aluminum coverings on its furnace, these prevent reaching temperatures greater than 620 °C, T_d was unable to be determined, for N-BK7, given this limited range.

Table 2.1: Thermal properties measured by DSC and viscometry for all glasses used in this study (value taken from supplier literature [62])*

Glass	DSC T_g [± 2°C]	T_{12} [± 2°C]	m
GeAsSe	272	248	32.8
$As_{40}Se_{60}$	190	172	52.6
$As_{20}Se_{80}$	104	81	38.1
N-BK7	557*	577	38.7

Table 2.2: Thermal properties measured by TMA for all glasses used in this study

Glass	$T_{g,d}$ [± .6°C]	T_d [± 2°C]	α_g [± .2 ppm/°C]	α_l [± 7 ppm/°C]
GeAsSe	251	290	18.1	67
$As_{40}Se_{60}$	176	200	23.5	89
$As_{20}Se_{80}$	89	115	37.4	103
N-BK7	571	N/A	8.8	57

The viscometry done on the chalcogenide samples show an interesting result. The T_{12} temperature for $As_{40}Se_{60}$ and $Ge_{17.9}As_{19.7}Se_{62.4}$ track closely with the T_g as determined by TMA ($T_{g,d}$). The $As_{20}Se_{80}$ T_{12} and dilatometric T_g values were not as close but were still within 7 °C accounting for error. In these chalcogenides it is safe to say that T_{12} occurs below and close to the glass transition temperature as determined by TMA. Differences in reported T_g values make it difficult to compare experimentally determined values among authors. There is a popular convention of claiming $T_g = T_{12}$; this convention in its pure form is used as a way of defining a single discrete value for T_g.[63] T_{12} can be directly measured using viscometry, the value of T_g however is not discrete, so equating it to T_{12} is a method of solidly defining it. However, in literature, this is often misused, authors who determine T_g using DSC often equate that value to T_{12} and hold that $T_g = T_{12}$ and the reciprocal are always true. Using the experimental tools at our disposal, it is preferable to measure the values independently, state the conditions under which they were measured, not relying on theoretical linkages of various properties when experimental connections can be determined with relative ease.

4 Fabrication of Ge-As-Se structural relaxation samples

Once synthesis and initial thermal characterization were complete, the samples were prepared for relaxation testing. The glass samples were designed to fit easily into the TMA as can be seen in Figure 2.5. The samples were designed to have a square cross section (~3 x 3 mm). This was done to ensure that heat transfer between the furnace environment and the center of the sample was expedited. Though a smaller cross section would have resulted in faster heat transfer, a balance was struck between heat transfer rate, physical stability in the TMA, sufficient relaxing volume, and ease of fabrication. The height of the samples was designed to be ~12 mm, this resulted in a 4:1 height to cross sectional ratio. The N-BK7 samples used in this study met the sample specifications in as-received condition.

The synthesis of ChG glass produced a near cylinder as shown in Figure 2.7a. The rounded bottom resulting from the ampoule shape was removed as shown by the cut lines, as was the meniscus that forms upon cooling in every glass melt of this nature. The cuts were made with a Buehler Isomet wafering saw, using a diamond impregnated circular blade. Once the top and bottom of the sample were removed, a right cylinder remained. This cylinder was turned on its side and diced into 3.1 - 3.25 mm “plates” as seen in Figure 2.7b. Each plate was then ground down to 3 mm thickness. The resulting plates were diced once again to reach the final overall shape of the samples (Figure 2.7c).

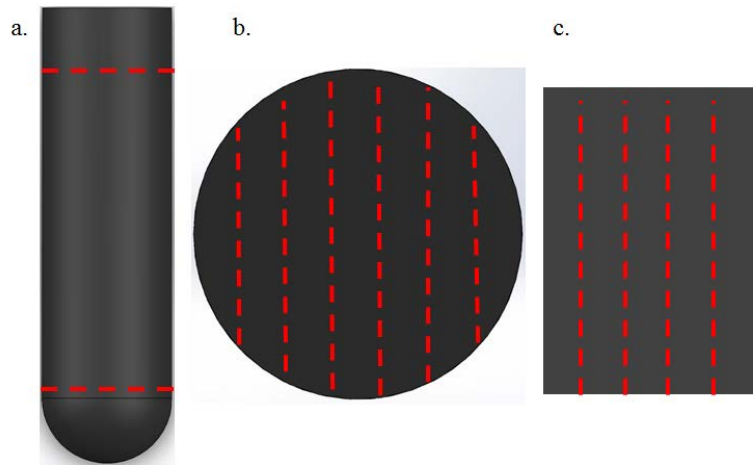

Figure 2.7: Schematic of relaxation sample fabrications, red dashed lines represent cuts

The tall samples with square cross sections were ground to a final 3 x 3 mm specification and cut to their final 12 mm height requirement. These samples were tested for their structural relaxation behavior.

CHAPTER 3

CHARACTERIZATION OF STRUCTURAL RELAXATION IN GLASSES

1 Introduction

Understanding structural relaxation in glass is one of the keys to understanding the glass transition range. Structural relaxation cannot be handled as a monolith, it must be broken down into its constituent parts. Study of structural relaxation in glass is not a direct investigation, as in so many other areas of scientific study, the evolution of measurable properties must be used to determine the behavior of glass structure. Among the most used properties for characterization of structural relaxation are enthalpy, volume, and density.[64] They are used because their behavior is directly dependent on the glass network structure, therefore if the glass network changes, the properties will change. The difficulty exists in deduction of the mechanisms of structural relaxation, it is one thing to measure property changes with time at a specific temperature and another thing entirely to understand in what way the structure and therefore properties change.

However, before delving into the evolution of glass during structural relaxation, the behavior of the measured properties had to be characterized. Once the characterization was sufficient, the real work of deciphering the glass network changes during relaxation could begin. The most widely used method for characterizing structural relaxation is through DSC measurements.[59,65-68] Among the characterization experiments done using the DSC, the most popular is the Tool-Narayanaswamy-Moynihan (TNM) model as the basis for first principles analysis.[20] The following section will detail both the TNM

model as well as other structural relaxation models, highlighting differences where important.

2 Characterization Methods

2.1 TNM model

The Tool-Narayanaswamy-Moynihan (TNM) model is the end result of piecewise contributions to the research of structural relaxation research by the scientists whose name it bears. Recall from Figure 3.1, the representative trend of a given material property in a glassy system. For the sake of description, *p* is defined as a representative material property that behaves according to the general trend in Figure 3.1. The evolution of a property, *p*, when the glass is held isothermally at a temperature near T_g can be written as Equation 5 where $p_{eq}=p(T,\infty)$ and $p=p(T,0)$.

Equation 5

$$\frac{dp}{dt} = \frac{p_{eq} - p}{\tau}$$

This expression simply shows that the rate of property change is a function of the distance from equilibrium. Equilibrium is graphically defined by the liquid equilibrium or "liquidus" line shown in Figure 3.1. In order to better describe the glassy state, Tool came up with what he considered a characteristic temperature to relate a glassy network to its equilibrium liquid structure. This temperature, the fictive temperature (T_f), is defined graphically as the temperature at which the tangent of the curve of *p(T)* in the glassy region intersects the liquid equilibrium line.

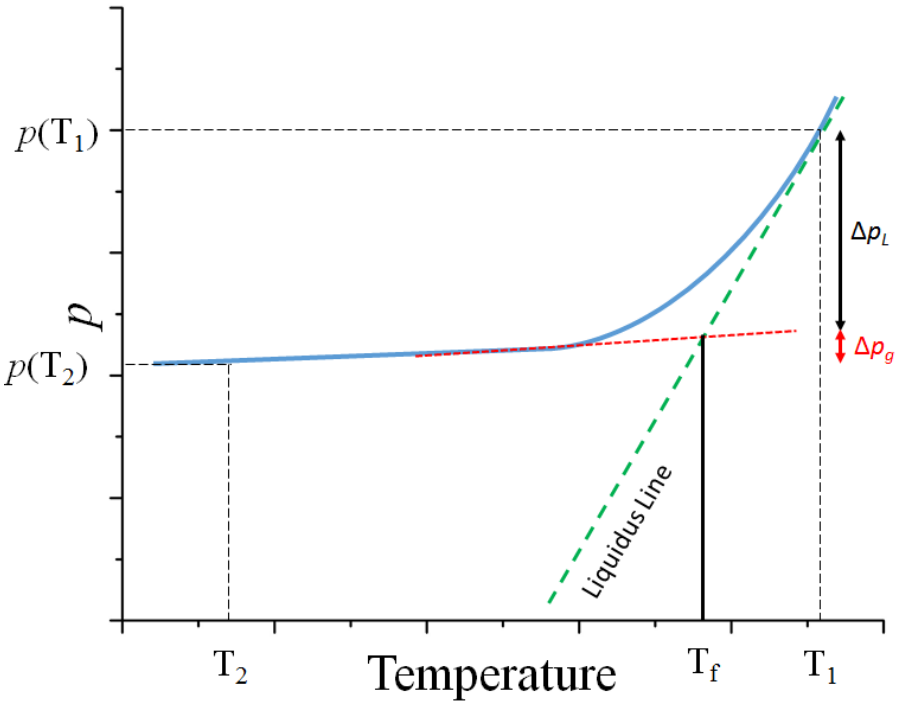

Figure 3.1: Graphical representation of the liquid and glass components of property change

Once the working space for the mathematical description of how glass properties shift through T_g is defined, the description and derivation of Tool can be presented. The value of property, p, at T_2 after cooling from T_1 can be described as $p(T_2) = p(T_1) + \Delta p_L + \Delta p_g$. The component Δp_L which occurs in the liquid regime (between T_f and T_1) can be described as $\Delta p_L = \alpha_L(T_f - T_1)$, where α_L is the liquid CTE defined by the liquidus line. Similarly, Δp_g is the component of the overall property change that occurs in the glassy or metastable solid state is described as $\Delta p_g = \alpha_g(T_2 - T_f)$, where α_g is the CTE of the glass. The expression for p as a function of temperature can be generalized further by substituting any temperature, T, for T_2 and substituting the general initial temperature, T_0, for the specific temperature T_1. That results in Equation 6.

Equation 6

$$p(T) = p_{eq}(T_0) + \alpha_L(T_f - T_0) + \alpha_g(T - T_f)$$

To further complicate the process, the vibrational component must be removed from the overall property change, *p(T)*. The elastic, instantaneous, or vibrational change in property can be described as $p_v(T) = p_v(T_0) + \alpha_g(T - T_0)$. In the case of glasses $\alpha_g = \alpha_v$ and is substituted as such. The property change due to structural relaxation is the total property change minus the vibrational or elastic component. Removing the vibrational leaves only the structural component, and this is represented by Equation 6 minus $p_v(T)$ which results in Equation 7.

Equation 7

$$p_s(T) = p(T) - p_v(T) = p_{eqs}(T_0) + \alpha_s(T_f - T_0)$$

Taking the derivative of Equation 7 with respect to time yields Equation 8.

Equation 8

$$\frac{dp_s(T)}{dt} = \alpha_s \frac{dT_f}{dt}$$

Then rearranging Equation 7 and adding time dependence to both sides gives Equation 9.

Equation 9

$$p(T,t) = p_v(T) + p_s(T,t)$$

If $t \rightarrow \infty$ then the value of p necessarily reaches equilibrium, meaning full structural relaxation has taken place. This allows the definition of the equilibrium property after infinite relaxation time in Equation 10.

Equation 10

$$p_{eq}(T) = p_v(T) + p_{eqs}(T)$$

Substituting Equation 9 and Equation 10 into Equation 5 and reducing we get Equation 11.

Equation 11

$$\frac{dp_s(T,t)}{dt} = \frac{p_{eqs}(T) - p_s(T,t)}{\tau}$$

Then combining that with Equation 8 and understanding that the expansion due to structural relaxation is the difference between the structural change of the property and the equilibrium value of the property, finally nets Tool's equation, Equation 12.

Equation 12

$$\frac{dT_f}{dt} = \frac{T_f}{\tau}$$

This expression of Tool's which seeks to define the change in fictive temperature (T_f) with time during relaxation is the basis of the TNM model. The expressions in Equation 12 have all been thoroughly defined, with the exception of τ. In order to accurately define τ, Tool looked towards a relationship between viscosity and relaxation time. As a way of getting from viscosity to relaxation time, Tool used the well-known

equation $\eta = G * \tau$, where G is the shear modulus of the glass and η is the viscosity.[69] Tool surmised that in a small range of viscosity and temperature, the viscosity would have some exponential relation to temperature. After a failed first attempt, he included a fictive temperature dependence in his expression. Equation 13 showcases his description of viscosity, where η_0, A_1, and A_2 are constants; this leads to Equation 14, where K is the bulk modulus ($= \frac{1}{G}$) and τ_0 is a constant, which is the description of τ that follows logically from that point.

Equation 13

$$\eta = \eta_0 e^{-(A_1 T + A_2 T_f)}$$

Equation 14

$$\tau = K\eta = K\eta_0 e^{-(A_1 T + A_2 T_f)} = \tau_0 e^{-(A_1 T + A_2 T_f)}$$

By substituting that τ into Tools original equation (Equation 12), the result is Equation 15.

Equation 15

$$\frac{dT_f}{dt} = \left(\frac{T_f - T}{\tau_0}\right) e^{(A_1 T + A_2 T_f)}$$

Upon further experimentation and study this expression of the relaxation time that Tool was derived was validated in certain cases. Initial studies seemed to back Tool's equation.[70] The break down in the equation came when Napolitano and Spinner as well as Ritland applied Tool's description to analysis of actual properties in an optical glass.

Their experiments described the evolution of the refractive index of a borosilicate glass after annealing, and the results showed that a single fictive temperature was not sufficient to describe the configurational relaxation behavior of the refractive index. [71,72] In essence the relaxation is more complex than a single exponential decay dependent on a single T_f or a single relaxation time. Napolitano and Macedo deduced that the relaxation of the refractive index should be described by a series of two exponentials which could accurately describe the data they obtained.[73] Their expression for the relaxation behavior of the refractive index as a function of time at a specific temperature in B_2O_3 glass while undergoing annealing is detailed in Equation 16, where *n* is the refractive index, and C_1 and C_2 are constants.

Equation 16

$$n(t) = n_{eq} + \frac{1}{2}\left(C_1 e^{-\frac{t}{\tau_1}} + C_2 e^{-\left(\frac{t}{\tau_2}\right)}\right)$$

The next major steps in the development of the TNM model came from the second gentleman after whom it is named, O.S. Narayanaswamy. His contribution to the theory is based on the idea of two isothermal conditions, one initial and one final. In this case you assumes a glassy system that is at a temperature T_1. As $t \rightarrow \infty$, $T_f \rightarrow T_1$. After the temperature has been held for a sufficient time, the system is at equilibrium meaning $T_1 = T_f$. Here, once equilibrium is reached at T_1 an "instantaneous", or nearly instantaneous temperature jump is made to a new temperature T_2 where it is held until equilibrium is reached, $T_f = T_2$. Figure 3.2 shows a representation of such a condition. From those

isothermal testing conditions the response of a property, referred to as M, of the system can be defined as shown in Equation 17.

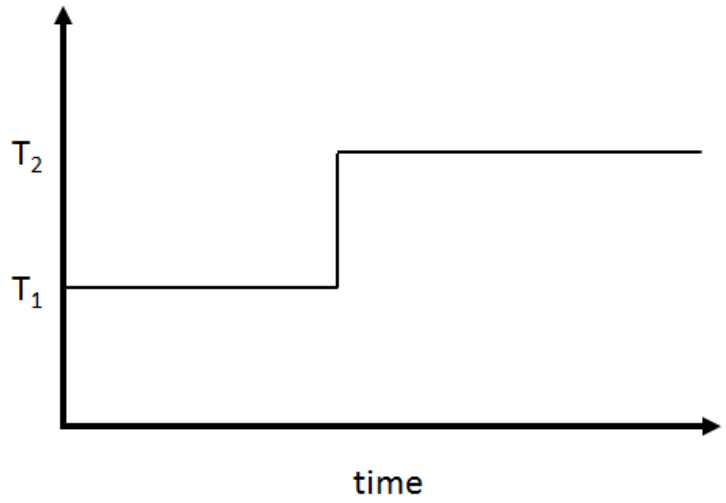

Figure 3.2: Depiction of isothermal structural relaxation, temperature versus time

Equation 17

$$M_p(t) = \frac{p(T_2, t) - p(T_2, \infty)}{p(T_2, 0) - p(T_2, \infty)}$$

Substituting Equation 9 into Equation 17 and adding the conditions t = 0, $T_f(0) = T_1$, and $T_f(\infty) = T_2$, simplies $M_p(t)$ to Equation 18.

Equation 18

$$M_p(t) = \frac{T_f(t) - T_2}{T_1 - T_2}$$

Narayanaswamy wanted to be able to write Equation 18 as a stretched exponential. The stretched exponential, or Kohlrausch-Williams-Watts (KWW) function is shown in Equation 19 as it would look for a property, *M*, where β is known as the stretching parameter.

Equation 19

$$M_p(t) = e^{-\left(\frac{t}{\tau}\right)^{\beta}}$$

When $\beta = 1$, the expression in Equation 19 is a single exponential; when $\beta < 1$, the exponential is called "stretched". Another way to model the same effect is to substitute a Prony series for the stretched exponential. A Prony series is a series of weighted exponentials as shown in Equation 20, it is capable of approximating a stretched exponential.

Equation 20

$$M_p = \sum_{n=1}^{N} w_n e^{-\left(\frac{t}{\tau_n}\right)}$$

In order to write M_p as a function of a stretched exponential, Narayanaswamy invoked the idea of thermorheological simplicity (TRS).[74] Understanding TRS is key to understanding the solution Narayanaswamy arrived at to describe relaxation in glasses. TRS assumes that the relaxation times that describe the property response, M_p, have the same temperature dependence. That is to say the relaxation response of each relaxation time is simply shifted in time but not different in the character of relaxation. Once this

assumption is made then all of the several relaxation times that are supposed to make up the system can be related to one another by a factor λ_n. If the only difference in the τ values that comprise a relaxation event is their position in time, then by considering a shifting factor they can all be made to overlap in a master curve. The first step towards this is a definition of the relaxation times as simply shifted in time from one another but leading to no difference in the shape of relaxation behavior at a given temperature. Equation 21 shows the simple way the relaxation times that follow TRS can be described, given that they differ from one another by some constant λ_n.

Equation 21

$$\tau_n = \frac{\tau}{\lambda_n}$$

Adding the scaling nature of τ set up in Equation 21 to the Prony series representation in Equation 20, and adding the expression $\beta \equiv \frac{t}{\tau}$ yields Equation 22.

Equation 22

$$M_p = \sum_{n=1}^{N} w_n e^{-\lambda_n \beta}$$

At this point the behavior of the system in which TRS is valid is only a function of the ratio β. So the response of the system plotted versus β should be the same for all temperatures as Figure 3.3 demonstrates.

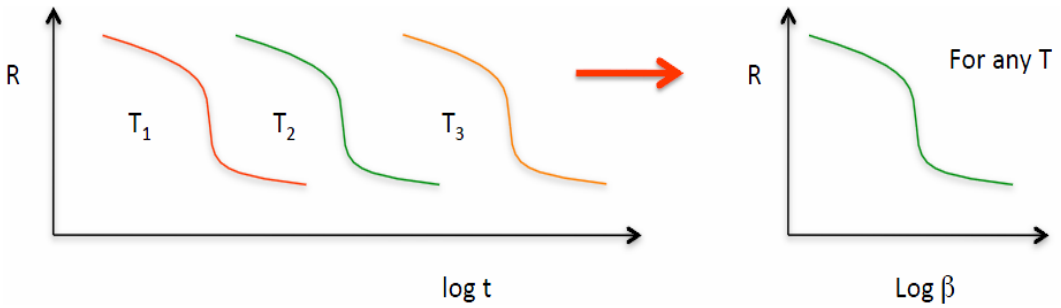

Figure 3.3: Example of the response of a system that obeys TRS, a plot of response versus β can be used as a master curve [75]

The final step is to convert the idea of a master curve into a mathematical entity. Narayanaswamy defined a reference temperature, T_r, and a corresponding time parameter at this temperature known as the reduced time (ξ). This reduced time can be related to relaxation time at any temperature by the expression $\beta = \frac{\xi}{\tau_r} = \frac{t}{\tau}$. If a system is said to relax at temperature T, in time t, then the amount of time it would take to relax that amount at T_r, is ξ, the reduced time. Equation 23 shows the expression Narayanaswamy chose for reduced time.

Equation 23

$$\xi = \tau_r \int_0^t \frac{dt'}{\tau_p[T(t')]}$$

Thus, the response of the system can be written as a function of reduced time and scaling factor now fully incorporating TRS behavior (Equation 24).

Equation 24

$$M_p(\xi) = \sum_{n=1}^{N} w_n e^{-\lambda_n \frac{\xi}{\tau_r}}$$

Now that the reduced time and exponentiality of M_p has been established, reduced time must be incorporated into the fictive temperature expression of the property response for M_p as well as $p(T,t)$. Equation 25 is the manifestation of Equation 18 with the substitution of reduced time ξ, for a temperature step experiment.

Equation 25

$$M_p(\xi) = \frac{T_f(\xi) - T_2}{T_1 - T_2}$$

Equation 25 is solved for $T_f(\xi)$, being sure to include the integration of M_p from 0 → ∞, and Narayanaswamy's contribution to the calculation of fictive temperature is revealed (Equation 26).

Equation 26

$$T_f = T - \int_0^{\xi} M_p(\xi - \xi') \frac{dT}{d\xi'} d\xi'$$

At this point in the derivation, if you supposed that M_p is a single exponential then Equation 26 reduces to Tool's equation (Equation 12) in terms of ξ. Then Equation 9 must also be expressed in terms of reduced time. This accomplished in much the same way, with the substitution and integration of M_p from 0 → ∞. Once this equation is solved, Equation 27 results.

Equation 27

$$p(T,\xi) = p(T,\infty) - \int_0^{\xi} \alpha_s M_p(\xi - \xi') \frac{dT}{d\xi'} d\xi'$$

An exponential form of M_p contains a relaxation time which is depicted as the reference relaxation time, τ_r, in Equation 24, but can be stated in a more general form as the relaxation time of a given property, τ_p. Narayanaswamy defined τ_p as a function of some material properties and a number of other fitting variables, although some authors consider even the fitting parameters material properties. The expression for the relaxation time of a property and the last major mathematical foundation piece of the TNM model is shown in Equation 28, where τ_0 is a fitting parameter, x is a non-linearity parameter, ΔH is the change in enthalpy during the change in temperature, and R is the ideal gas constant.

Equation 28

$$\tau_p = \tau_0 exp\left[\frac{\mathrm{x}\Delta\mathrm{H}}{RT} + \frac{(1-x)\Delta H}{RT_f}\right]$$

With the definition of an appropriate relaxation time, the suite of TNM equations is complete. Equation 26, Equation 27, and Equation 28 are the three TNM equations. The acronym TNM stands for Tool-Narayanaswamy-Moynihan. The "TN" contribution to the TNM model is nearly complete, they involve the theory and mathematics of modeling relaxation behaviors based on the knowledge of four basic parameters. Moynihan provided an experimental analogue with which to check the validity of the "TN" model which was soon to include his name.

The practical use of the TNM model begins with the three equations demonstrated above and a few assumptions. First, an equation must be assumed to describe the relaxation response of a given property. Equation 19, the KWW or "stretched exponential equation was introduced as a commonly accepted model, and has been verified on various material properties.[76-78] The KWW equation is assumed to accurately represent the evolution of some intrinsic material property. The result of this assumption is that M_p is defined in the form of Equation 19, with a dependence on the reduced time, ξ as outlined by Equation 26, the assumed property evolution is detailed in Equation 29.

Equation 29

$$M_p(\xi - \xi') = e^{-\left(\frac{\xi - \xi'}{\tau_r}\right)^{\beta}}$$

The next step is to find an expression for ξ-ξ'. The reduced time, defined in Equation 23, minus the derivative of the reduced time and rewritten to include heating and cooling rate dependence, simplifies to Equation 30, where $q = \frac{dT}{dt}$ is the quench rate.

Equation 30

$$\xi - \xi' = \tau_r \int_{T'}^{T} \frac{dT''}{q\tau_p(T'')}$$

Equation 26 must now be simplified to be solvable. The expression for T_f can be broken up into 'N' sections, so that Equation 31 results.

Equation 31

$$T = T_0 + \sum_{i=1}^{N} \Delta T_i$$

As Equation 32 shows, this operation removes reduced time from the integral in Equation 26, while keeping the dependence on reduced time of M_p.

Equation 32

$$T_f = T - \int_{T_0}^{T} M_p(\xi - \xi')dT$$

Then, M_p is substituted into Equation 32, and $(\xi\text{-}\xi')$ from Equation 30 is substituted into M_p. The integral from $T_0 \rightarrow T$ can be expressed as a summation and the expression for T_f takes the form of Equation 30.

Equation 33

$$T_f = T - \sum_{i=1}^{N} \Delta T_i exp\left[-\left(\int_{T'}^{T} \frac{dT''}{q\tau_p(T'')}\right)^{\beta}\right]$$

The final expression of T_f is found by converting the integral within the exponential using the summation expression for temperature. The result is, Equation 34, to be numerically solved to obtain the fictive temperature after a change in temperature over a period of time.

Equation 34

$$T_f = T - \sum_{i=1}^{N} \Delta T_i exp\left[-\left(\sum_{j=1}^{N} \frac{\Delta T_j}{q_j \tau_{p_j}}\right)^{\beta}\right]$$

The final piece of the puzzle is taking the expression for τ_p from Equation 28, and removing the fictive temperature dependence of the current step. That is to say that in Equation 28, the temperature and fictive temperature can equivalently be referred to as T_j and $T_{f,j}$. The solution is to make the fictive temperature term in that equation refer to the fictive temperature from the previous step (*j-1*). If that is done, Equation 28 takes the new form of Equation 35.

Equation 35

$$\tau_{p_j} = \tau_0 exp\left[\frac{\mathrm{x}\Delta\mathrm{H}}{RT_j} + \frac{(1-x)\Delta H}{RT_{f_{j-1}}}\right]$$

The fictive temperature dependence is now tied to the fictive temperature of the previous step. This works well for two reasons: (1) the intial condition of T_f at $t = 0$ is known and (2) if the steps used are small enough, the assumption does not have a negative effect on the outcome. The final step to doing a calculation is to use Equation 34 and numerically solve it, iterating until a solution for T_f is reached at a desired time. While this discussion has reviewed the theoretical side of the TNM model, for the experimental validation, data collected by DSC is necessary. The following section defines this portion of the analysis.

2.1.1 TNM by DSC

The TNM equations were developed over a couple of decades and were refined and updated as new experimental methods and data became available. Moynihan recognized the need for an experimental link between what was at the time the TN model and measurable, experimentally repeatable material data.[79] The link between experimental data and the TNM model is the expression found in Equation 36.

Equation 36

$$\frac{dT_f}{dT} = \frac{dT_f}{dt}\frac{dt}{dT} = \frac{1}{q(t)}\frac{dT_f}{dt}$$

The left side of Equation 36, is the quantity that can be measured via DSC, while the right side can be calculated using the TNM model, where *q(t)* is the cooling or heating rate of the glass.[80] In order to obtain the fictive temperature dependence on the temperature of relaxation, a link must be made between that quantity and measureable values in the DSC. This link begins with a first principles look at enthalpy in a system analogous to the one described in the last section (i.e. $T_0 < T_f$). The core equations are layed out in Equation 37 and Equation 38.

Equation 37

$$H(t) = H_{eq}(T_f) - \int_{T}^{T_f} C_{P,g}\, dT'$$

Equation 38

$$H(T) = H_{eq}(T_0) + \int_{T_0}^{T} C_P dT'$$

The two equations above, define the temperature-dependent enthalpy change. For Equation 37, starting with the enthalpy of the system at T_f, remember $T < T_f$, the change in enthalpy is represented by the area under the heat capacity curve of the glass from the current system temperature to the fictive temperature. The equilibrium enthalpy at the fictive temperature minus that change in $C_{P,g}$, defines the current enthalpy at temperature T. Equation 38 deals with the enthalpy-space from the initial temperature to the current temperature. It follows the same concept just from the other side, simply adding the area under the C_P curve to the equilibrium value at $H(T_0)$. The final term to define before starting the mathematical operations is H_{eq}, Equation 39 defines the path from enthalpy at the initial temperature to enthalpy at the fictive temperature.

Equation 39

$$H_{eq}(T_f) = H_{eq}(T_0) + \int_{T_0}^{T_f} C_{P.L} dT'$$

Setting Equation 37 equal to Equation 38 and substituting in Equation 39 then simplifying yields Equation 40.

Equation 40

$$\int_{T_0}^{T} C_P dT' = \int_{T_0}^{T_f} C_{P,L} dT' - \int_{T}^{T_f} C_{P,g} dT'$$

Subtracting $\int_{T_0}^{T} C_{p,g} dT'$ from both sides and splitting that integral on the right side yields Equation 41.

Equation 41

$$\int_{T_0}^{T} (C_P - C_{P,g}) dT' = \int_{T_0}^{T_f} (C_{P,L} - C_{P,g}) dT'$$

The left side is obtained by a simple combination of the integrals, while the right side is obtained by splitting the $\int_{T_0}^{T} C_{p,g} dT'$ term that was added. This is done by understanding that Equation 42 is valid, using the integral from T_0 to T_f minus the same integral from T_f to T, then taking the negative of that integral to cancel the right-most term in Equation 40.

Equation 42

$$\int_{T_0}^{T} C_{P,g} dT' = -\int_{T_0}^{T_f} C_{Pg} dT' - \int_{T_f}^{T} C_{P,g} dT' \text{ and } -\int_{T_f}^{T} C_{Pg} dT' = \int_{T}^{T_f} C_{P,g} dT'$$

One last step is necessary, that is, to use the fundamental theorem of calculus to extract fictive temperature from the expression. First the chain rule must be used on the composite functions in Equation 41, then the fundamental theorem must be applied to achieve Equation 43.

Equation 43

$$\left[C_P(T) - C_{P,g}(T)\right] = \left[C_{P,L}(T_f) - C_{P,g}(T_f)\right] \frac{dT_f}{dT}$$

This expression can then be solved for the fictive temperature term as in Equation 44.

Equation 44

$$\frac{dT_f}{dT} = \frac{\left[C_P(T) - C_{P,g}(T)\right]}{\left[C_{P,L}(T_f) - C_{P,g}(T_f)\right]}$$

The goal of representing the left side of Equation 36 in terms of measurable DSC parameters has been achieved. All of the terms on the right side of Equation 44 are measurable by DSC. Figure 3.4 shows an example heat capacity plot, with the important terms marked.

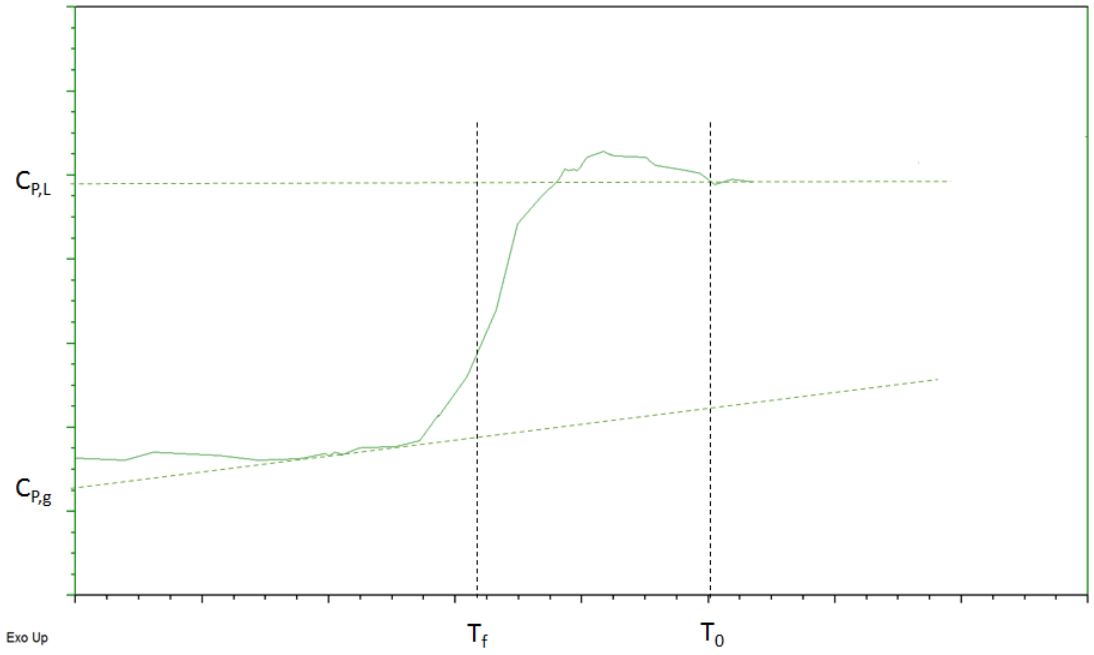

Figure 3.4: Example C_P curve showing measurement of heat capacities for TNM validation

The numerator of Equation 44 is obtained by taking the area between the C_P curve and the line representing the temperature dependent glassy heat capacity, $C_{P,g}$, this corresponds to the integral on the left side of Equation 41. The denominator is determined by taking the area of the trapezoid formed by the temperature limits, T_f and T_0, and then

the glassy and liquid heat capacity lines representing the contribution of $C_{P,L}$ and $C_{P,g}$ to the overall heat capacity change in the system. Knowing these values gives an expression for $\frac{dT_f}{T}$ which when substituted into Equation 36, is equated to the result of the TNM equations for a given glass. The result of Moynihan's work allows unknown parameters of the TNM model to be experimentally determined and applied to the broader model which can then be used in predicting fictive temperature and property change in a glassy material.[81]

2.1.2 TNM by dilatometry

The TNM suite of equations are typically applied to relaxations measured by DSC however, there a small number of instances of the TNM model's which employ dilatometry. The first was a study on As_2S_3 glass which is an analogue to the As_2Se_3 glass used in this dissertation. That study used the TNM equations to fit experimental data. [20] Additionally the author, Jiri Malek, used some facets of the dilatometric data that was gathered to infer the constant value of at least one of the fitting parameters, ΔH sometimes also labeled as Δh^*, which denotes it as the "apparent activation energy". The nature of the study done by Malek is similar in some senses to the study done for this dissertation as Chapter 4 Section 3.1 will detail. The main difficulty found in using the TNM model in this way is that it remains simply a set of four, or in Malek's case, three fitting parameters that are matched to the data. These parameters are embedded in a model that was mathematically derived from a reasonable physical understanding, however that does not ensure the physical meaning of these parameters.

A further study of amorphous selenium (α-Se), showed that the TNM parameters, most notably β and x from Equation 35, varied between measurements of heat capacity via DSC and volume change via dilatometry.[82] This carries two important conclusions both of which can be true at the same time (1) volumetric relaxation and enthalpy relaxation do not necessarily have the same behavior at a given time and temperature of relaxation, and (2) TNM parameters, which rely on fitting experimental data, do not universally describe relaxations even within the same material. It is important to remember that models are just that, models; they are filled with assumptions and suppositions. The treating of models as scientific fact is a major cause of scientific uncertainty and error. Models are absolutely useful and necessary, but the model must never be treated as if it is the actual end-all description of the material system. Models are only a tool to be used for a better understanding of the material not a substitute for experimental data.

3 Structural Relaxation Theory

Theories attempting to explain structural relaxation or the results of relaxation have abounded since the beginning of glass science. The effort to classify the glass transition as a true transition has relied on structural relaxation experiments to provide evidence for or against the many theories that have been posited over the years. This section details some of the main theories endeavoring to describe the glass transition and in doing so shedding light on how glasses react. In order to discuss topics like the “zero-point entropy” of glass or the issue of some models showing residual entropy at absolute zero, it is necessary to analyze how

the excess entropy and other properties change to bring the glass to those disputed temperatures and behaviors.

3.1 The Kauzmann Paradox

A defining discussion point in glass science is the nature of structural relaxation, naturally this leads to discussions of the limits of relaxations. If relaxations become longer and longer processes at what point do they cease or is there a limit to the allowable configurations in which to relax at some point. One point of theory at which to look for answers to these questions is the Kauzmann Paradox. The idea of the Kauzmann Paradox was put forward by Walter Kauzmann in 1948.[4] The evolution of certain thermodynamic properties such as entropy where predicted at lower temperatures by measuring them in the glass transition region (Figure 3.5).

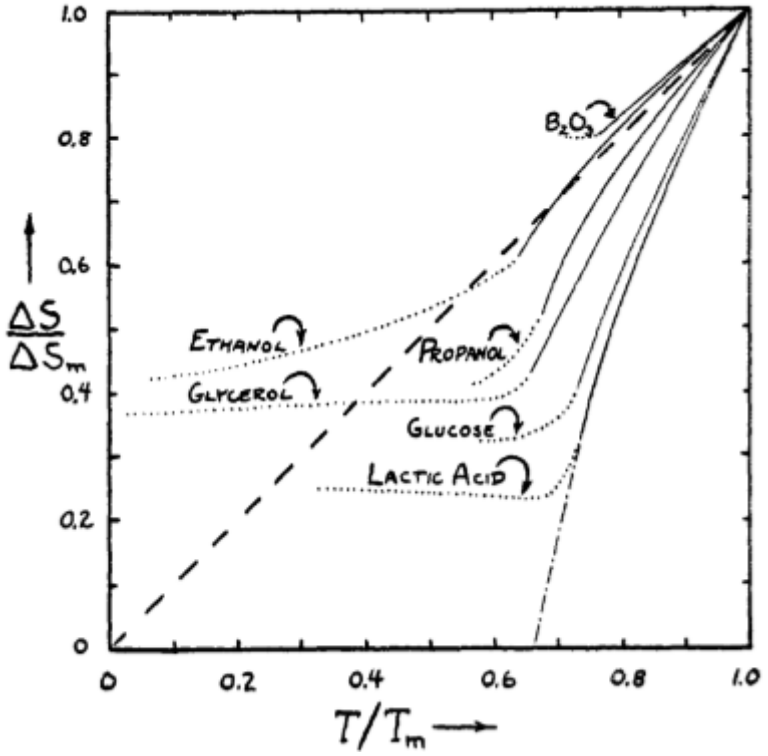

Figure 3.5: Kauzmann paradox, the liquidus lines of each material extrapolate to negative entropy.[4]

This caused problems resulting from the fact that the so called “excess entropy” that glass has over the crystalline phase would, as predicted from the higher temperature extrapolations, continuously cross over the crystalline equilibrium. If this phenomenon occurred it would mean that at a certain temperature the glassy “phase” or more correctly the glassy state of the material would be entropically favorable over the crystalline arrangement of atoms. This was of course a paradox and was named after Kauzmann for his description of it. The necessity of considering an entropy issue for volume relaxation is important. The work done in this dissertation concerns the configurational change in volume of a glass between two thermodynamic states. A change in volume at constant

temperature, as these tests are isothermal, leads to a necessary change in entropy in most materials. In this way the two are linked.

Much work has been done in relation to Kauzmann's Paradox by later authors to address this question of a paradox.[83] Kauzmann himself theorized that the paradox was prevented or resolved due to the interaction of two energy barriers in the material. The first was an energy barrier between the equilibrium liquid and the crystalline state which kept the liquid from crystallizing. The second was the energy barrier that prevented rearrangement in the glass between the metastable solid and the equilibrium liquid. He theorized that when approaching the "Kauzmann Temperature" (T_K) those two barriers would approach the same height and the glass would crystallize just at the Kauzmann temperature. Mauro et. al. claimed that Kauzmann's explanation was unnecessary because it made the mistake of assuming that the entropic properties of the glass can be extrapolated from above T_g which they claim was not the case.[84] Adam, Gibbs and DiMarzio made further arguments that acknowledge the usefulness of a Kauzmann temperature but find different resolutions to the paradox.[1,9] Still others have done simulations to prove that a glass with the same enthalpy as the equilibrium liquid cannot possible have an entropy lower than the crystal.[85] Hence, the debate remains unresolved.

3.2 Gibbs-DiMarzio and Adam-Gibbs Cooperatively Rearranging Regions

The Kauzmann Paradox was further pursued by Gibbs and DiMarzio, who substituted a temperature denoted T_2 in place of T_K.[9] In pursuing the idea that a paradox was unacceptable, they developed a theory that suggested that T_2 was T_g when the system

was given an infinitely long time to relax. This then allowed for the prediction of a true thermodynamic phase transformation at T_2. According to their theory they believed that either T_g was the experimental T_2 given a very long time for relaxation, or the values of T_g and T_2 where strongly linked to one another. Bestul and Chang took this concept and did rigorous and detailed experiments on the values of T_g and T_2 for a large number of glass forming liquids.[86] Using parameters from the Williams-Landel-Ferry (WLF) equation and an entropy based modification of them done by Goldstein, they calculated the excess entropy at T_g for 40 substances, all glass formers.[87] Upon doing these calculations they came to the realization that for their vast sampling of glass forming liquids the T_g/T_2 value was between 1.14 and 1.53 for all of them. They also recorded the difference between T_2 and T_g in all cases. In addition, they found that the glass transition of most of the materials they measured occurred when the excess entropy of the system dropped to ~ 0.7 calories per "bead". A bead was their term for a polymer chain or one unit of a polymer. This data was quickly used by Adam and Gibbs to bolster their theory of the glass transition as definitively tied to T_2 which they claimed was a true thermodynamic transition.

Adam and Gibbs further used this result in the development of their own theory for resolution of the Kauzmann Paradox. Their description of the glass was based on the fact that it had an excess of entropy at the glass transition and reduced to no excess entropy at T_2. The entropic based approach they took stated that as the entropy in a system decreased so did the number of possible configurations the glass could be in. As the excess entropy decreased to essentially zero the glass would eventually be constrained to one discrete configuration and would not reach the Kauzmann Paradox.

Adam and Gibbs built off of this theory to develop the theory of Cooperatively Rearranging Regions (CRR). This theory stated that as entropy decreased with temperature, and the number of available configurations was reduced, the nature of structural relaxation would have to be much more long range and therefore take longer times. As the temperature decreased below T_g, one atom or structure could no longer move independent of the rest, at the extreme case of being just above T_2, if one atom wanted to change configuration, essentially the entire piece of material would have to change configuration to accommodate it because of the very low entropy and lack of configurations available.

3.3 Energy Landscape Theory

The energy landscape theory (ELT) is a theory based on considering the positions of atoms and their interactions in the view of being on a "potential energy hypersurface". This surface is defined by potential energy wells in which atoms prefer to sit at the lowest possible energies. The arrangement of these energy wells defined the spacing of the atoms and the configuration of the glass. It is important to note that when the system in question is constant volume the hypersurface is an energy landscape, however when the volume is changing, as in most experiments, it is more correctly an enthalpy landscape. The two behave similarly and can be talked about with essentially no distinction; energy is most commonly used. Major work has been done on the initial definition of ELT by Stillinger who used models of slightly super cooled systems to observe that atoms spent more time in certain low energy zones until they obtained enough energy to "hop" out and reach a more preferred, lower energy configuration.[2] The landscape is made up of energy wells

separated by “ridges” and “saddle” states. Ridges are sharp transitions between wells while saddles provide lower energy transitions from well to well or serve as local energy minima depending on their curvature. Figure 3.6 shows a visualization of a potential energy landscape and the major components that factor into configuration change from basin to basin.

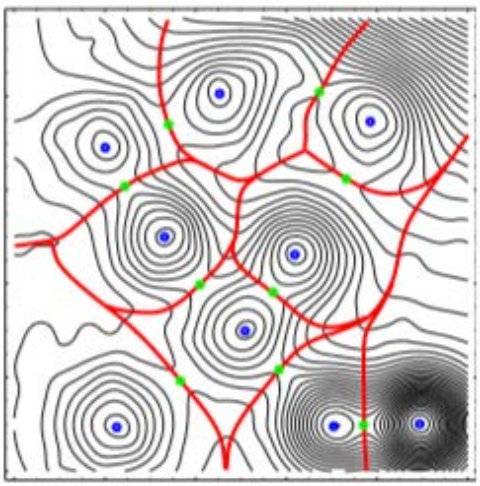

Figure 3.6: Potential energy landscape, blue dots are inherent structures, red lines are ridges, and green dots are first order saddle transition [88]

The ELT contains important concepts for the interpretation of experimental results regarding configurational change in glasses. The first is the concept of an ergodic system at temperatures above the percolation temperature transition temperature (T^*). The idea of percolation in glasses near the transition temperature is explained by Carmi as the disappearance of pathways or saddles for atoms to reach a different configuration as temperature decreases below T^*.[3] At higher temperatures ($T>T^*$), according to the percolation view in ELT, the glass is capable

of sampling essentially all nearby configurations and behaves ergodically. However, when the temperature is dropped below the percolation temperature, links between certain basins are removed which leads to regions that have intrabasin movements within them but cannot move outside of their region. Those regions are called metabasins (MB) and lead to broken-ergodic systems. In the temperature regime where MBs appear, relaxations and change in configuration can occur within different MB's leading to multicomponent relaxation. This concept will be important later in this dissertation.

Using the idea of MBs as a basis for expanding the ELT into a description of relaxations, it is theorized that primary relaxations, known as α-relaxations, are due to interMB transitions while secondary, β-relaxations are due to intraMB transitions.[89] These relaxations are often approximated by the KWW function and the relaxation times for interMB relaxations can be approximated by Equation 45, where S_{conf} is the configurational entropy, ν is the attempt frequency, *k* is the Boltzmann constant, *T* is temperature in Kelvin, and *B* is the barrier energy.

Equation 45

$$\tau_\alpha(T, T_g) = \nu^{-1} exp\left[\frac{S_{conf}(T_g)}{k}\right] exp\left[\frac{B(T_g)}{kT}\right]$$

ELT is the most modern, recent product of the desire to understand the glass transition temperature and the phenomena that occur near to and because of it. This includes structural relaxation; the idea of an energy landscape will be raised in the next chapter of this dissertation.

CHAPTER 4

VOLUMETRIC STRUCTURAL RELAXATION MEASUREMENT AND MODELING

1 Introduction

Volumetric structural relaxation data is essential for understanding annealing behavior of optical components. This same annealing behavior effects thermal forming processes such as PGM, for glasses during cooling. Infrared glasses such as those in the Ge-As-Se system demonstrate larger changes in volume during cooling than most common oxide glasses like N-BK7. This dramatic change in volume and shape during cooling or post process annealing leads to changes in optical properties.[90] There is no way to anneal glass in ambient conditions and not change the volume, however if volume relaxation is understood, its effect can be taken into account during the design of the PGM mold tooling. The alternative to annealing the glass is leaving the structural stresses in the optic after processing. This can have a number of adverse effects, for one, the stress left in the glass can increase the probability of cracks forming in the optic. Additionally, stress effects the optical properties like refractive index, changing the intended optical behavior of the final part. Although stress effects do not always cause unacceptable optical changes in a molded optic, it is useful to understand how far out of equilibrium the material is as a way of estimating the stress within the optic.

2 Summary of material systems

2.1 N-BK7

The N-BK7 samples used in this study were received from Schott North America in the form of 3 x 3 mm cross section beams of approximately 100 mm length. The beams were cut down to 12 mm in length and then fine ground on both ends to enable vertical free standing. Characterization of N-BK7 thermal properties was done in the same way as characterization of the Ge-As-Se glasses. In addition energy dispersive x-ray spectroscopy (EDS) was done on N-BK7 in order to assess its basic constituent elements. The results of the EDS analysis showed a glass containing large amounts of both silicon and boron along with oxygen. In this glass system, boron and silicon are the network formers. Also present in the system are small amounts ($\leq$ 5 atomic %) of sodium, potassium, and barium. These constituents are known as network modifiers in glass science.[91] A network of boron and silicon oxide forms a network in which each network former has all free bonds taken up by oxygen and each oxygen would have every bond taken up by a network former. The addition of network modifiers serve to create non-bridging oxygen (NBOs) in the glass network. NBOs occupy free volume in the network, and these positively charged species create a charge imbalance which forces an oxygen to only bond to one network former. The negative charge associated with the oxygen balances out the charge of the anion and is called non-bridging because it does not covalently bond into the network. This has the effect of weakening the structure, lowering connectivity, and dimensionality as well as most thermal properties. The inclusion of small amounts of alkali in the melt drastically

reduced the melting temperature and T_g of the glass system and inhibit crystallization by clogging diffusion pathways in the glass network.

2.2 Ge-As-Se System

The infrared materials used for the work in this dissertation were synthesized, fabricated, and characterized according to Chapter 2. The structural nature of these glasses was discussed in detail in Chapter II, Section 2.

3 Experimental procedure

The development of experimental procedures and methods for characterizing structural relaxation was spawned by the need to understand the behavior of glasses during cooling and post process annealing in PGM. Following the lead of research done on structural relaxation by Scott Gaylord, N-BK7 was chosen as the proof-of-concept material for this development.[60,92,93]

3.1 Dilatometric experiments

The experimental procedure for the measurement of volumetric relaxation was the same for all of the chalcogenide compositions as well as N-BK7. The procedure was originally published in a paper this author wrote detailing the relaxation procedure which will be reiterated in this dissertation.[38]

As detailed previously, the samples for relaxation were fabricated to a 3 x 3 mm cross section and 12 mm height. They were then placed vertically in the TMA as shown in Figure 2.5. One of the keys to making any measurement of glass thermal, mechanical,

or optical properties is ensuring that the thermal history of the glass is known or can be determined. The term thermal history is a euphemism for the structure of the glass. However, since the structure of a certain glass composition is strongly dependent on the quench rate from liquid (see Figure 3.1) and any subsequent annealing times, the overall concept of the glass behavior being tied to its processing conditions is called the thermal history. Any measurements that are made, therefore, are dependent on the thermal history of the glass. In order to take measurements in a frame of reference that allows for a comparison of the results, the thermal history a.k.a. structure must be known. Rather than do experiments to determine the structure of each sample, the typical method is to heat each sample to a certain temperature, usually just above T_g. In the temperature range above T_g, the structure will reach equilibrium in a matter of minutes. This was done to all samples prior to the rest of the test. Each relaxation test began with a 5 °C/min ramp from room temperature to $T_{g,d}$ + 10 °C in order the set the thermal history of the glass. The temperature was then held at $T_{g,d}$ + 10 °C until volume equilibrium was reached (see Figure 4.1). The only runs that did not contain this step were runs with initial relaxation temperatures greater than $T_{g,d}$ + 10 °C.

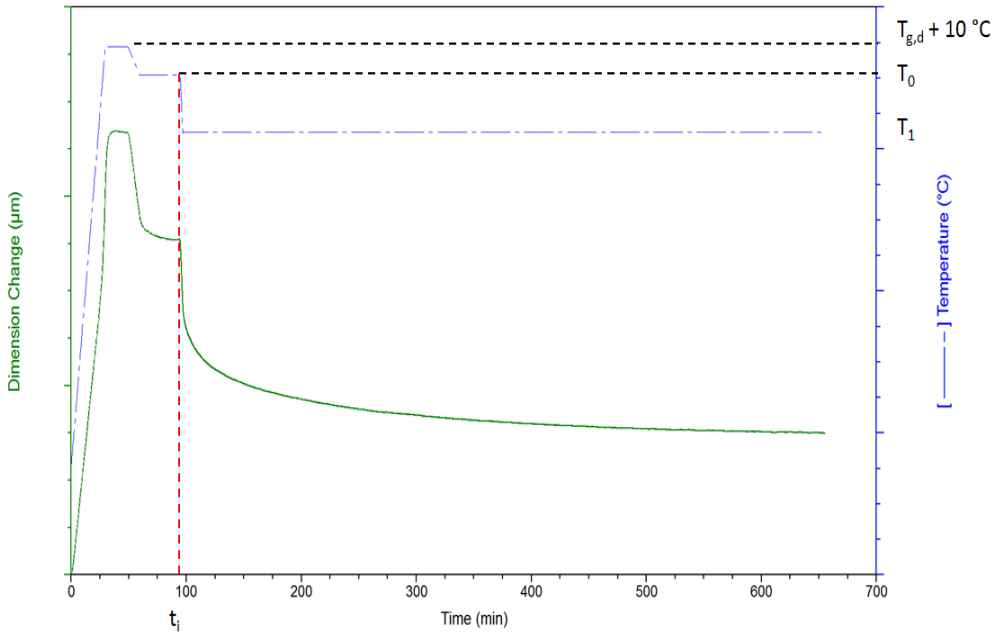

Figure 4.1: Example plot of temperature and dimension change versus time for a TMA relaxation experiment; the green curve (solid line) is dimension change and the blue curve (dashed line) is temperature

After thermal and structural equilibration, the temperature was ramped down at 1 °C/min to the initial testing temperature, T_0 ($T_{g,d}$ + 10 °C > T_0 for most cases). The samples were then held at T_0 until structural equilibrium was reached. For purposes of this dissertation, structural equilibrium as measured by TMA was defined as the length vs time plot reaching a linear, constant slope behavior. Once equilibrium was reached the temperature was ramped down as fast as possible (~10 °C/min) to the final testing temperature, T_1. Figure 4.1 is a representative plot of the temperature regime as well as the reaction of glass height to the temperature protocol described. The temperature jump, $\Delta T = T_0 - T_1$, was varied in these experiments. In the case of the N-BK7 proof of concept, ΔT = 10 °C. For the As-Se and Ge-As-Se compositions ΔT = 5, 10, 20, and 30

°C. The system is held at T_1 until structural equilibrium is reached. The data acquired during these runs was then processed and analyzed using MATLAB and a method developed by the author.

3.2 Data analysis

Analysis of experimental data is just as important as gathering that data. Not all of the data gathered from an experiment is scientifically relevant and even less is purely tied to the phenomenon being studied. The analysis for this length/volumetric relaxation data involves several steps. First the data which relates to configurational structural relaxation must be parsed from data that does not relate. Then effects from experimental parameters must be removed as much as possible leaving only the data related to the phenomenon in question. Once the data has been properly processed it can then be fitted and described mathematically.

3.2.1 Data processing

The first step in processing the data collected from the TMA experiments described in the previous section, is to remove the irrelevant ramp up and equilibration sections that do not pertain to structural relaxation. The phenomenon in question occurs from the initiation of the temperature down step from $T_0 \rightarrow T_1$. The time at which the temperature down step is initiated by the program was called t_i. The data from t_i to the end time of the test, (t_{end}), was extracted from the whole, a representation of this relaxation data can be seen in Figure 4.2.

Following this major parsing of data, the phenomena occurring during the temperature down step and subsequent isothermal hold was evaluated. It is known that in the glass transition region, and even far below it in the case of chalcogenides, the physical response of the glass to temperature change can be described by Equation 46.[94]

Equation 46

$$\Delta property = vibrational\ component * \Delta T + configurational\ component * \Delta T_f$$

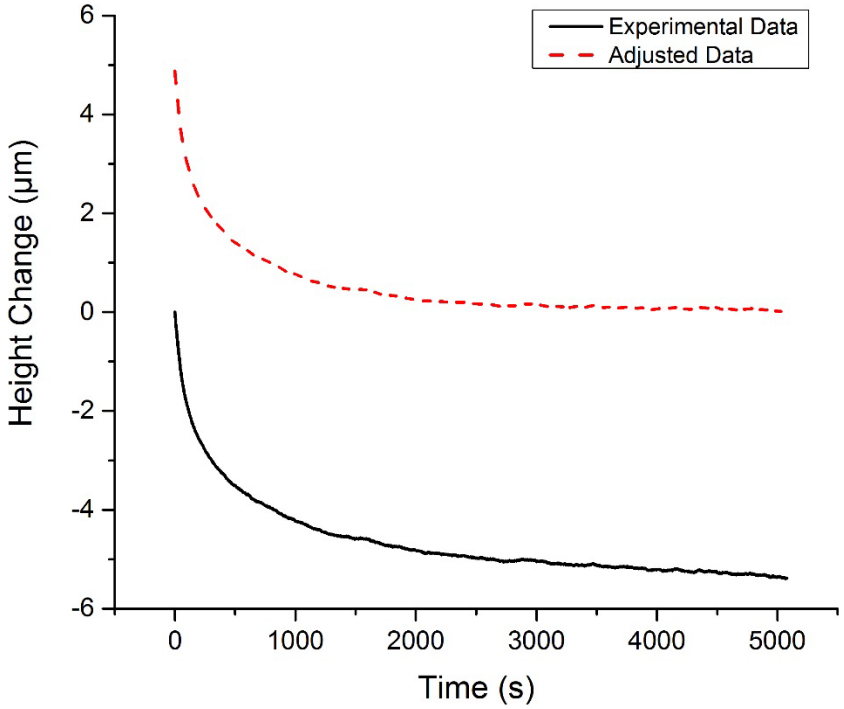

Figure 4.2: Experimental relaxation data and adjusted relaxation data, in a plot of height change versus time

The first order of business was to remove the vibrational component of the length/volume change. There were two options for doing this, the first was to create a function dependent on the CTE and use it to remove the effects of CTE on each data point. This would be done as follows: the data points within the time envelope from the initiation

of the temperature jump t_i, to the time at which the sample reached an isothermal state, t_0, would all be shifted according to Equation 47, where q is the "quench rate" or ramp rate of the temperature transition from $T_0 \rightarrow T_1$, and L_{intial} is the length of the sample at $t = 0$.

Equation 47

$$\Delta l_{vib}(t) = \alpha_{vib}[q * (t - t_i)] * L_{initial}$$

The data between t_i and t_0 would have the change in length due to CTE removed by Equation 47, additionally, the data from $t_0 \rightarrow t_{end}$ would be shifted by the full contraction or expansion amount defined by Equation 47 if $t = t_0$. However, this method of removing the CTE effects was not chosen, because $(t_0 - t_i) << (t_{end} - t_0)$. Rather than risk the assumption of q as being linear and possible unintended effects on the short time part of the relaxation behavior, a second option was preferred.

The second option was to calculate or model the precise value of $(t_0 - t_i)$ and shift the data to remove that value, making $t_0 = 0$. This option was chosen due to the fact that the time taken to reach isothermal is small compared to the time for the entire test. A simple thermal finite element model (FEM) was created to simulate the time taken for the center of the relaxation sample to reach the isothermal temperature at T_1. COMSOL Multiphysics was used to create a 2-D axisymmetric model using convection boundary conditions. This model was run, for each experiment, using the T_0 and T_1 values specific to that experiment as well as the heat capacity, thermal conductivity, and dimension values specific to the sample in question. The temperature of the center of the sample was calculated by the model and the time taken for the sample to reach within 10% of T_1 was

calculated. The variable t_0 was set equal to that calculated time and the entire data set was shifted in time to make $t = 0$ the starting point of the data set. The center of the sample typically reached equilibrium within 30-90 seconds of t_i. Once the data that fell into the non-isothermal regime of the sample was removed, no CTE effect remained present in the data. These data operations were done within the MATLAB program written by the author with input and assistance from Dr. Vincent Blouin.

Equation 46 is true for the structural relaxation measurements done in this study, however it is incomplete given the experimental conditions in this test. In addition to configurational and vibrational changes in sample height, there is also a temperature dependent viscous component to the height change that is not directly related to the configurational change that was targeted for characterization.[95] At temperatures in and around the glass transition region, the glass will "slump" or viscously flow, over a given period of time, due to the force of gravity on the sample. This behavior is evident in Figure 4.1, as $t \rightarrow t_{end}$ the dimension change curve reaches a constant, negative linear slope. This is the same slope associated with the glass structure reaching equilibrium at a specific T_1. The constant slope exhibited by the height change property is not equal to zero. This means that there is a constant, linear decline in sample height at each discreet temperature for these glassy materials. This viscous flow is not related directly to the configurational component of interest.

Equation 46 can be abbreviated and rewritten as Equation 48, where α_g is the CTE of the glass, α_{config} is the height change component related to structural relaxation, α_{visc} is

the temperature dependent viscous height change component of the change in height, and $\Delta T_f = T_f - T_1$.

Equation 48

$$\frac{1}{3}\Delta V = \Delta l = L_{initial}[\alpha_g \Delta T + \alpha_{config}\Delta T_f + \alpha_{visc}(T_1)t]$$

The goal of this study is to capture only the configurational component of relaxation; therefore the effects of the vibrational and viscous material responses must be removed. Having described the removal of the vibrational component, it is necessary to detail the removal of the viscous component. To do this, the slope of the change in height versus time curve is taken after a time at which the sample reached structural equilibrium. This operation was done as follows: four times were picked by the program user, two near the beginning of the viscous linear section (t_{d1a} and t_{d1b}), and two near t_{end} (t_{d2a} and t_{d2b}). The midpoint of each pair of points was found by taking the mean of the points between t_{d1a} and t_{d1b} and the mean of the points between t_{d2a} and t_{d2b}. Those points ($mean(t_{d1})$ and $mean(t_{d2})$) were used in combination with the mean time calculated from the same points to calculate the slope of the viscous response of the sample as in Equation 49.

Equation 49

$$\alpha_{visc} = \frac{mean(t_{d2}) - mean(t_{d1})}{\frac{1}{2}[(t_{d2a} + t_{d2b}) - (t_{d1a} + t_{d1b})]}$$

This value was taken as the viscous component of length change during the experiment. The viscous component was then removed. Since the length change due to flow is time dependent, there is no change due to viscosity at t_0 and a maximum change at t_{end}, due to this the component of viscous flow can be removed by substituting the value calculated in Equation 49 into Equation 48. The effect is essentially a rotation about the point t_0 and the final result is an adjustment of the long time section that corresponds to structural equilibrium from a negative constant slope to a constant slope of zero. A representation of the change can be seen in Figure 4.2

Having removed all extraneous material responses from the data, only configurational length change remained. The relaxation curve was shifted so that the minimum was equal to zero for the sake of calculation simplification. The next step in the process was fitting the data.

3.2.1(a) Curve fitting

The date to be fit was normalized to the maximum length change in the data. This resulted in a relaxation curve beginning at a y-axis value of one, at t_0 and relaxing to zero at t_{end}. The equation used for the fit was a Prony series (Equation 20). In the context of the TNM model, it is an equation used to approximate the KWW function (Equation 19). However, the Prony series has two major advantages over the KWW function and hence was chosen as the model for this relaxation data. First the Prony series has the ability to define multiple distributions of relaxation times spread across varying magnitudes of time, while the KWW function can only define one distribution of relaxation times.[96] The

KWW function is known to fit relaxation data, with the caveat that the system it is describing be fairly close to equilibrium and experience a relatively small amount of overall relaxation. Second, the Prony series is mathematically simpler and easier to solve and manipulate. The Prony series is a mathematical solution to what is known as the Generalized Maxwell Model (GMM).

The rational for this method can be deduced from the original Maxwell model, and the Generalized Maxwell Model itself. A simple Maxwell element is pictured in Figure 4.3.

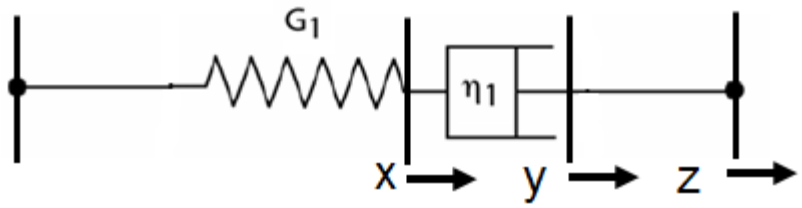

Figure 4.3: Mechanical representation of a single Maxwell element

The physical representation of a simple Maxwell element contains a spring and a damper in series. There are two modes in which this system can operate, one is constant strain mode where force exerted on the system remains constant and the displacements *x*, *y*, and *z* change to keep the system in equilibrium. The case that is of interest for this dissertation is the second case in which the total elongation of the system, *z*, is a constant value. In this second case the force on the system decays by some function which can be reached by solving the system mathematically. In the TMA experiments detailed in the section above, the "instantaneous", or fast change in temperature relative to the time of the test, is in effect an instantaneous change in thermodynamic properties. The property that

was specifically targeted in this research was volume or length. When the temperature is suddenly changed, the thermodynamic equilibrium volume or length of the sample is instantaneously changed. Related to the model, it is the equivalent of putting a constant displacement on the model pictured in Figure 4.3. For the simple Maxwell element, the force on each component is equal to the overall force on the system. So in this case $F_x=F_y=F_z$. The force for the spring is defined as Equation 50, where k is the spring constant in units of [force/distance].

Equation 50

$$F_x = k * x$$

Likewise, the force on the damper is expressed by Equation 51, where η is the viscosity of the fluid in the damper (not necessarily the material itself), A is the cross sectional area of the damper, and d is the diameter of the plunger inside the damper.

Equation 51

$$F_y = \eta \frac{A}{d} \frac{dy}{dt}$$

Due to the fixed elongation condition of this system in this case, the total change in displacement of x and y must be equal to zero as described in Equation 52.

Equation 52

$$\frac{dx}{dt} + \frac{dy}{dt} = 0$$

Then the derivative of Equation 50 with respect to time must be taken and $\frac{dx}{dt}$ solved for, then $\frac{dy}{dt}$ must be solved for in Equation 51 and both solutions must be plugged into Equation 52. The net result is Equation 53.

Equation 53

$$\frac{1}{k}\frac{dF_z}{dt} + \frac{d}{A}\frac{F_z}{\eta} = 0$$

Finally, in order to solve for F_z, the Laplace transform was taken, the equation solved and the inverse Laplace transform taken to achieve a solution in time domain, the result is Equation 54.

Equation 54

$$F_z(t) = C * e^{-t*\left[\frac{k*d}{\eta*A}\right]}$$

The expression in the exponential $\left[\frac{k*d}{\eta*A}\right]$ is the reciprocal of the relaxation time, τ. So an alternative way to write Equation 54 is shown in Equation 55.

Equation 55

$$F_z(t) = C * e^{-\frac{t}{\tau}}$$

Equation 55 is a single exponential describing the behavior of the force in the system during time, this value decays over time. The force is at a maximum at *t=0* and decreases in magnitude until the force reaches zero at some value of time. This is precisely the same behavior seen in the volume or height change of the glass sample during structural

relaxation. The length goes from a max value (normalized to 1) to a minimum value (normalized to 0). The change of thermodynamic state that is initiated by the change in temperature puts a nearly instantaneous force on the system due to the thermodynamic disequilibrium. The structure is under stress to change in some way to reduce this force, in the case of a temperature decrease, this force will cause a loss in height and volume. The closer to the equilibrium value of volume the sample goes, the lower the remaining force on the structure to relax. This also illustrates that larger ΔT values create larger forces and larger amounts of length and volume change in a given glass.

The simple Maxwell element description of the glass would be adequate if not for the fact that the majority of glassy materials are known to have more than one simple reaction to structural pressure, or "fictive pressure" as Gupta styles it.[97] There are multiple relaxation events that occur in a glass, all of which, when combined, make up the overall structural relaxation behavior. Though the simple Maxwell model can describe a single relaxation adequately, it cannot account for a relaxation process that may contain multiple relaxation times that vary significantly in magnitude. For a solution to this material problem, the GMM is appropriate. The GMM simply depicts a number of simple Maxwell elements in parallel. The force responses of these elements are additive. Therefore, the solution to a GMM that has been elongated or forced to contract, as in the simple Maxwell element example above, is simply a superposition of the solutions for a single element. The result is a Prony series (Equation 20). This is the model that was chosen for its relevance to the experimental setup, property of interest, and material behavior of the glasses that were analyzed

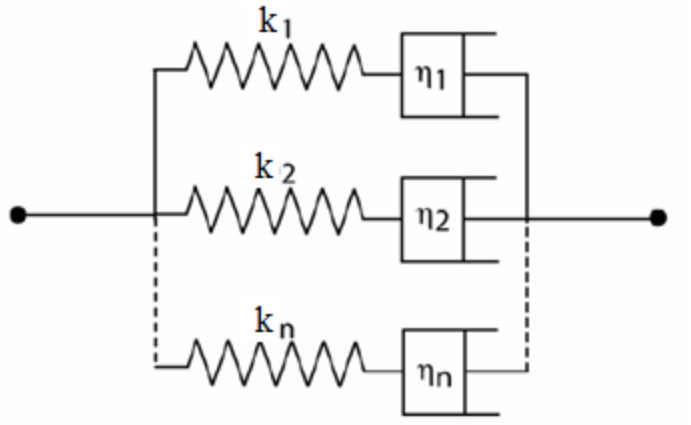

Figure 4.4: Mechanical representation of the Generalized Maxwell model

If the data was fit with a Prony series using a nonlinear approach, the solver would attempt to optimize the solution using both w_i and τ_i values. This is a computationally intense process and would require large amounts of memory. However, since it was assumed that the relaxation times describing the curve exist somewhere between t_0 (which equals zero) and t_{end}, it is reasonable to assume that some combination of these relaxation times will lead to an acceptable fit. For this reason it was decided to input a vector of relaxation times to the solver, in doing so the necessary computation is restricted to optimizing the weight, w_i, values that correspond to the input relaxation times. A similar computational method was used in the work of Tschoegle's dissertation.[98] Detailed MATLAB code involved in the processing and fitting can be seen in Appendix A.

Generic results obtained from initial curve fitting will be discussed in this section in order to frame the discussion of the curve fitting method and refinement of that method towards a useful and reasonable expression of material response. Detailed results will be dealt with in the next section.

The method described above and mathematically treated in Tschoegel's dissertation, requires an input vector of relaxation times, τ_i. The more values in the input vector, the more time and processing power was needed for the program to fit the model to the data, this is a limiting factor in that an infinite number of relaxation times could be input but it would take an infinite amount of time for the solver to complete that calculation. As with most computational operations, there exists a fine balance between resolution and solving time. At the other end of the spectrum, it is possible to guess values of τ_i and hope that the fit is adequate. This approach was taken by Vallet and Kadali in their Masters work regarding stress relaxation and stress retardation in silicate glasses.[99,100] Although the approach he used of choosing 3-4 relaxation times and varying them to manually improve the fit resulted in short fitting times, the results were at times unnecessarily arbitrary.

A method of fitting relaxation data and refining the precision of the fit with as few assumptions and arbitrary decisions as possible was developed, for the purposes of this dissertation research. The fitting of relaxation data in order to characterize it appears to be a part of the experimental process when observed in a chronological way with reference to the experiment. However, if the acquisition of data and the fitting or modeling of that data are considered as separate operations it becomes clear that the methods necessary for fitting experimental data should be no different than methods used in pursuit of pure modeling based studies. That is to say that best practices in fitting and modeling data are not unique to purely computational studies. Following this logic, it was decided to begin fitting by inputting a vector of relaxation times with what was considered a large step size. The input

vector, τ_i, was defined as described in Equation 56, where $\tau_1=0$ and the final relaxation time $\tau_N = t_{end}$.

Equation 56

$$\tau_i = \tau_{i-1} + 20$$

This resulted in a step size, $\Delta\tau$, of 20 seconds. An experimental run where $t_{end} =50000\ s$, would contain one thousand steps (i.e. $N = 2500$). It is also important to identify the relevant information that the fit will provide. The purpose of using a Prony series is to classify relaxation behavior in terms of the relaxation times and the relative strength of those times. These τ_i and w_i values are the output parameters of interest.

Inputting the relaxation time vector as well as experimental data to the curve fitting program produces a vector of weights that corresponds to the vector of relaxation times. The weights are then plotted versus the relaxation times, Figure 4.5 demonstrates a common fit with a $\Delta\tau$ of 20 seconds. Once the spectrum was analyzed, the input τ_i vector was modified to "zoom in" and decrease the step size in the regions that the previous fit had weighted as significantly nonzero. This had the effect of increasing the resolution in those specific areas where peaks were shown to exist in the initial rough fit. Applying this method helped to reduce solving times while not sacrificing resolution in areas with relaxation times that described the data. Figure 4.5 shows an example of a rough ($\Delta\tau = 20$) spectrum compared to a higher resolution ($\Delta\tau = 1$) fit.

Decreasing the step size farther leads to longer solving times, often approaching 72 hours of computing time. Higher temperature tests naturally lasted for shorter amounts of

time and were able to be fitted with smaller step sizes. This was sometimes necessary as the relaxation events happen faster at higher temperatures. In general two regimes of step size determination were used, the first was for high temperature, $T_1 \geq (T_{g,d}$ - 10 °C), were subjected to an initial analysis where $\Delta\tau$ = 20 s and a refined analysis where $\Delta\tau = 1\ s$. The second regime was $T_1 < (T_g$ -10 °C) which included an initial analysis where $\Delta\tau$ = 50 s and a refined analysis where $\Delta\tau = 5\ s$.

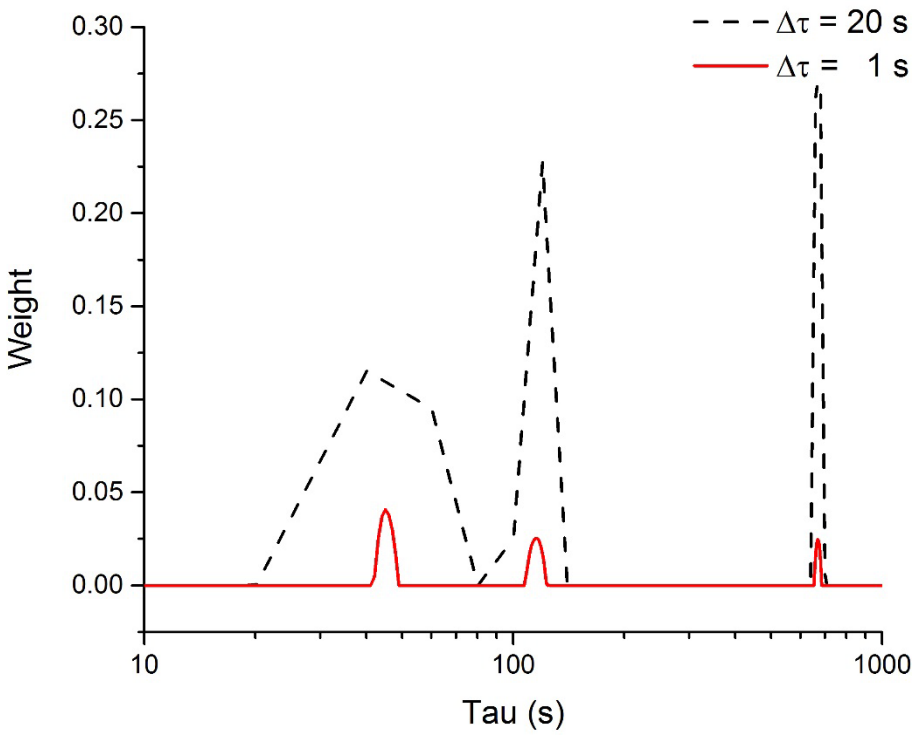

Figure 4.5: Weight versus relaxation time spectrum for a step size of 20 seconds and 1 seconds (black dashed line and solid red line respectively)

Figure 4.5 shows the presence of several distributions of relaxation times. These distributions are located roughly an order of magnitude distant from one another in time. The height of the peaks can be deceiving. According to the definition of the Prony series,

all the weight terms must add up to one. In the case of multiple distributions of relaxation times, the area under the curve is equivalent to the weight of the particular feature in question. In order to test the distribution of relaxation times around each peak, the weight and relaxation time distributions were used to create a curve. This was done for each peak independently, each curve was then fit with the KWW function (Equation 19). As discussed after the introduction of the KWW function, a β of one is descriptive of a pure exponential. Each of the individual distributions, when fit by the KWW function returned a value of $\beta \approx 1$. This means that although there is some slight distribution of relaxation times, when taken as a part of the whole, the distribution is so small as to be insignificant. This finding allowed each distribution of relaxation times to be treated as a single exponential and approximated as such.

Given that each relaxation feature behaved in what could be approximated as an exponential fashion, the final characterization steps were simplified. Rather than regard the spectrum as a number of discreet distributions, it is possible to view them as a number of discreet simple exponentials. Once each data set was fitted with the highest resolution set of relaxation times, and the weight versus relaxation time curve looked smooth and well resolved, the value of τ_i at the maximum weight for each peak was recorded. This operation identified the most dominant relaxation time in each discreet distribution. Those peak relaxation times, which varied in number from 1 to 4 depending on T_1, were used as the input relaxation time vector for a new curve fit. Instead of having 1000's of τ_i values, only 1, 2, 3, or 4 were input to the solver. The solver was then run to find the weights of those single relaxation times. This was the final iteration of fitting and produced the desired, end

product parameters. Although the analysis of relaxation time distributions discussed above indicated that the distributions could in fact be approximated by single exponentials, further verification was done to confirm this.

Once a "high resolution" fit was done (i.e. $\Delta\tau = 5$ *s)*, the area under each peak was calculated by integration. After the final fitting was done using the single exponential approximation for each distribution, the height of each single relaxation time was compared to the area under the curve of the high resolution fit. These values were close matches, indicating that the approximation was valid. The weight corresponding to a discreet distribution of relaxation times was equal to the weight of a single relaxation time used to approximate that distribution. This meant that weighting information was preserved through the approximation and no valuable material behavior data was lost. After applying this method to the spectrum shown in Figure 4.5, the result is Figure 4.6.

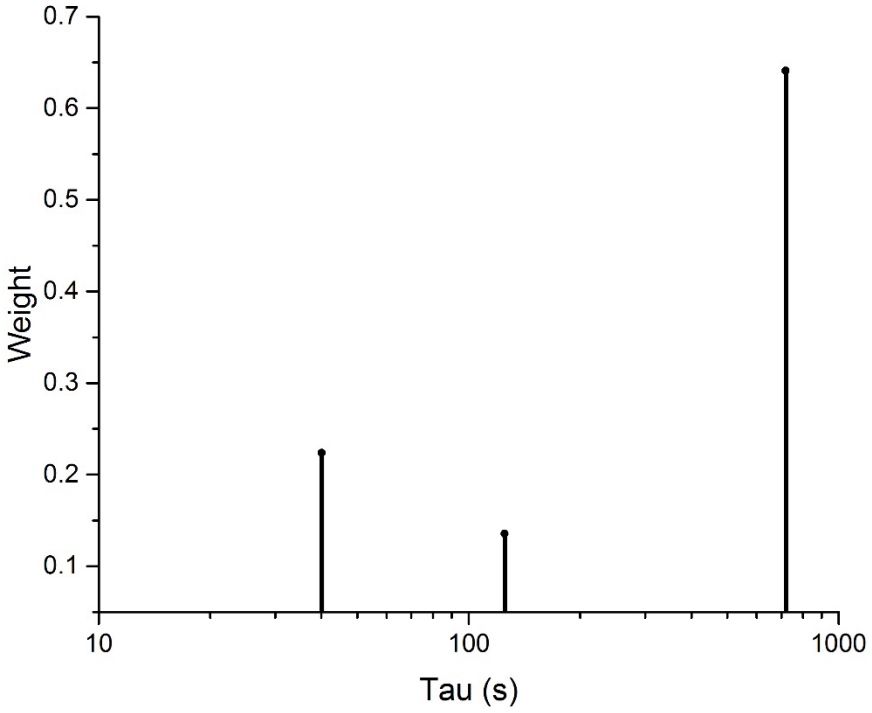

Figure 4.6: Weight versus relaxation time using single exponential terms to approximate distributions with drop lines from the data points for perspective

Another check on the validity of approximating three relaxation time distributions with three single exponentials is the quality of the fit as quantified by the R^2 value. "R^2" is computed by taking the sum of the squares of the distance of the data points from the best-fit, normalizing that by the sum of the squares of the distance of the data points from the mean y-axis value of the data. That number is then subtracted from unity. The closer to one that R^2 is, the better the fit with an R^2 of unity being a perfect fit. The quality of the fit can be used to gauge whether or not the assumptions made were reasonable. In the case of the spectra shown in Figure 4.5 and Figure 4.6, the high resolution step contained hundreds of relaxation times and R^2 = .999371. For the corresponding 3-term fit, R^2 = .999368. This extremely small difference lends credence to the assumption that, if

identified correctly, a 3-term Prony series can essentially match the quality of a fit obtained by a ~300-term Prony series. This result has nothing to do with the Prony series itself, it only means that this data can be described just as accurately by a small number of terms which leads to a more manageable set of structural relaxation parameters.

The spectrum shown in Figure 4.6 is representative of the final form the structural relaxation characterization took. The lines extending vertically down are just to give the appearance of height. Figure 4.6 displays a relaxation behavior comprised of 3 exponential terms (a 3-term Prony series). The largest relaxation time is weighted heaviest meaning it contributes to the overall relaxation behavior the most. Figure 4.7 shows this data expressed in component form. When plotted as individual exponentials, the contribution of each can be clearly seen, with the relaxation times and weights being taken from Figure 4.6.

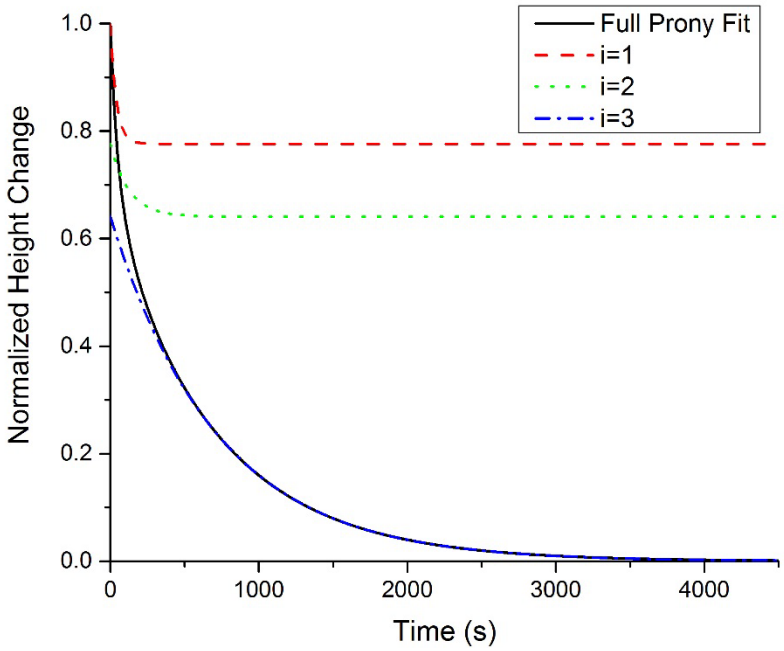

Figure 4.7: Normalized Height Change versus time; Prony series plotted with its individual components

Having demonstrated the experimental and data processing steps necessary for characterization of length (or volume) structural relaxation in the chosen glasses, tt now remains to detail the results obtained from these experiments and enter into a discussion as to their scientific and technological meaning.

4 N-BK7 relaxation experiments

The results of the experimental studies detailed in the previous chapter, are extensive. N-BK7 relaxation data was gathered for $\Delta T = 10\ ^{\circ}C$, and included eight T_1 values. In the case of the chalcogenide glasses, each of the three glasses was tested using $\Delta T = 5, 10, 20, \text{and } 30\ ^{\circ}C$, at an average of approximately eight T_1 values per condition, the total number of experiments numbers very nearly one hundred. The approach that will be taken is to express the characterized relaxation curves and plot the resultant final Prony

fits for each. Then the author will endeavor to interpret the results and frame them in such a way as to promote discussion. The results and discussion of N-BK7 will be treated separately from the discussion of the chalcogenide ternary. The relaxation behaviors of the two glass families will be used in comparison when beneficial.

N-BK7 was initially measured as a proof of concept to validate the efficacy of this dilatometric method of structural relaxation measurement. It was also chosen due to previous research on this glass by Scott Gaylord in his Masters work.[92] Gaylord derived TNM parameters for N-BK7 through DSC measurements this serves as a good way to compare the predictions of the TNM model to the realities of the actual fictive temperature change versus time measured in the TMA. The TNM and other material parameters found in his thesis can be seen in Table 4.1.

Table 4.1: Material inputs for TNM calculation of Tf change in N-BK7 from Gaylord's thesis [92]

Property	N-BK7
$\alpha_g \pm .1\ 10^{-6}/K$	8.2×10^{-6}
$\alpha_L \pm 1\ 10^{-6}/K$	54×10^{-6}
E/R ± 5%	71,704 K
x ± 5%	.708
B ± 5%	.774
$\tau_0 \pm 5\%$	3.56×10^{-36} s

The first step in researching the structural relaxation behavior of N-BK7 was to compare the length/volume relaxation behavior determined by TMA with the TNM predicted relaxation behavior. Using the properties from Table 4.1 and the data measured by TMA for a temperature down step from 567 to 557 °C, the normalized length relaxation behavior was compared. Figure shows the TNM prediction and the actual normalized length change of N-BK7 glass.

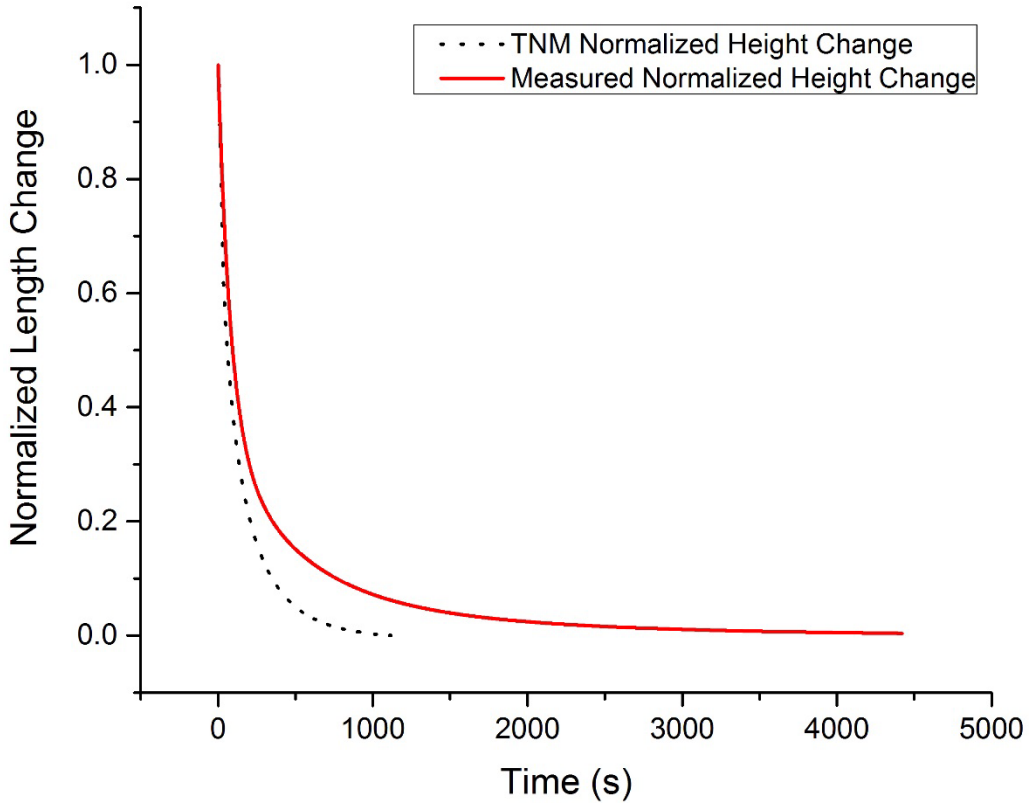

Figure 4.8: Normalized length change versus time determined by TNM prediction (black, dotted line) and actual measured normalized length change determined by TMA (red, solid line)

Although the short time relaxations are comparatively well predicted by the TNM model, at around 40% of relaxation remaining, the model diverges severely from the

measured relaxation behavior of the material. This same behavior is observed all across the temperature spectrum in this material as well as the chalcogenide glasses. This fact, coupled with the apparent difference in behavior of enthalpy relaxations and volume relaxations in these glasses led to the necessity of utilizing different characterization tools than the TNM model and parameters as described by DSC measurements.[82]

4.1 N-BK7 Results

TMA length relaxation experiments were carried out on N-BK7 as described in the previous section. Experiments were done with $\Delta T = 10$ °C and $T_1 = 542, 547, 552, 557, 562$. Once obtained, the relaxation data was processed and fitted according to the protocols developed by this author and detailed in the last section. The Prony series fits of the data had an average R^2 of $.998663 \pm .000986$. Due to the quality of the fit it is possible to plot the fitted curves as an accurate representation of the relaxation data. One of the secondary benefits of fitting experimental data is that the fit acts as a sort of filter, reducing the prevalence of any noise in the data and presenting a cleaner picture of the relaxation behavior of the material. The relaxation curves for $\Delta T = 10$ °C in N-BK7 are plotted in Figure 4.9.

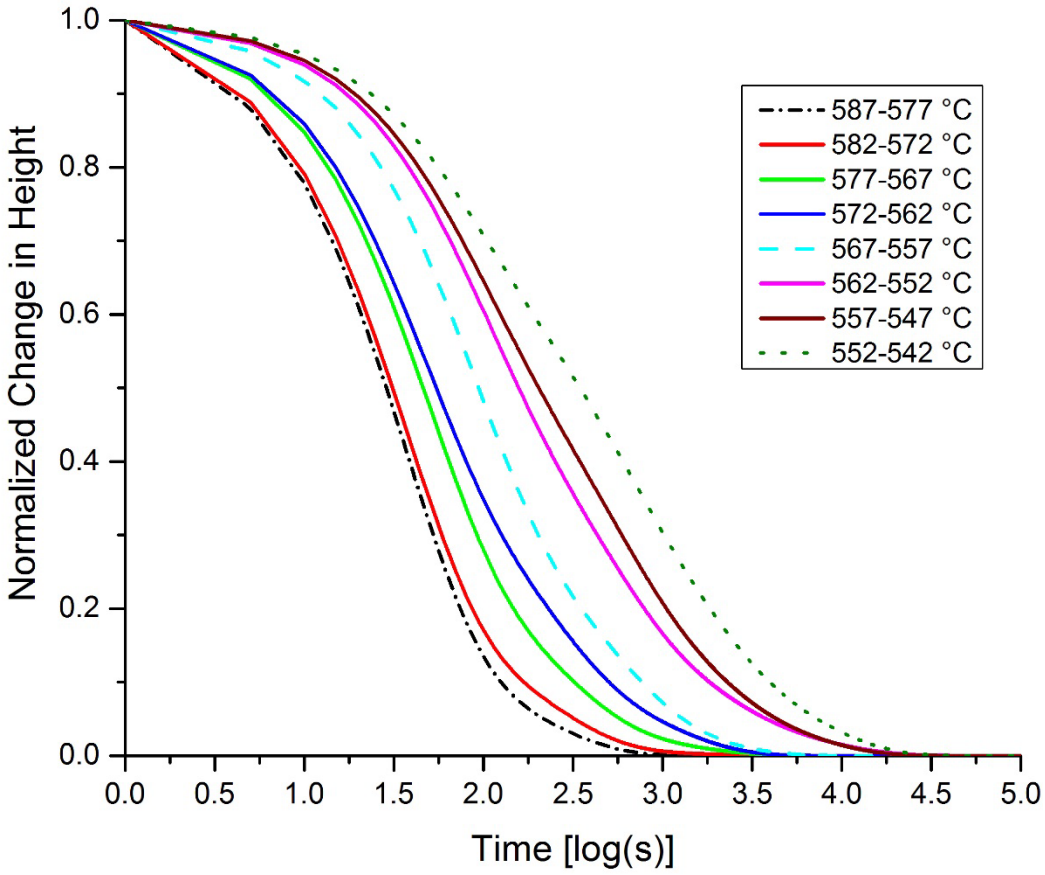

Figure 4.9: Normalized change in height versus time in log seconds, of N-BK7 for ΔT = 10 °C

The figure shows the relaxation curves of N-BK7 plotted in a semilog-x plot. This enables differences in relaxation behavior at long and short times to be clearly seen and accentuates the uniqueness of each curve. As expected, the test with the highest T_1 (577 °C) relaxes fastest, while the test with the lowest value of T_1 (542 °C) relaxes slowest. This behavior is expected based on the temperature dependence of glass relaxations.[20,101] The exponential nature of the relaxations is observable by visual inspection. Fitting the data with the Prony series makes it possible to quantify the nature of that exponential relaxation and use that data to identify relaxation modes within the glass.

The Prony series spectrum of a relaxation is the w_i term of the Prony series plotted versus the τ_i term, or the Prony weights versus the Prony relaxation times. The spectrum is meaningful because it directly displays the relaxation times that exist in the overall relaxation behavior and weights them, showing how much each contributes to the total. An example of such a spectrum can be seen in Figure 4.6. The spectrum characterizing structural relaxation behavior of a specific temperature can be plotted and compared to the spectra from other temperature conditions. Varying the values of T_1 and ΔT allow the relaxation behavior to be quantified as a function of both temperature and magnitude of temperature change. Since the characterization of N-BK7 was intended to be a proof of concept, multiple values of ΔT were not fully tested.

The Prony series spectra of multiple T_1 conditions is best expressed as a function of $T_1/T_{g,d}$, this allows relaxation behavior to be compared across various glass systems without the magnitude of the glass transition temperature limiting the comparison. The dilatometric glass transition temperature is used because the phenomena observed in these relaxation tests were volumetric in nature and not enthalpic, therefore if there is a disparity between T_g and $T_{g,d}$ (which there is) then the dilatometric classification of $T_{g,d}$ is more suitable for the definition of the glass transition in this case. Figure 4.10 shows the Prony relaxation spectra for N-BK7.

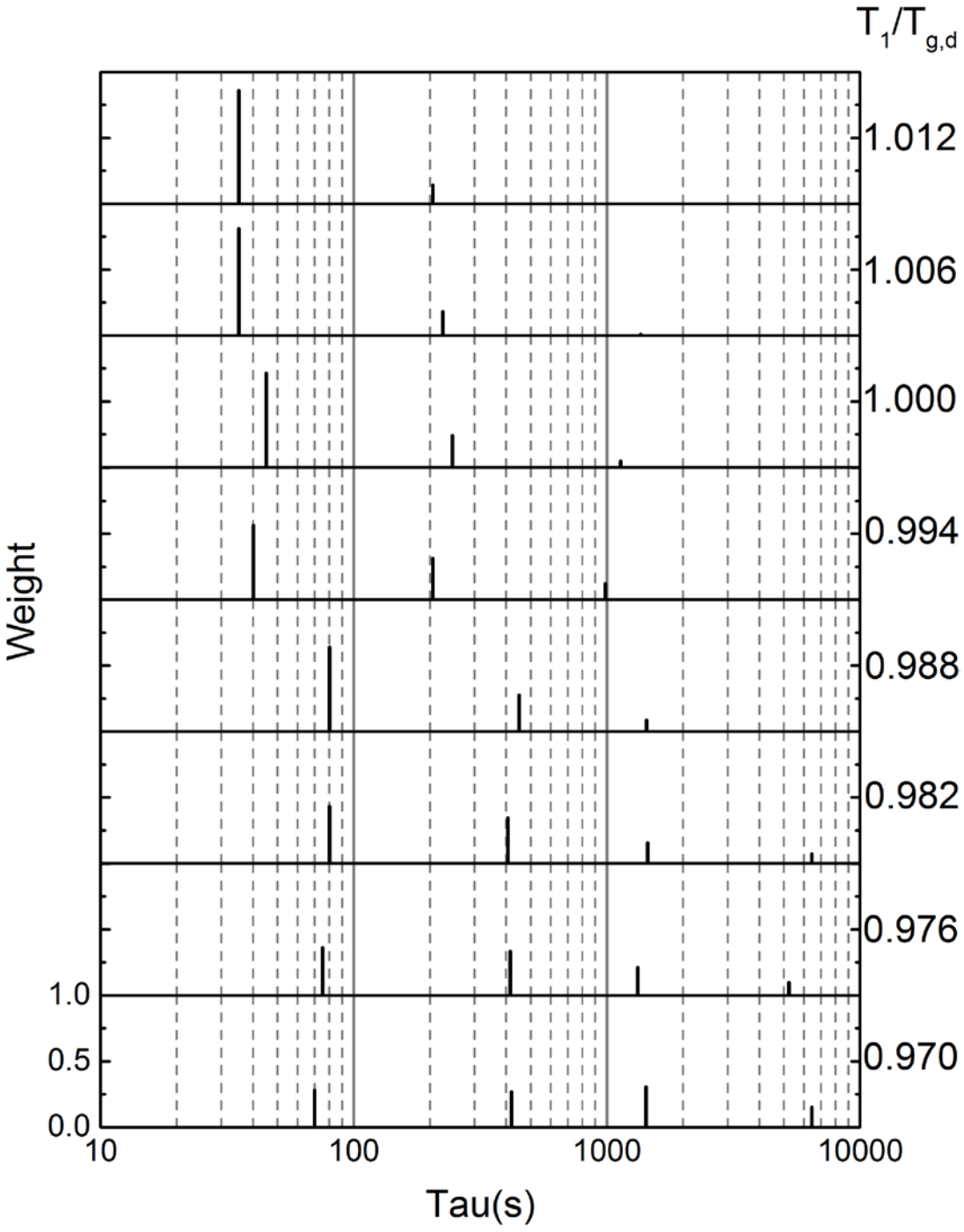

Figure 4.10: Prony spectra of structural relaxation in N-BK7 for ΔT = 10 °C

4.2 N-BK7 Discussion

The Prony series spectra of N-BK7 relaxation in Figure 4.10, depicts the temperature evolution of structural relaxation behavior for $\Delta T = 10$ °C. It is possible to draw a number of qualitative conclusions from the outset.

First, the striking aspect of these spectra is that there exist multiple, significantly weighted relaxation times for each temperature condition. These relaxation times are separated from one another by an order of magnitude in many cases. The existence of a given number (2-4) of relaxation times points towards the existence of multiple exponential relaxations occurring within the glass during structural relaxation. Since the test is isothermal, the differentiation between various relaxation times at a set temperature cannot be based on a temperature dependence. Due to the constant temperature of each test one can assume a constant viscosity since viscosity is strongly tied to temperature in these glasses.[58,63] Considering a material with a constant viscosity during the test, the most likely factor differentiating relaxations on a time scale would be the size of the relaxing structure or region.

The next qualitative observation that can be made is related to the disappearance of relaxation features as T_1 increases. At the lowest temperatures, a maximum of 4 terms make up the series. Extending this idea in the material behavior realm, if it is assumed that each exponential represents a relaxation event or mode in the glass, then certain relaxations are no longer observed as the temperature is increased. This mimics the idea of constraint theory, in which temperature dependent constraints related to the energy landscape in the

glass disappear as the energy of the system is increased.[102] Whether this behavior directly relates to constraints or not, it is clear that some of the structural phenomena that enable relaxation do not exist or do not contribute to relaxation in a measurable way at higher temperatures. It makes sense to expect larger regions or structures associated with long time relaxations to be dissolved as a structure or unit at higher temperatures and therefore have no effect on the structural relaxation behavior.

Additionally, the weight trends, which are treated with more detail below, show a reasonable response to temperature. At the highest temperature conditions, the short time relaxations are dominant. As the temperature is decreased, and the number of peaks changes from 2 to 3, the weighting of the peaks for $T_1/T_{g,d}$ = 1.000 show the weight of relaxation mechanisms decreasing with longer relaxation times. This continues into the 4 peak regime as well. Only when the temperature is further decreased do the longer relaxation times begin to dominate or have an equal share in the relaxation behavior of the whole. This phenomenon would seem to indicate cooperative rearrangement at lower temperatures, where slower and larger relaxing regions depend on each other moving in order to relax.

Further discussion of the results demands different viewpoints of the data in order to extract a number of behavioral characteristics from the system. Figure 4.11 shows a plot of relaxation time (note: it is in log(s)) versus $T_1/T_{g,d}$). This plot shows that apart from a strange discontinuity just below $T_{g,d}$ the relaxation times associated with each peak are nearly constant throughout the entire temperature range. This would suggest that the size of each feature does not change with temperature only the relative contribution to the

relaxation of the system changes. The near constant relaxation times across the entire experimental temperature range indicate that these values could be treated as fixed in any model of N-BK7 relaxation. Having τ_i values that are independent of temperature simplifies the model and means that the weights are the values that carry the temperature dependence linked to the difference between relaxation behaviors. This is not the case for all glasses, the chalcogenides showed relaxation times that varied substantially with changing temperature.

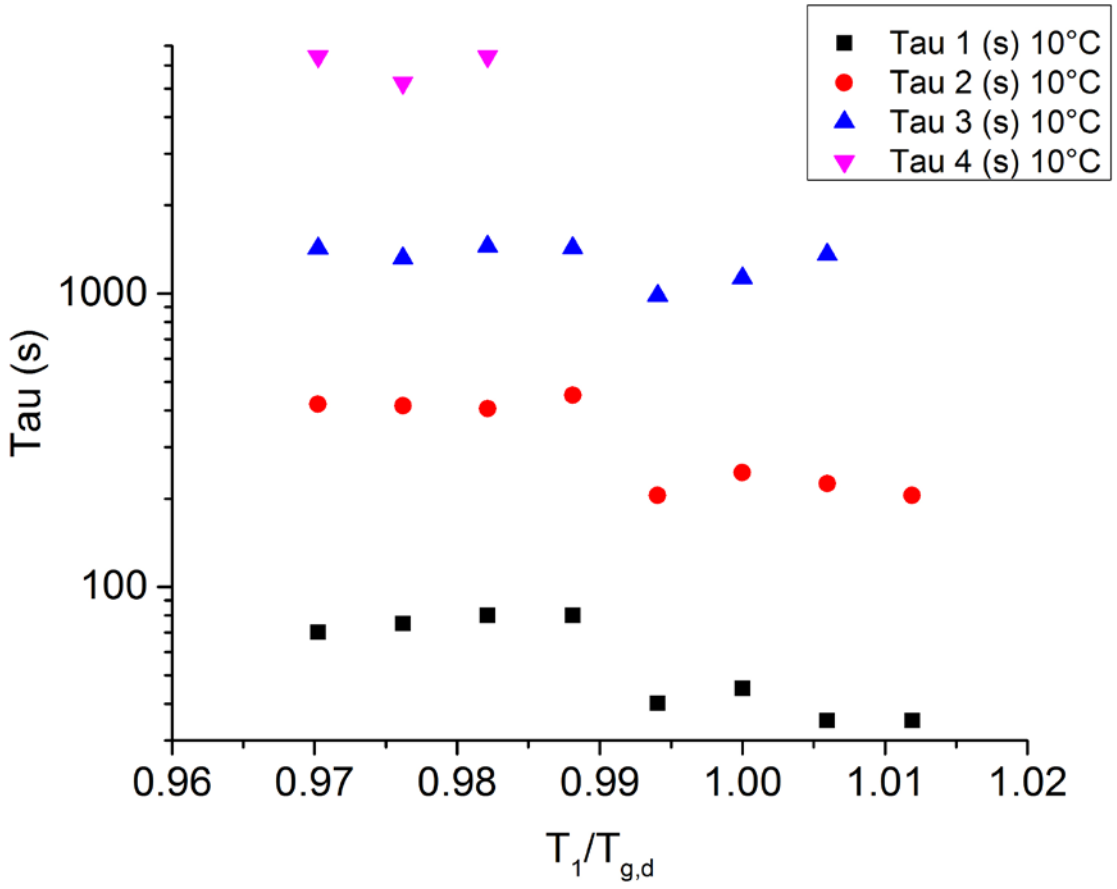

Figure 4.11: Relaxation time in log(s) versus $T_1/T_{g,d}$ in N-BK7 for ΔT = 10 °C

Given the constant nature of the relaxation times in N-BK7, the focus turns towards the weight values (w_i). Though it appears as if the structures or regions that relax during structural relaxation do not change size with temperature, the contribution of each unit must change with temperature. The weights are an indication of how much of the total relaxation takes place in a mode related to a relaxation time. Figure 4.12 shows the weight versus $T_1/T_{g,d}$ behavior of N-BK7. These same trends can be observed in Figure 4.10, however they are much easier to distinguish when plotted separately. The weights change linearly with temperature and in a manner consistent with reasonable trends. The first or shortest time features gains precedence as the temperature increases while all other features decrease in importance. Due to temperature limitations on the TMA, higher temperature could not be probed to discover at what temperature N-BK7 reached relaxation behavior characterized by a single exponential.

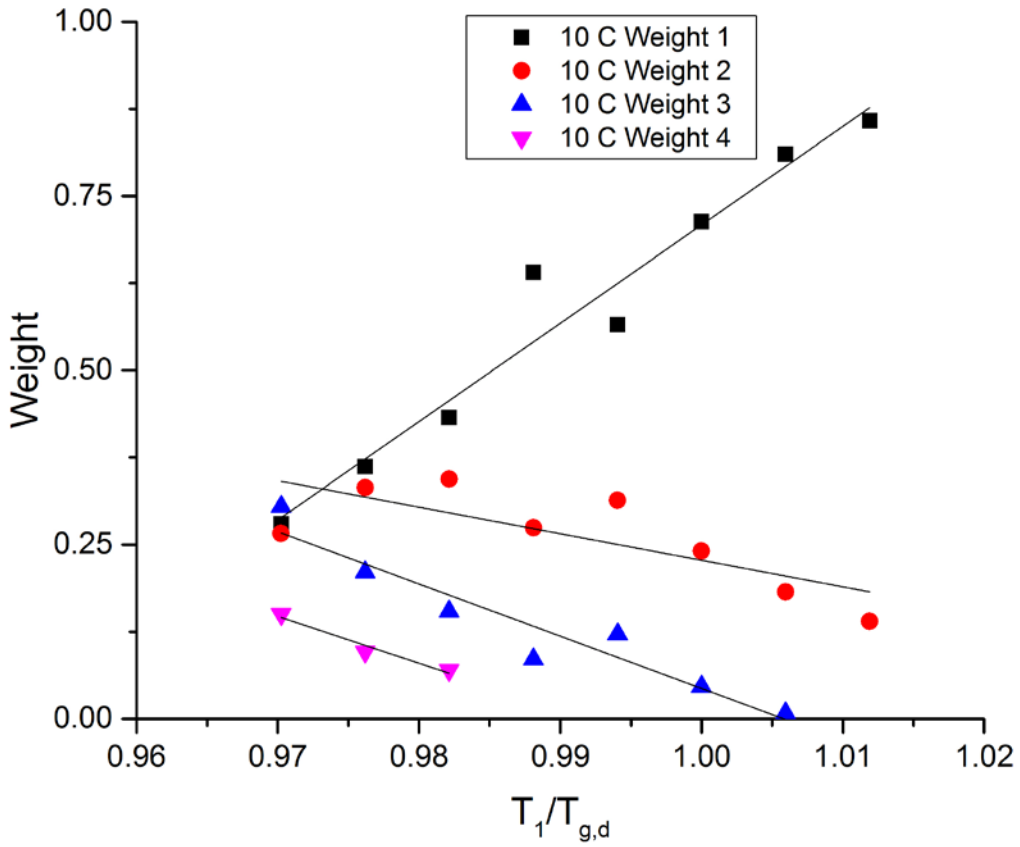

Figure 4.12: Weights versus normalized temperature in N-BK7 for ΔT = 10 °C

In order to facilitate the quantification of relaxation behavior in this temperature range it is possible to extend the weight trends and predict when the 2nd peak will disappear, leaving single exponential relaxation as the result. Figure 4.12 also contains linear best fit lines that provide slope and y-intercept data. The fit parameters are recorded in Table 4.2. Each set of parameters corresponds to one of the relaxation behaviors and can be expressed in equation form as a function of temperature as in Equation 57.

Equation 57

$$w_i(T_1) = m_i * T_1 + b_i$$

Table 4.2: Prony weights and relaxation times versus $T_1/T_{g,d}$ best fit parameters

i =	τ_i	*Slope* (m_i)	*y-intercept* (b_i)	R^2
1	*58*	*14.11*	*-13.40*	*.944*
2	*321*	*-3.81*	*4.04*	*.528*
3	*1300*	*-7.50*	*7.54*	*.891*
4	*6040*	*-6.72*	*6.66*	*.924*

Since the relaxation times are approximately constant with temperature, they can be set for all T_1 values within the tested range. This leaves the general Prony series representation for structural relaxation of N-BK7 expressed in the form of Equation 58, where R is defined by

Equation 59.

Equation 58

$$\alpha_{config}(T_1) = R * \sum_{i=1}^{N} \left(m_i \left(\frac{T_1}{T_{g,d}} \right) + b_i \right) e^{-\left(\frac{t}{\tau_i}\right)}$$

Equation 59

$$R = \frac{\Delta l_{config}}{L_{initial}}$$

4.2.1 Application of developed configurational model

One constructive way to validate a material model is use a model based on an aggregation of data to predict values that were measured in the development of that model. The Prony series model of configurational length/volume change depicted in Table 4.2 was applied, using Equation 58, to a case where $\Delta T = 10\ °C$, T_1 = 557 °C, $T_{d,g}$ = 567 °C, and R = 4.93E^-4. The resulting prediction of $\alpha_{config} * \Delta T_f$ versus time is shown in Figure 4.13.

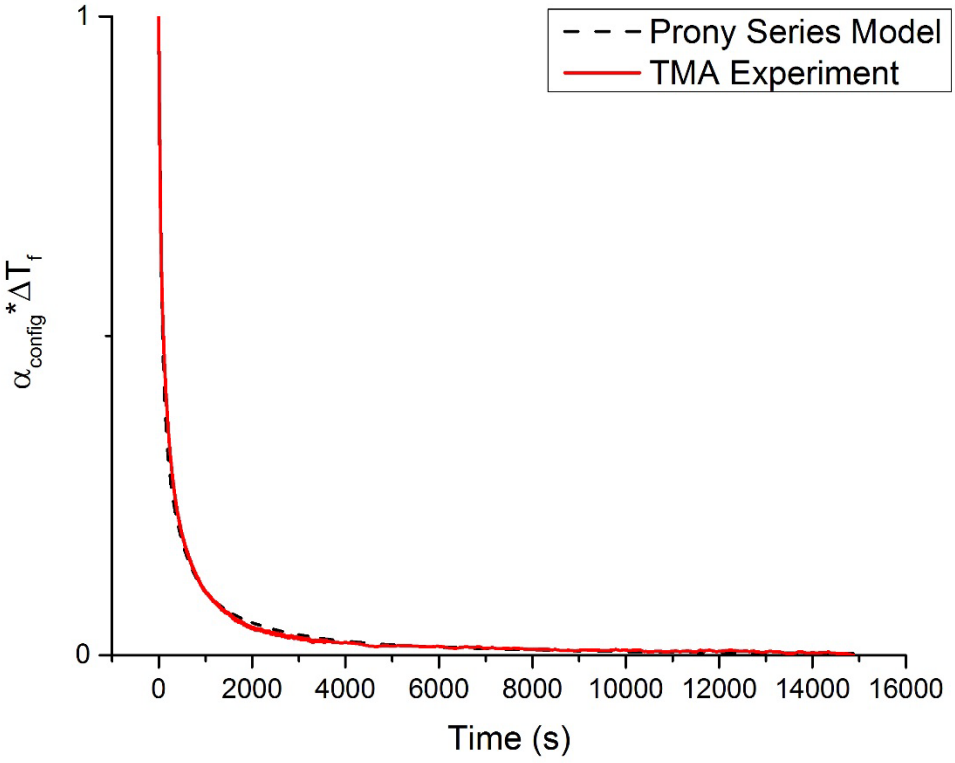

Figure 4.13: Normalized configurational change in height versus time for the Prony series prediction (black, solid line) and the actual measured value (red, solid line) for a jump from 567-557 °C in N-BK7

The Prony series based model for structural relaxation appears to represent the relaxation behavior of N-BK7 well when used in a predictive sense. In order to better understand the discrepancies between modeled values and measured values, it is helpful to plot the data from Figure 4.13 in a semilog-x plot. Figure 4.14 shows model versus experimental structural relaxation data plotted with time on a log scale. This helps exaggerate the differences and understand the strength and weaknesses of the model. An additional tool to quantify the precision of the prediction is to calculate the R^2 between the model and the experimental data. As mentioned previously, the average R^2 for the original fitting with the Prony series, or the quantification of how well the Prony series method fits

the original data was R^2 = .998663 ± .000986. When all of the available data was fitted and incorporated in a model to predict configurational length/volume change as a function or temperature and time, and that model was applied as seen in Figure 4.13 and Figure 4.14, the result was a reasonable prediction of configurational change based on the model. It was expected that the R^2 for prediction would be lower than the R^2 for direct fitting. The average R^2 for predictive modeling of each test relaxation was found to be .953463 ± .048553. The conclusion is that the model predicts length/volume change as a result of structural relaxation acceptably well for a majority of uses.

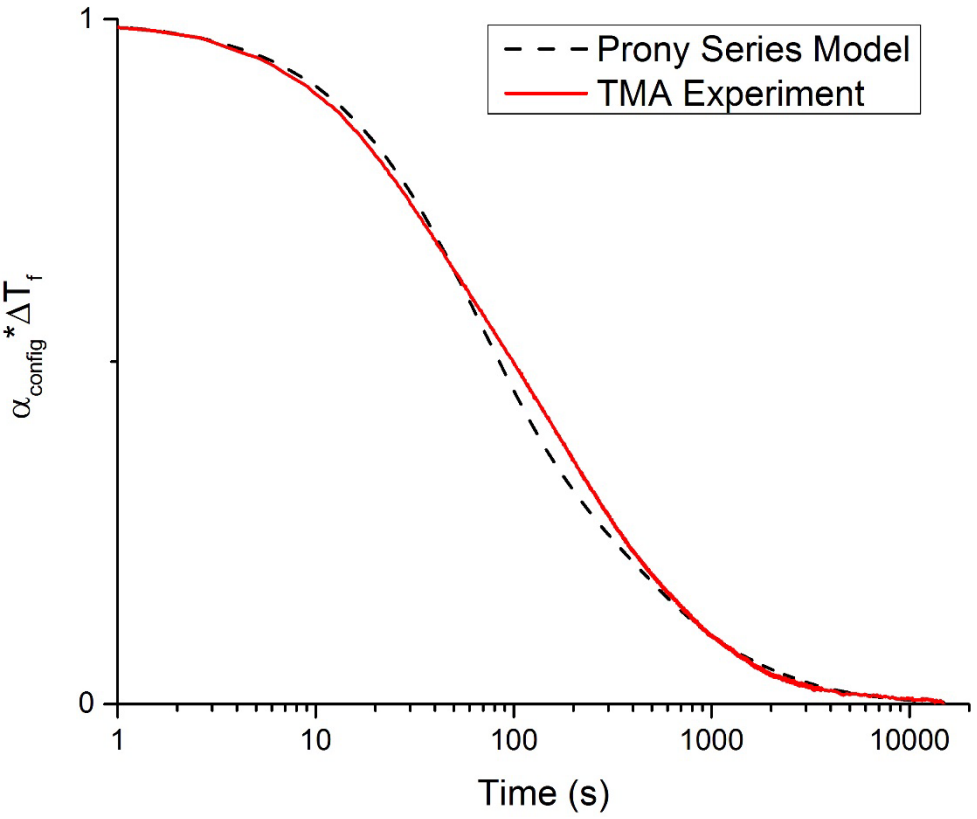

Figure 4.14: Log-x Normalized configurational change in height versus time for the Prony series prediction (black, solid line) and the actual measured value (red, solid line) for a jump from 567-557 °C in N-BK7

As in any modeling, assumptions must be made and mathematical care must be taken to ensure that the model stays within the bounds of the real system. Error from the fitting of experimental data compounds with error in modeling the trends of the fitting parameters gained from analyzing the data. A number of these issues arise with this model but can be dealt with using good mathematical sense.

The first issue was that the linear trends applied to weight terms as a function of T_1, as defined by Equation 57. This equation accurately represents the change of weight terms while those weight terms are greater than zero. The weight terms in the Prony series must be greater than or equal to zero, and the sum of those weights must be equal to one as in Equation 60.

Equation 60

$$\sum_{i=1}^{N} w_i = 1$$

However, when the weights are expressed as a linear equation, once they pass below zero, mathematically they keep getting more and more negative. This adversely effects the Prony series because it causes the sum of the weights to be less than unity. The fix for this is simple, once a weight is equal to or less than zero its value should be set at zero. This can be done easily with a simple 'IF-THEN' logic statement. The effects of this problem are not completely mitigated however.

The linear trends of weights do not always maintain the perfect summation to one because the trends are derived from experimental data that rarely follow perfect

mathematical laws. The end result is that a combination of weights may end up summing to somewhat more or less than one. This presents an issue for prediction of configurational length/volume change, because if the weights add up to 0.8 for example, then the total height change will be 20% less than the true value. Likewise if the weights sum to greater than one, the opposite problem occurs. The fix for this issue is also relatively simple. If, for instance, the temperature condition is such that there are two Prony terms that describe the data, and their weights sum to 0.8, with $w_1 = .6$ and $w_2 = .2$, then the two weights can be proportionally increased to reach a sum of one without changing the relationship between them. Using this method, the relative strength of their contributions remain intact while also satisfying the condition to sum to unity. In the example listed here this would involve adding (.6/sum) times the missing 0.2 in weight to the w_1 and (.2/sum) times the missing 0.2 in weight to w_2. The resultant sum of weights is equal to one with the relative contributions of each weight preserved. The resulting model realistically predicts configurational change in N-BK7 glass within the range of temperatures studied.

There are a couple of further restrictions on the model. The first is that it may not accurately predict at temperatures lower than 542 °C for N-BK7. It is expected, however, that the model should accurately predict relaxation behavior up to the temperature at which the behavior turns to single exponential behavior. Once single exponential behavior has been reached a simple temperature or energy dependent exponential should suffice to characterize behavior.[73,103] According to the model, as defined by the values in Table 4.2, N-BK7 should reach single exponential relaxation behavior at ~ 618 °C which is a T_1/T_g of 1.089.

4.2.2 Technological application

Compared to the lack of applicable and useable models for this kind of data, this result is relatively simple and could be applied in a range of applications. In the scientific community this modeling system could be used to predict the effects of heat treatments on material properties and quantify the disequilibrium of a glass system. Additionally it could be used to help determine the effective quench profile that a glass undergoes during the melt-quench processing method. This would help establish the thermal history of the glass and could be used as a method for ensuring consistent and repeatable processing during the quench process in glass making.

Industrially speaking this characterization method, which could be done on readily available horizontal dilatometers, would be a useful tool for glass makers to have. It would allow them to decide how much of the structural stress they would like to anneal out of the glass in order to meet specifications without any additional waste in time. Currently, glass manufacturers make sheets or plates of glass and anneal them for very long times to ensure full annealing, but if their standard glasses were characterized using this method, they could predict exactly how long was necessary for the amount of annealing they wished to do. This would save time and heating costs for their annealing lehrs.

All of this data could be acquired using the normalized change in volume versus time because in many cases the exact dimension change may not need to be known, only the percent of relaxation that is complete. In high tech industries such as optical manufacturing, specifically in PGM, the exact dimension changes of a lens could be

modeled using FEM software to characterize the results of annealing steps to reduce effects such as stress birefringence in an optic. Understanding the shape change of an optic during cooling or annealing would then lead to the ability to predict the exact mold shape that needed to be machined for that PGM process, saving thousands in iteration costs and possibly months in time.

5 Ge-As-Se system relaxation experiments

The Ge-As-Se material system was chosen for characterization for a number of reasons. First, it is one of the most commonly found chalcogenide glass systems in industry and academia. Second, much supporting research has been done on glass properties and structure, allowing any data gathered in this study to be leveraged with wider community knowledge. And finally, this system contains within it several interesting elements including changes in dimensionality, connectivity, and coordination throughout different areas of the same glass system. These differences are vital to understanding the causes and effects of relaxation behaviors in these glasses, while still maintaining a system that is comprised of similar constituents. The TMA analysis described in the preceding chapter was done on three glasses in the Ge-As-Se system. The high selenium, low dimensionality and coordination $As_{20}Se_{80}$, the stoichiometric and 2-D, excellent glass forming $As_{40}Se_{60}$, and the higher coordination, higher dimensionality, stoichiometric $Ge_{17.9}As_{19.7}Se_{62.4}$. These were isothermally relaxation tested at various temperature below, at and slightly above $T_{g,d}$. The magnitudes of the temperature jumps during the test were set at ΔT = *5, 10, 20, and 30 °C*. Each composition was fully tested at each ΔT condition. The results from these tests are detailed in the sections below. For the sake of brevity, the ΔT = *10 °C*

condition was used as the illustrative case, the full sets of data will be discussed as appropriate.

5.1 $As_{40}Se_{60}$ results

$As_{40}Se_{60}$ is the binary, stoichiometric composition chosen for this study. This glass is made up of $AsSe_{3/2}$ pyramids that forma a puckered layer structure in a 2-D configuration. Each layer of pyramids is weakly attracted to other layers by van Der Waal forces. These sheets make up a bulk glass by "crumpling" like a piece of paper. This glass is considered an ideal glass former with a coordination number of $\langle r \rangle = 2.4$.[18] This glass was synthesized and fabricated into samples as describes in Section 12. The samples were tested in the TMA and analyzed, for the data listed below ΔT = 10 °C unless otherwise noted. $T_{g,d}$ = 176 °C and the tests covered the values of T_1 from 151 to 191 °C. Figure 4.15 shows the relaxation curves resulting from TMA experiments on $As_{40}Se_{60}$.

The relaxation curves were fit with the standard Prony series method detailed earlier in this dissertation. The fitted relaxation curves are plotted in Figure 4.15, these relaxation curves are accurate representations of experimental data with the average R^2 = .999190 ± .000774.

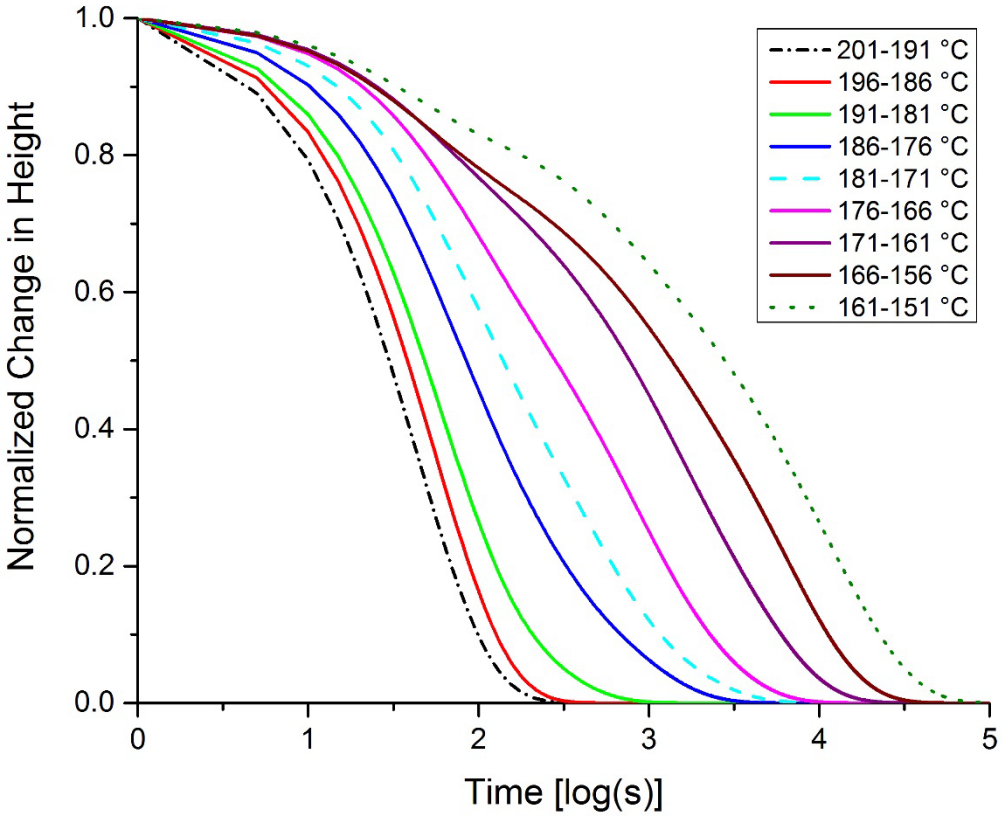

Figure 4.15: Normalized change in height versus time in log seconds, of $As_{40}Se_{60}$ for ΔT = 10 °C

The Prony series spectra for $As_{40}Se_{60}$ can be seen in Figure 4.16. The relaxation times show a maximum of 4 peaks. In the case of this glass, the number of peaks decays steadily from 4 to 3 and so on until reaching single exponential relaxation behavior at the two highest temperature conditions tested.

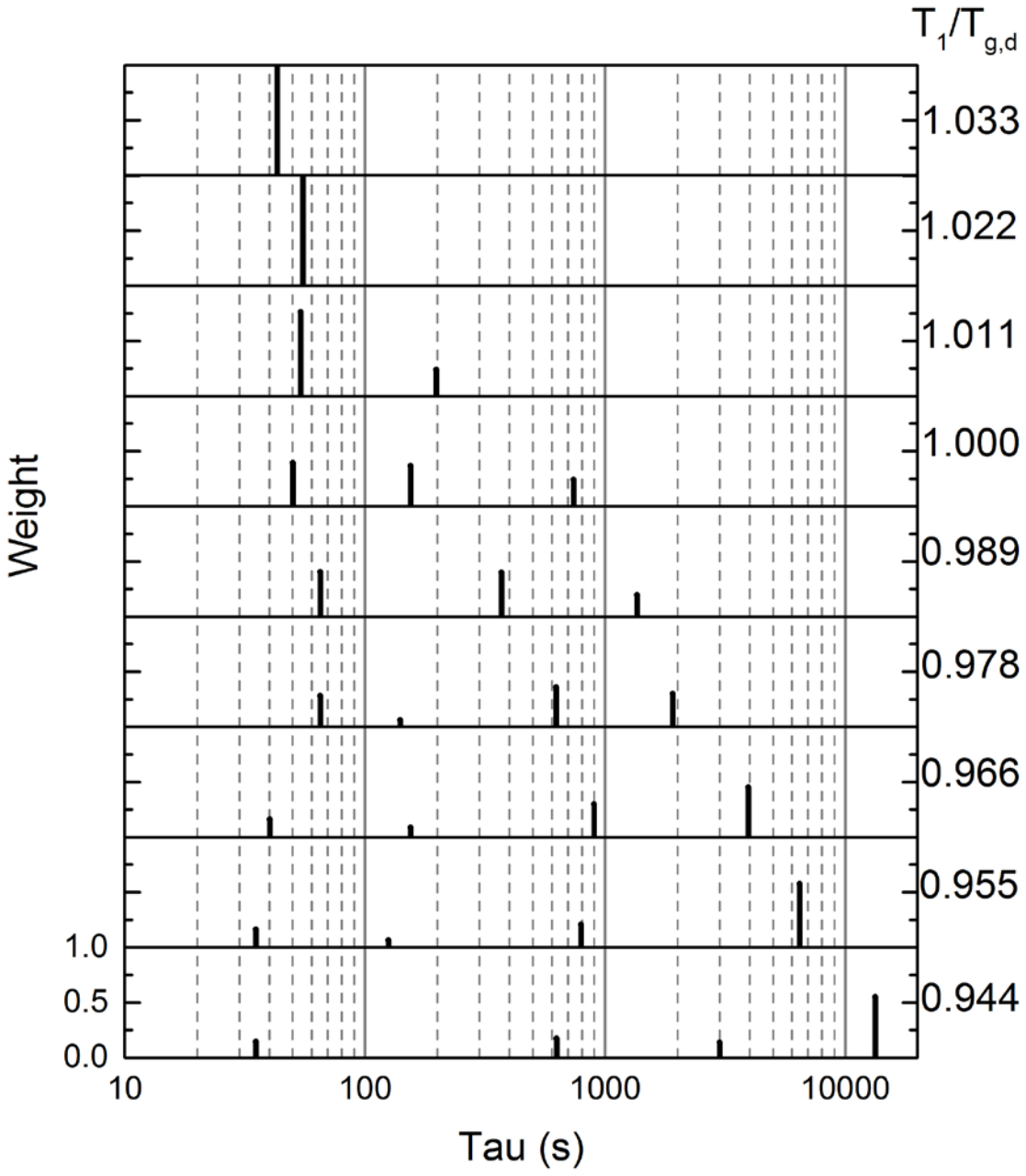

Figure 4.16: Prony spectra of structural relaxation in $As_{40}Se_{60}$ for ΔT = 10 °C

5.2 $As_{20}Se_{80}$ results

$As_{20}Se_{80}$ is a binary glass containing arsenic and selenium. It is nonstoichiometric and has an excess of selenium. This leads the formation of short selenium chains consisting of between two and three selenium per chain between arsenic atoms. The details of which were outlined in Section 12, and can be read about in more detail in the XPS paper on the subject.[49] This glass was synthesized and fabricated into samples as detailed in Section 12. The samples were tested in the TMA and analyzed, for the data listed below ΔT = 10 °C unless otherwise noted. $T_{g,d}$ = 89 °C and the tests covered the values of T_1 from 60 to 100 °C.

The relaxation curves were fit with the standard Prony series method detailed earlier in this dissertation. The fitted relaxation curves are plotted in Figure 4.18, these relaxation curves are accurate representations of experimental data with the average R^2 = .998266 ± .002803. This glass showed what may be considered odd relaxation behavior, as the jump from 75 – 65 °C displays. The relaxation curve beginning at unity dips below that of the next highest temperature jump then crosses that curve again to move into a longer time behavior as expected. The curves crossing is something that will be shown on a smaller scale for the other chalcogenide compositions in future sections. This behavior emphasizes the effect of relaxation events that are spread over relaxation times orders of magnitude different from one another. A short time relaxation may occur for a structure or group of structures within a larger volume that displays longer time relaxation behavior. The relaxation curves of $As_{20}Se_{80}$ show that the short time relaxations at lower T_1 values may actually lead to faster relaxation than tests with higher T_1 values, although that is the

case only for the beginning of the relaxation process. At longer times when larger relaxations take over predominance the usual trend of slower relaxations at lower T_1 values is once again established. The Prony series spectra pulled from the fitted curves are shown in Figure 4.18. As in the case of N-BK7 and $As_{40}Se_{60}$, the maximum number of peaks observed is four.

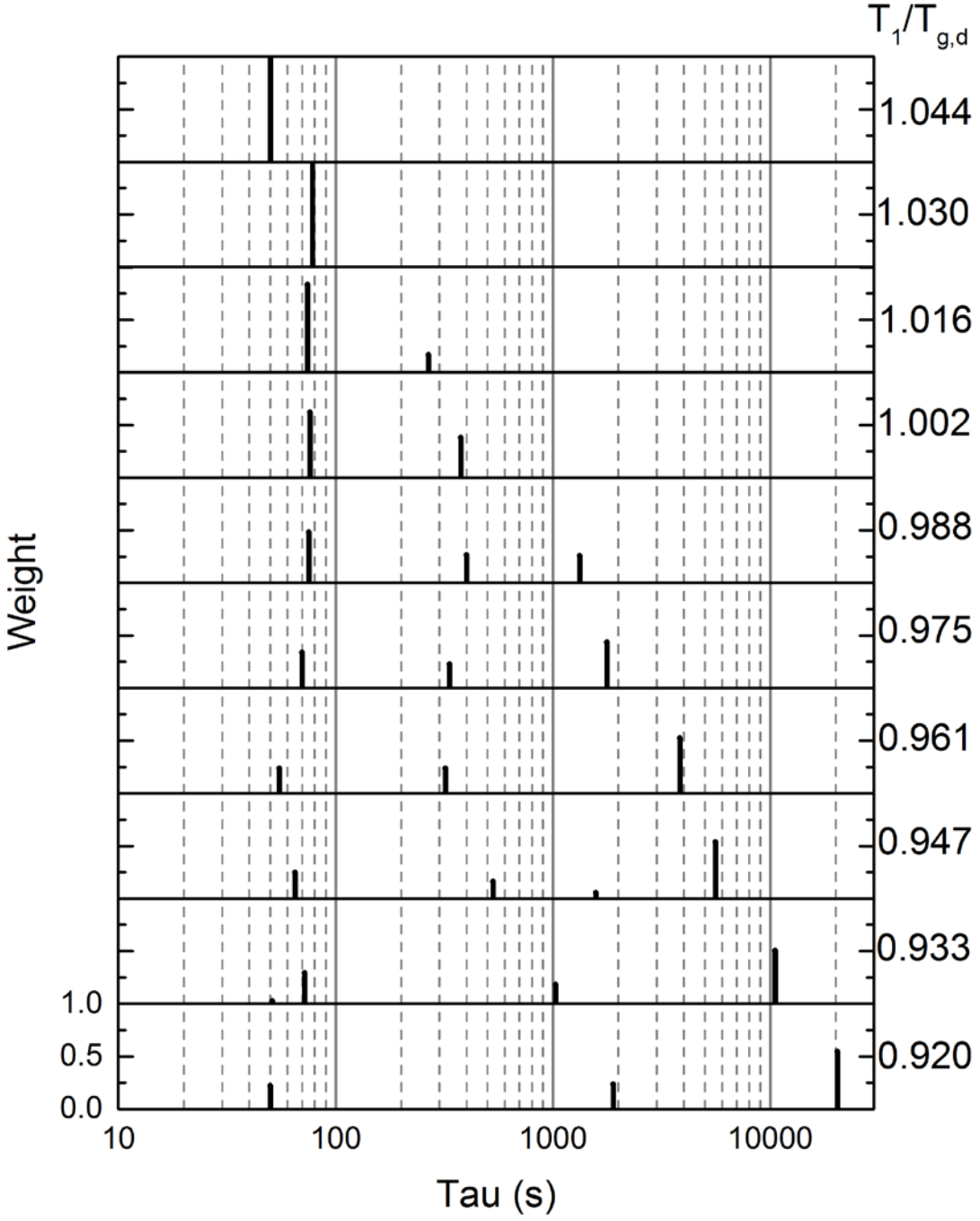

Figure 4.17: Prony spectra of structural relaxation in As40Se60 for ΔT = 10 °C

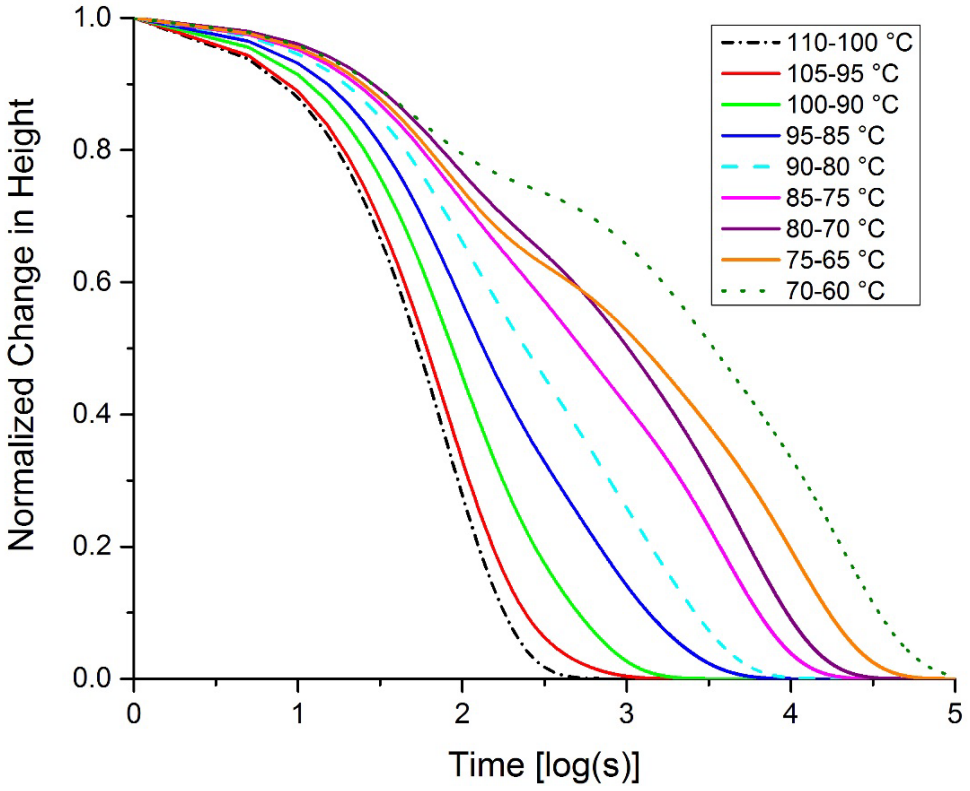

Figure 4.18: Normalized change in height versus time in log seconds, of $As_{20}Se_{80}$ for ΔT = 10 °C

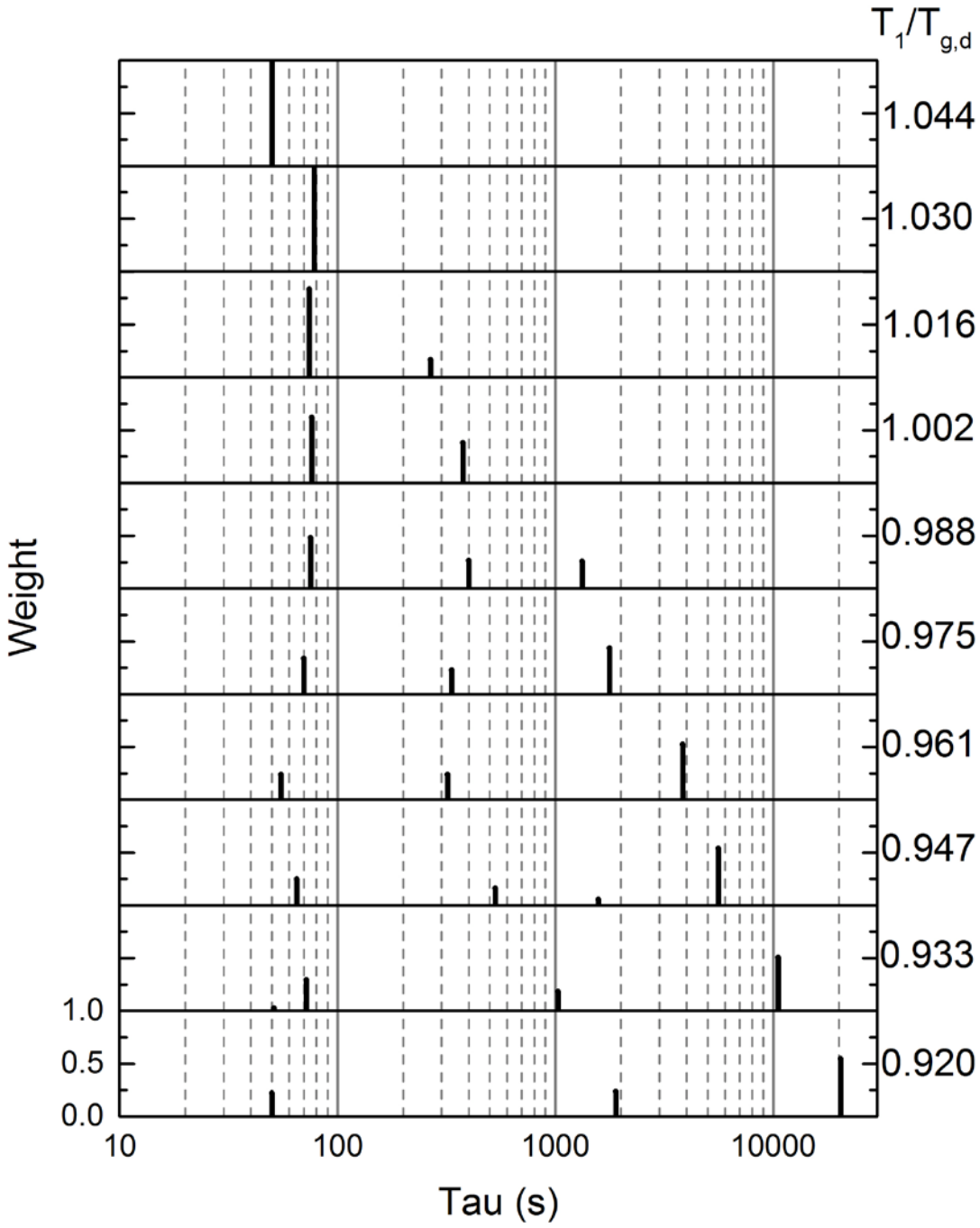

Figure 4.19: Prony spectra of structural relaxation in As20Se80 for ΔT = 10 °C

5.3 $Ge_{17.9}As_{19.7}Se_{62.4}$ results

$Ge_{17.9}As_{19.7}Se_{62.4}$ is a germanium containing glass selected to test the effect that a germanium has on the structural relaxation behavior of glasses in the Ge-As-Se ternary system. This composition was selected due to its location on the stoichiometric tie-line between $As_{40}Se_{60}$ and $Ge_{33.3}Se_{66.6}$. The addition of germanium to the glass network serves to cross link the puckered layers comprised of $AsSe_{3/2}$ pyramidal units. Rather than being attracted by van Der Waal's forces alone, germanium bonds directly to selenium and crosslinks the network. In polymer terms it serves to polymerize the glass network leading to a higher average number of bonds per atom (CN = 2.56). The overall bonding scheme is similar to that of N-BK7 but containing different constituents. In both cases the glass is made of a mix of 4-coordinated atoms (Si and Ge), 3-coordinated atoms (B and As) and a 2-coordinated set of atoms (O and Se). The main difference being the presence of an alkali (Na) in the N-BK7 that this glass does not have. The samples were tested in the TMA and analyzed, for the data listed below ΔT = 10 °C unless otherwise noted. $T_{g,d}$ = 251 °C and the tests covered values of T_1 from 235 to 285 °C.

The relaxation curves were fit with the standard Prony series method detailed earlier in this dissertation. The fitted relaxation curves are plotted in Figure, these relaxation curves are accurate representations of experimental data with the average R^2 = .997959 ± .001708. The Prony series spectra pulled from the fitted curves in Figure 4.20 are shown in Figure 4.21.

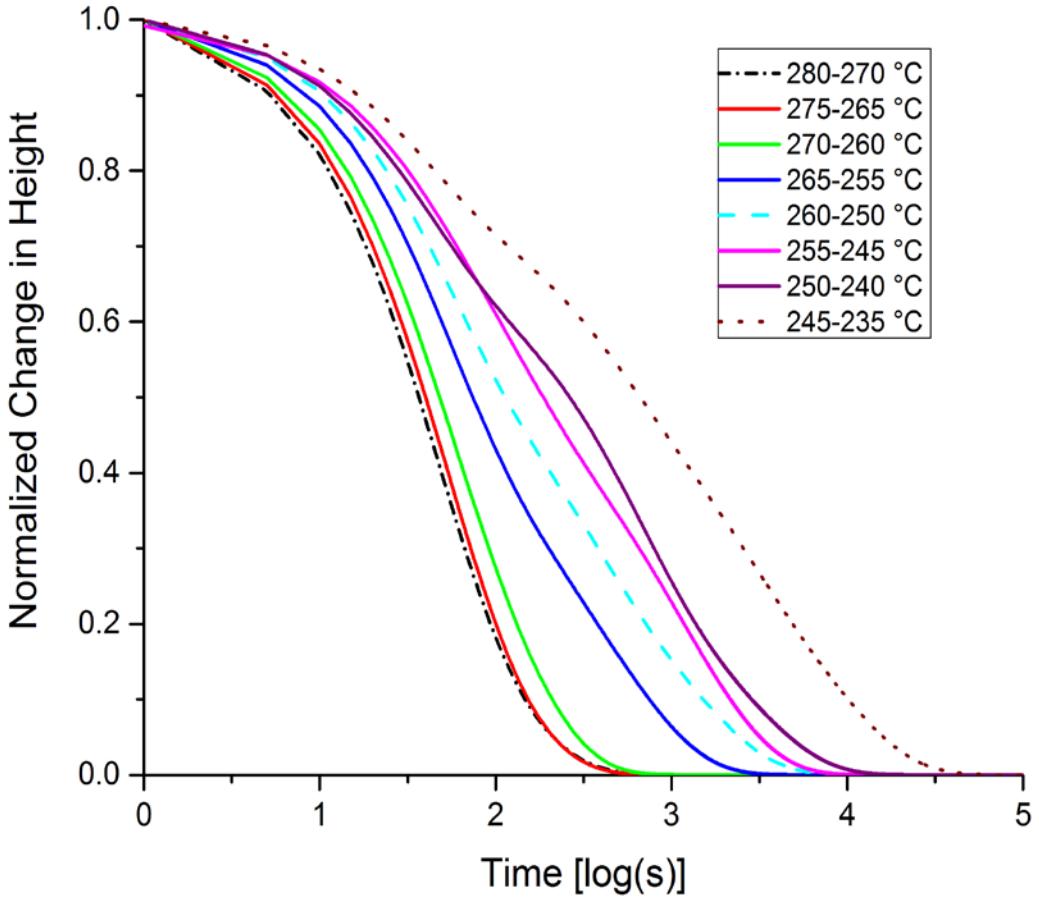

Figure 4.20: Normalized change in height versus time in log seconds, of $Ge_{17.9}As_{19.7}Se_{62.4}$ for ΔT = 10 °C

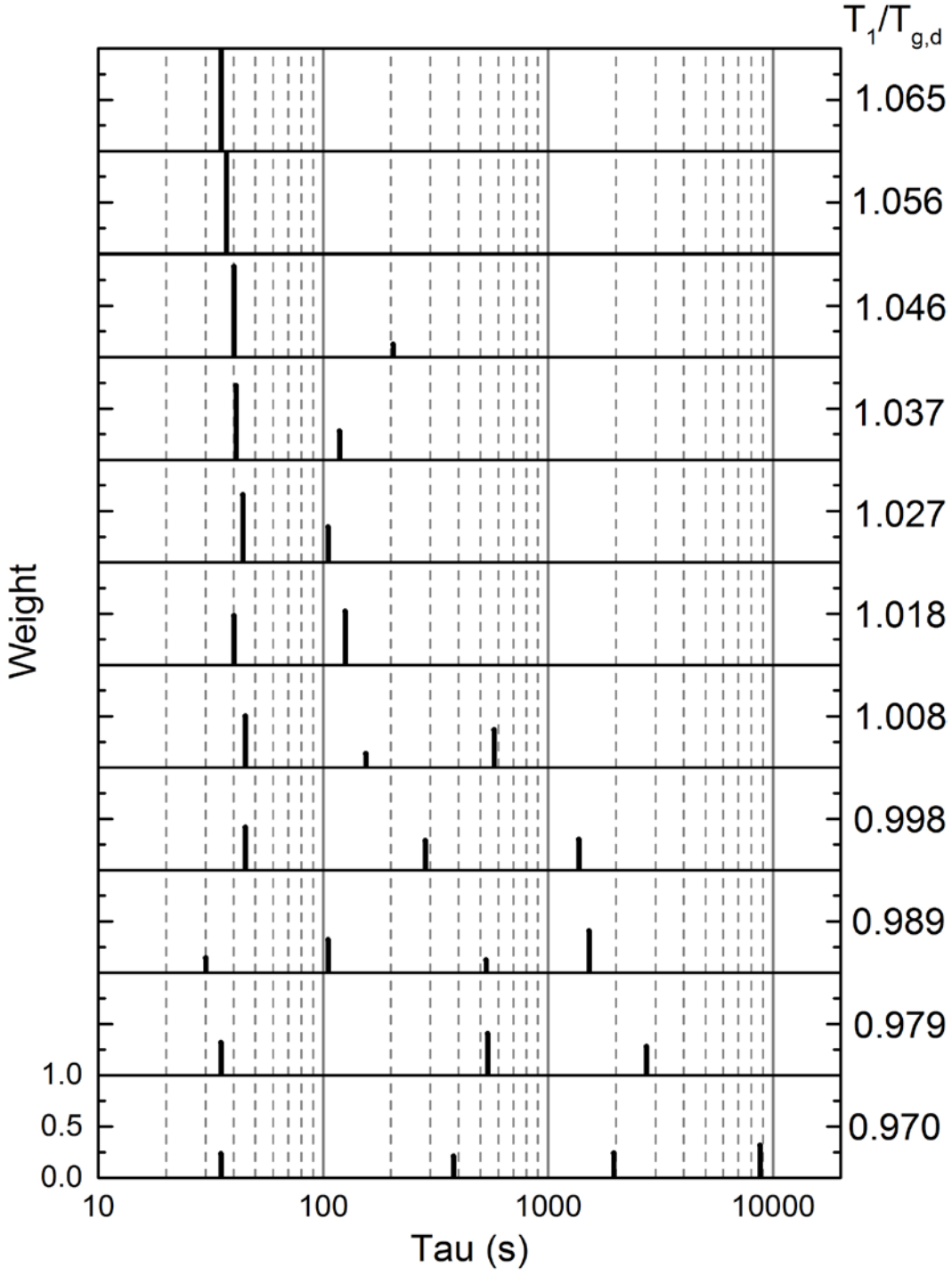

Figure 4.21: Prony spectra of structural relaxation in $Ge_{17.9}As_{19.7}Se_{62.4}$ for ΔT = 10 °C

6 Ge-As-Se system relaxation discussion

Volumetric structural relaxation experiments were done on $As_{40}Se_{60}$, $As_{20}Se_{80}$, and $Ge_{17.9}As_{19.7}Se_{62.4}$. The experimental results produced by Prony series fits of the data were described in Section 5. This section will detail the processing of the experimental data and theoretical conclusions drawn from it. The behavior of the glass network in the region of the glass transition temperature is a topic of nearly constant study in the glass science community.[50,64,104-107] The main components of the relaxation experiments and subsequent fitting, produce a number of useful sets of data that will be considered and discussed in this chapter. The relaxation times and weights will be valuable in gaining insight into structural behaviors of the glasses as they relax. Activation energies of relaxation were calculated from the change in relaxation time with temperature, these can be used to get a picture of the energy needed by the material to relax.

The total change in length (or volume) between two thermodynamic states, as measured by isothermal structural relaxation experiments, is the lone thermodynamic information that can be taken from these experiments. The total configurational height change of each sample was quantified and the results detailed below in Section 6.5. The results point to a reduction in configurational volume change and therefore entropy change with decreasing temperature. The downward trend of this property is such that a change of zero is expected at temperatures not far below $T_{g,d}$. The trending towards zero of either the configuration volume change between equally spaced thermodynamic states or the entropy trend that infers, matches with the trends highlighted by Kauzmann as well as

Adam and Gibbs. The $T_{g,d}/T_2$ ratio was calculated and is reported below, these values fall within the expected norms reported by Bestul and Change.

6.1 Volumetric effective activation enthalpy

In Section 2.1.2 the work of Malek in deriving apparent activation energies from volume relaxations in As_2S_3 was detailed. A comparison of the only similar study done on chalcogenides to the data shown in this dissertation is warranted. Although the physical meaning connected to the results shown by Malek are only as good as the physical meaning of the TNM parameters, the results of an analysis of this data through his lens may be helpful technologically if not scientifically. Malek plotted length change as measured by TMA versus log time and extended the tangent of that curve at the inflection point all the way to the x-axis (Figure 4.22). His argument was that the time at which the extrapolated tangent hit the x-intercept (t_m) corresponded to a condition at which the glass had almost fully relaxed. Therefore relaxation behavior could be considered free of any nonlinearities.

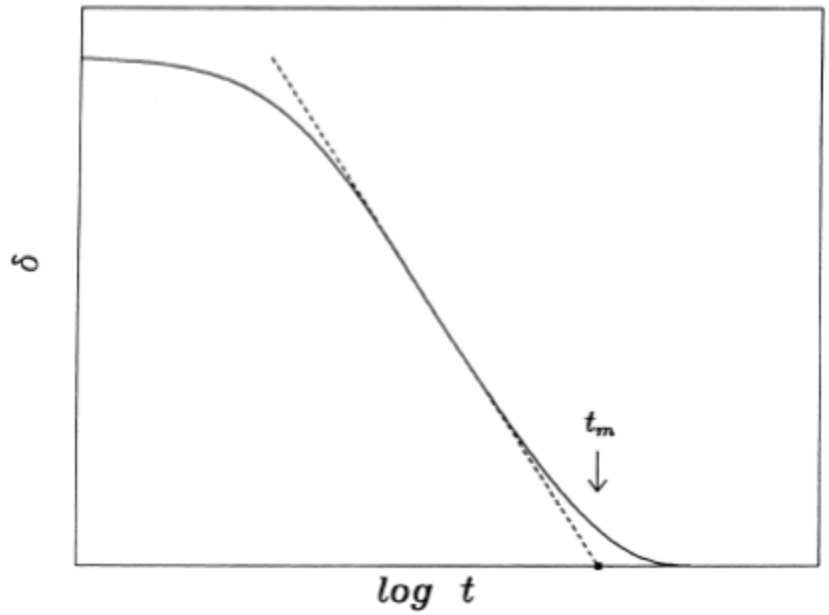

Figure 4.22: Plot of height change versus log time and extrapolation of the inflection point tangent for an As_2S_3 relaxation curve [20]

The relaxation curves of the three chalcogenide glasses discussed in this dissertation (Figure 4.15, Figure 4.18, and Figure 4.20) where analyzed according to the method described above. Once the t_m values were determined for each glass, they could be analyzed using TNM parameters. By using the time value near the completion of the relaxation it allows the non-linearity parameter of Equation 35 to be considered unity (x=1) and that equation can be simplified to Equation 61.

Equation 61

$$\tau = A * exp\left[\frac{\Delta h^*}{RT}\right]$$

If the t_m values are then plotted on a log of t_m versus *1/T* plot then the slope of an apparently linear trend would be equal to $(\Delta h^*/R)*log(e)$ and the y-intercept would be equal

to ln(A). The goal of this analysis was to calculate the effective activation energy or enthalpy and study any correlation with coordination number. Figure 4.23 shows the results of such a t_m plot. The effective activation enthalpy calculated from that plot was 251 kJ/mol. This represents the effective relaxation activation enthalpy for $As_{40}Se_{60}$ as characterized by this method. The same method was carried out on $As_{20}Se_{80}$ and $Ge_{17.9}As_{19.7}Se_{62.4}$. The tabulated activation energies are listed in Table 4.3 and the activation enthalpies are plotted versus CN in Figure 4.24. The results show a strikingly linear trend in activation enthalpy versus coordination number. This trend could be used to predict the general relaxation characteristics of other compositions between the studied compositions. Pairing the activation data with coordination data would allow a scientist or technician to be able to measure one relaxation curve for an unknown glass and predict the relaxation behavior at various temperatures for that glass. The enthalpy values obtained will be compared to data gathered by a different method in the following sections.

Table 4.3: Tabulated effective activation enthalpy and coordination number

Composition	$<r>$ (CN)	Δh^* (kJ/mol)
$As_{20}Se_{80}$	2.2	161 ± 5
$As_{40}Se_{60}$	2.4	251 ± 15
$Ge_{17.9}As_{19.7}Se_{62.4}$	2.56	303 ± 5

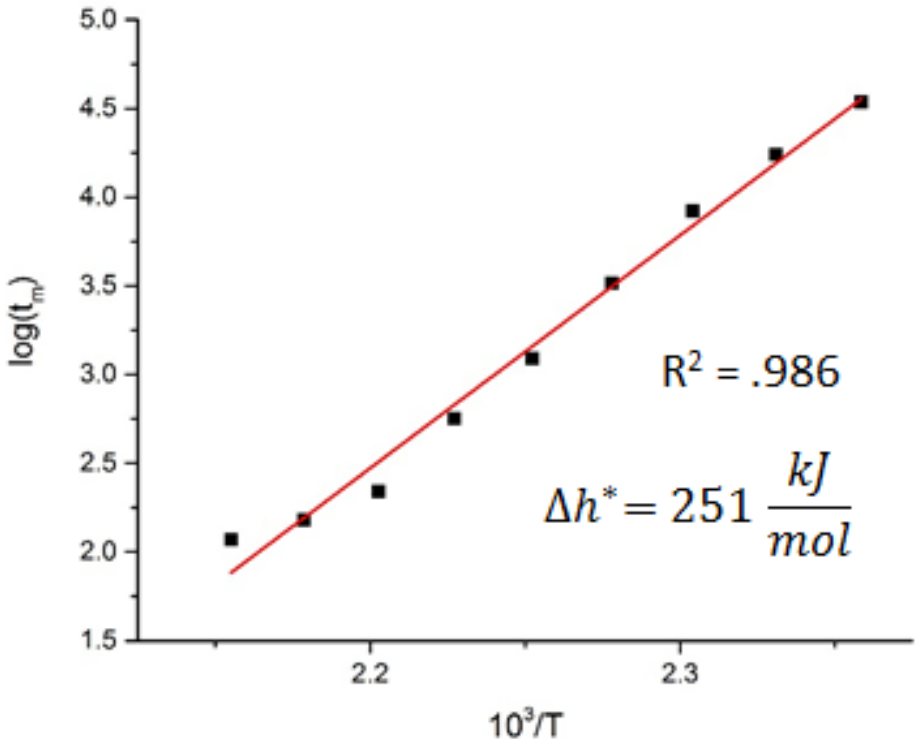

Figure 4.23: Plot of log(t_m) versus 1/T with the slope yielding effective activation energy for $As_{40}Se_{60}$

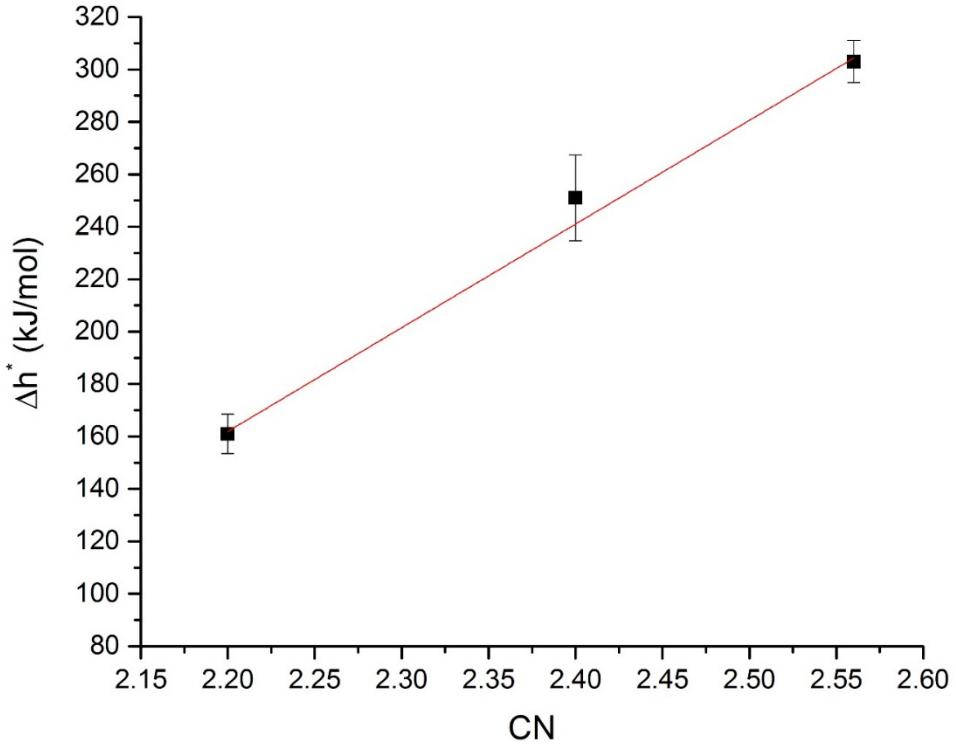

Figure 4.24: Effective activation enthalpy versus coordination number for glasses listed in Table 4.3

6.2 Relaxation time observations

As material scientists and more specifically glass scientists, we want to know why certain relaxation behaviors are observed under certain conditions. The data presented above is measured from experiments. It is important to adhere as much as possible to the measured data or mathematical expressions accurately describing it. For this reason it is necessary to turn our attention to the material science question of why these relaxations occur in the manner that they do, what causes them, and what can be deduced about their nature from the extensive amount of data gathered and analysis done.

The first step is a quantification of the significance of a given relaxation time. The analysis above has condensed all of the data gathered on this glass to a series of weight and

relaxation time pairs. The relaxation times describe a volume relaxation event occurring in the material as experimentally measured by TMA. The relaxation times at a given temperature, and therefore the events they indicate, occupy different magnitudes of time in most cases. It is common to see a relaxation time in the 10's (s), one in the 100's (s), and another in the 1000's (s) and so on. Structural relaxation events occurring in the same liquid at the same temperature can have different relaxation times for two main reasons: one, they are cooperative in nature, meaning the later relaxations can occur only after the earlier relaxations have taken place. The second possibility is that the units or structures that the longer relaxation times describe are larger in size than the shorter time relaxation mechanisms. Given the fact that the time separation of relaxations is often an order of magnitude, the evidence points to the latter possibility. If relaxations were delayed only until earlier relaxations had finished but were the same size, the gaps between relaxation times should at least be consistent. However, this is not the case; frequently the gaps between relaxation times are such that the idea of a difference in size being directly responsible for a difference in relaxation time is most likely. Taking the ELT view of the glass network, these various relaxation times may correspond to different MBs in the enthalpy landscape. This would mean that the relaxations indicated by the relaxation times are intra-metabasin relaxations and therefore would not directly affect one another. This supports the idea that the relaxation times shown are not directly linked.

The Prony relaxation spectra shown above for each individual glass will be looked at in detail. In order to get a better idea of the behavior of relaxation times with respect to temperature, the relaxation times are plotted versus normalized temperature. The

temperature normalization is T_1 in Kelvin divided by the dilatometric glass transition temperature ($T_{g,d}$) in Kelvin. This normalization is done so that the differences in $T_{g,d}$ between the various compositions is not a factor when comparing their relaxation time behavior to one another. Figure 4.25 shows a plot of the relaxation times versus $T_1/T_{g,d}$ for $As_{40}Se_{60}$. For all data presented, the error is within the data points unless otherwise indicated.

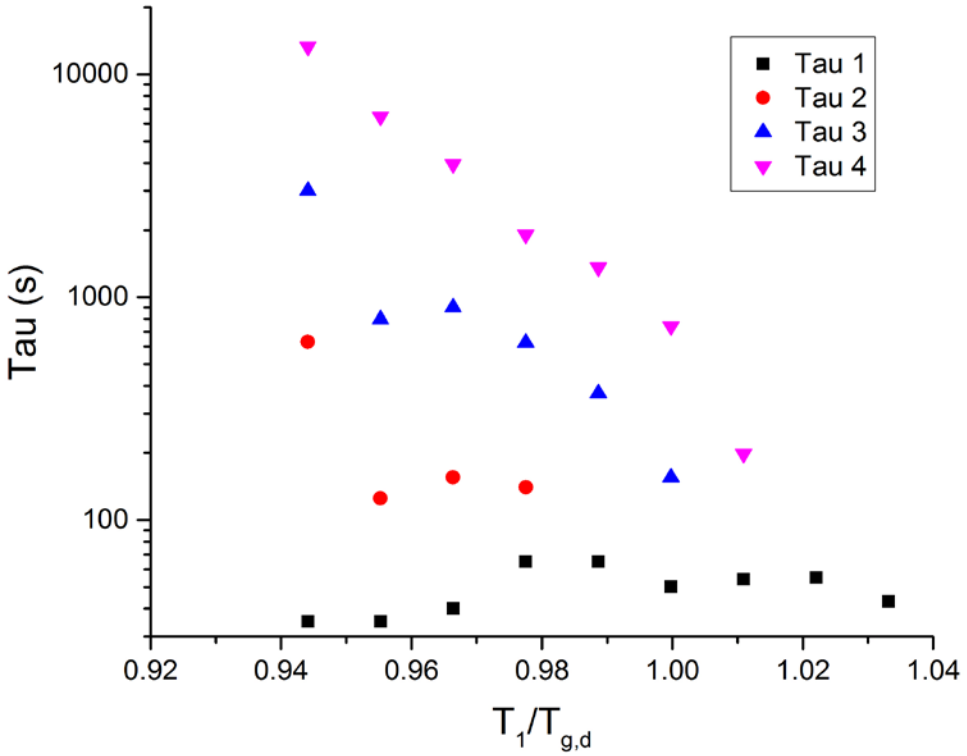

Figure 4.25: Relaxation time versus $T_1/T_{g,d}$ in $As_{40}Se_{60}$ for ΔT = 10 °C

The first thing noticeable about the relaxation times in Figure 4.25 are the trends with temperature. Unlike N-BK7 this glass contains mechanisms that relax in a nearly linear manner on a log plot, which indicates an exponential relationship with temperature. Given that structural relaxation is a process in which the configuration of the glass must

change to suit a new thermodynamic equilibrium, this equates to some sort of movement of structures in the glass, it is not surprising that the trend of relaxation times for this glass and the other glasses have an exponential relationship to temperature. This indicates a thermally activated process similar in nature to diffusion. The more stable relaxation times in N-BK7 are discussed in section 4.2 of this chapter.

Figure 4.26 and Figure 4.27 show the relaxation time trends of $As_{20}Se_{80}$ and $Ge_{17.9}As_{19.7}Se_{62.4}$ respectively. The under coordinated $As_{20}Se_{80}$ shows a linear trend of relaxation times versus temperature on a log scale as does the highly cross-linked Ge-As-Se composition. Despite their differences in connectivity and even composition they appear to behave within the same general rubric with regard to structural relaxation.

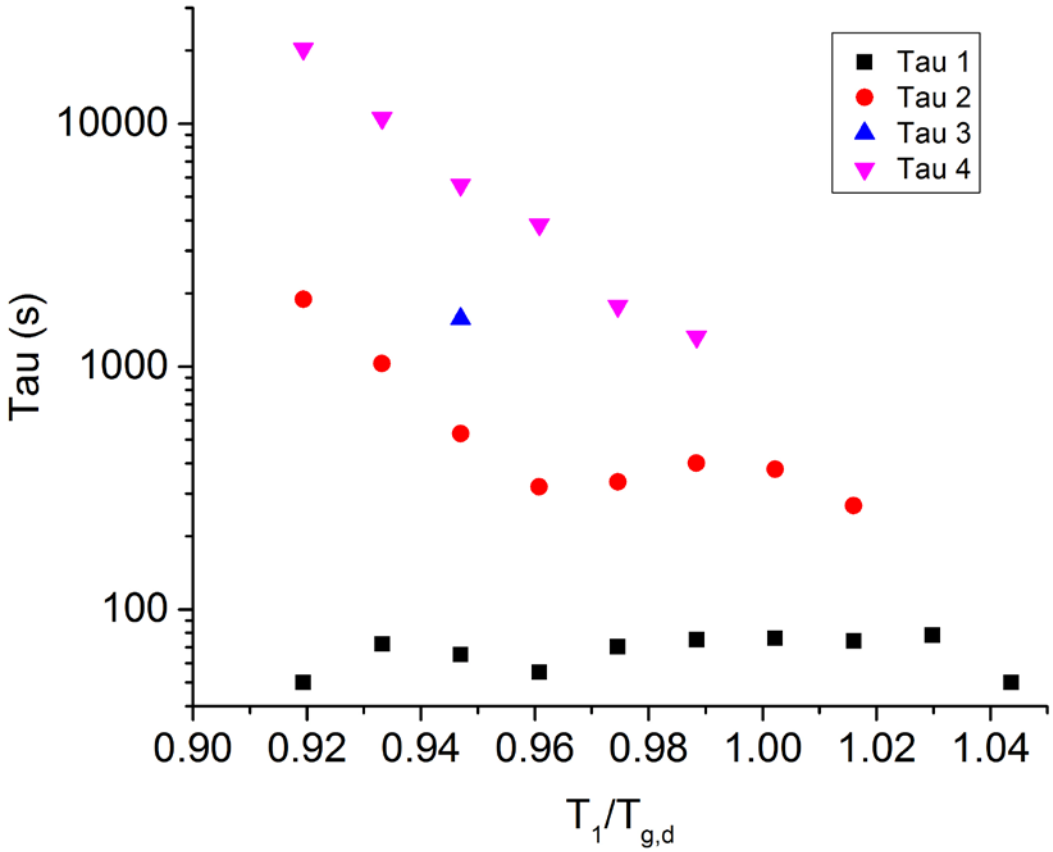

Figure 4.26: Relaxation time versus $T_1/T_{g,d}$ in $As_{20}Se_{80}$ for ΔT = 10 °C

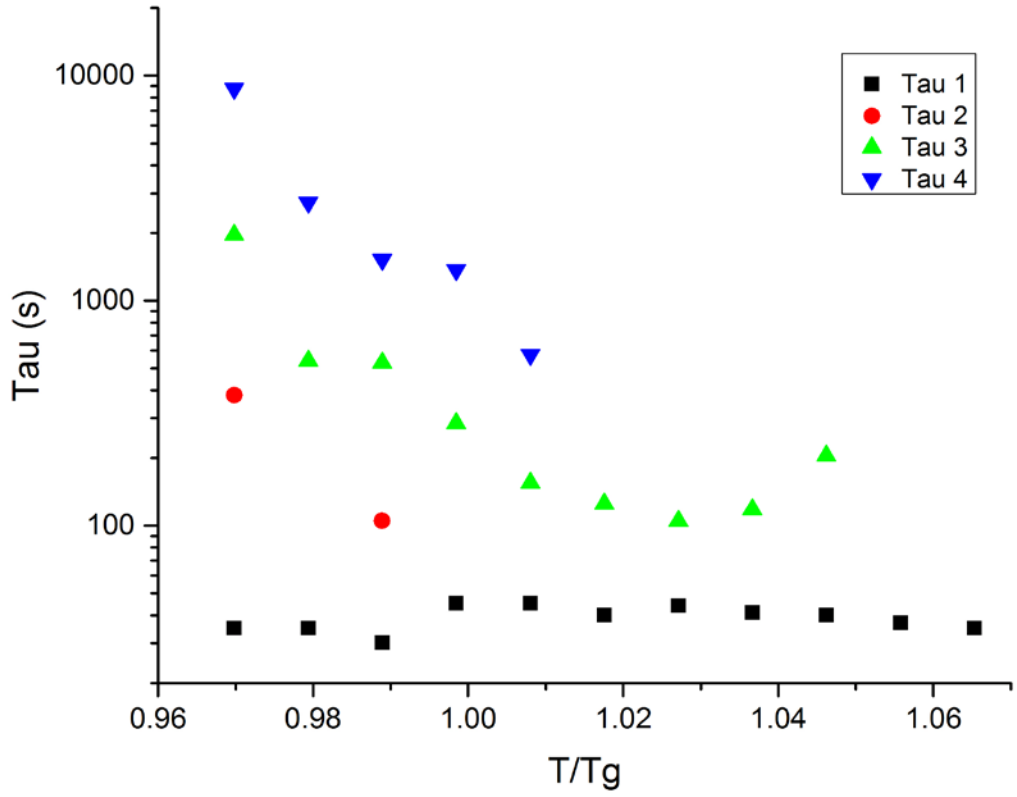

Figure 4.27: Relaxation time versus T1/Tg,d in $Ge_{17.9}As_{19.7}Se_{62.4}$ for ΔT = 10 °C

One of the major things to notice in these spectra is that all of the chalcogenide glasses reaches single exponential behavior by just above a T_1/T_g of 1.00. Although N-BK7 did not display single relaxation behavior within the temperature range measured, it was projected to reach that point at ~ 1.06 or T_1 = 891 K (618 °C). The Ge-As-Se glasses reach single exponential behavior at a $T_1/T_{g,d}$ range of 1.02-1.05, highlighting the similarities in relaxation time behavior between glasses in different families. Similarities in trends and behaviors over wide ranging glass compositions suggests the future ability to generate models and explanations of structure that apply on a fundamental level. The

ability to extend structural relaxation models to glasses from various families would be a large scientific and technological advantage.

Next, it is important to notice, that the relaxation times corresponding to the first peak seem to fluctuate differently than the longer time relaxation parameters. The Tau 1 does appear to undergo significant changes in the same areas of temperature as the other relaxation features, however, these changes are harder to understand. It is possible that the 1st set of relaxation times are somewhat limited in their sensitivity to structural change due to their proximity to the beginning of the test. As described in Section 3 of this chapter, analysis using the Prony series is carried out on data that has had the effects of CTE removed. This means that purely configurational relaxation remains. The proximity of the 1st set of relaxation times to the beginning of the test and the removal of the linear thermal expansion may in some way cause the 1st relaxation times to be artificially stable, especially when the overall relaxation behavior is described by several relaxation times. As the relaxation times of an exponential term decreases, that exponential begins to look more and more like a very steep straight line, to the point that a fast relaxation could be approximated by a straight line. It is unclear if the removal of the linear portion of instantaneous thermal expansion by parsing the data after the time at which it reaches thermal equilibrium in some way causes an inability to accurately view trends in the first relaxation. This is a potential limitation of this method.

Additionally, as can be seen in each of these cases, the steady decrease in number of relaxation peaks as the temperature increases is a phenomenologically important observation. The longer time peaks lose significance until they disappear. This supports

the idea of temperature dependent constraints.[102,108-110] An alternative view is the ELT which leads to many of the same conclusions as constraint theory. The metabasins which form structures or regions, relax when under enough pressure from thermodynamic changes. As the temperature of the test increases, the amount of energy within the glass network also increases. At certain energies, in the region of T_g and $T_{g,d}$, ergodicity is restored. The enthalpy landscape that dictates the configuration of the glass network does not necessarily change with temperature, but the amount of energy that the material has to move from one energy basin to another in the landscape is increased. With an increased overall energy the components of the glass have an increased probability of escaping from their energy basins into a more favorable configuration.[84] Constraints are essentially the product of the enthalpy landscape that causes certain structures to be formed. When the constraints holding a region or group of structures together dissolve, that structure is no longer an independent relaxing region and then devolves in the relaxation behavior of smaller regions or structures held together by higher temperature/energy constraints. This explains why the number of detectable relaxation events decreases towards one as the temperature is increased. Evidence for this interpretation in the data, can be seen in the plots of relaxation time versus $T_1/T_{g,d}$.

The presence or absence of certain relaxations is conspicuously noticed when they appear inconsistent. For instance the Tau 2 feature in Figure 4.27, at the lowest measured temperature the relaxation is described by four relaxation times. However, the next temperature does not contain that relaxation time. The disappearance of relaxation time with temperature is not surprising based on the arguments submitted above, but the

reappearance of a relaxation time could be viewed as unexpected. The enthalpy landscape argument is again valid. At the lowest temperature the landscape is such that the mechanism for relaxation is probabilistically favored. The next highest temperature leads to a thermodynamic state that does not make the mechanism that leads to that relaxation likely. Then as the temperature increases that relaxation is again facilitated by the enthalpy landscape and is experimentally detectable. This phenomenon is seen once in the case of $Ge_{17.9}As_{19.7}Se_{62.4}$ and there is an instance of a relaxation time appearing only once in the case of $As_{20}Se_{80}$ as shown in Figure 4.26.

Another interesting behavior seen in the relaxation times is a region where the slope of the times undergoes a rather abrupt change. This artifact appears in all 3 compositions at a $T_1/T_{g,d}$ of ~ 0.96 for $As_{40}Se_{60}$ and $As_{20}Se_{80}$ and ~ 0.99 for $Ge_{17.9}As_{19.7}Se_{62.4}$. At least one peak in each composition shows a plateauing of the relaxation time with respect to temperature. All of the samples measured to comprise this data were fitted with the same routine, but between the compositions there is a wide range of test temperatures. The fact that this "jog" in the slope of the relaxation times occurs in a similar $T_1/T_{g,d}$ window for each composition lends credence to its validity as a discrete behavior that occurs in all of these glasses when approaching $T_{g,d}$. It is possible that this flattening of the curve could be indicative of the glass network beginning the transition from a glass to a super cooled liquid. There is evidence in the literature to support the perspective of viewing these glasses as a mixture of glass and super cooled liquid while in the transition region.[64] A possible description of the cause for this type of trend could be found by considering the disposition of the glass kinetics at low, medium, and high temperatures within the measured

region. On the lower temperature end of the experiments, the time to completely go through structural relaxation became prohibitively long from an experimental point of view. The viscosity and density of the glass increased as the temperature decreased, this leads to the restricted kinetics that make the glass possible in the first place. At these high viscosities the changes in density of the glass network are more meaningfully than changes in the kinetics. Below a certain temperature there is almost no movement on the 10s of hours' time scale, but as the temperature is increased towards T_g the density begins to reduce more quickly with temperature, deviating from its low temperature linear path. Figure 3.1shows a representation of property change versus temperature, in the case of density it is displaying a reciprocal density trend. There may exist a region where the change in density dominates the relaxation time behavior. At a certain point the kinetics take over as the dominant relaxation time determinant. The slopes of the low temperature sections of the relaxation time curves in question are higher than the slopes after the plateau region, this would also support the idea of density controlled relaxation times at lower temperatures and kinetics controlled relaxation times at higher temperatures. In the region where the effect of density or, inversely, free volume would dominate, the relaxations would occur due to movements of atoms or structures from configurations of higher energy to those of lower energy with little cooperation from neighboring atoms or structures. The amount of space in which to relax would have the dominant impact on the speed of relaxations causing them to be highly sensitive to temperature. At a certain temperature, the amount of cooperative movement on the part of neighboring atoms or structures would increase to the point of having almost as much impact on relaxation times as the amount

of space in which to move. This corresponds to the flat region of the curve when the density or amount of space in which to move is no longer restricting the relaxation, but the kinetics still are. Then the higher temperature side of the experimental space is comprised of dominant kinetics increasing relaxation speed until only one, single exponential relaxation event suffices to provide all of the necessary configurational change with changing thermodynamic state (i.e. temperature).

A useful exercise is the comparison of this feature between the chalcogenide compositions considered here. This comparison would be useful here, but will carry more meaning if dealt in Section 6.4 expanding on the meaning of relaxation time with temperature.

6.3 Relaxation weight observations

The second parameter to analyze is the weighting term of each peak. These weights show the strength of the relaxation features relative to all other relaxation features. When a relaxation time has a significantly nonzero weight it contributes to the relaxation behavior of the material. This is the second parameter that can be plotted as a function of temperature and used to identify the relaxation behavior of certain structures within the glass. Although the weights are Prony series parameters, it is anticipated that they may hold somewhat less direct correlation to physical properties because they simply indicate the relative importance of each relaxation time. For the present state of discussion the weights will be used in a utilitarian manner to better understand the evolution of the peaks

as described by their corresponding relaxation time. Figure 4.28 is a plot of the weights versus $T_1/T_{g,d}$.

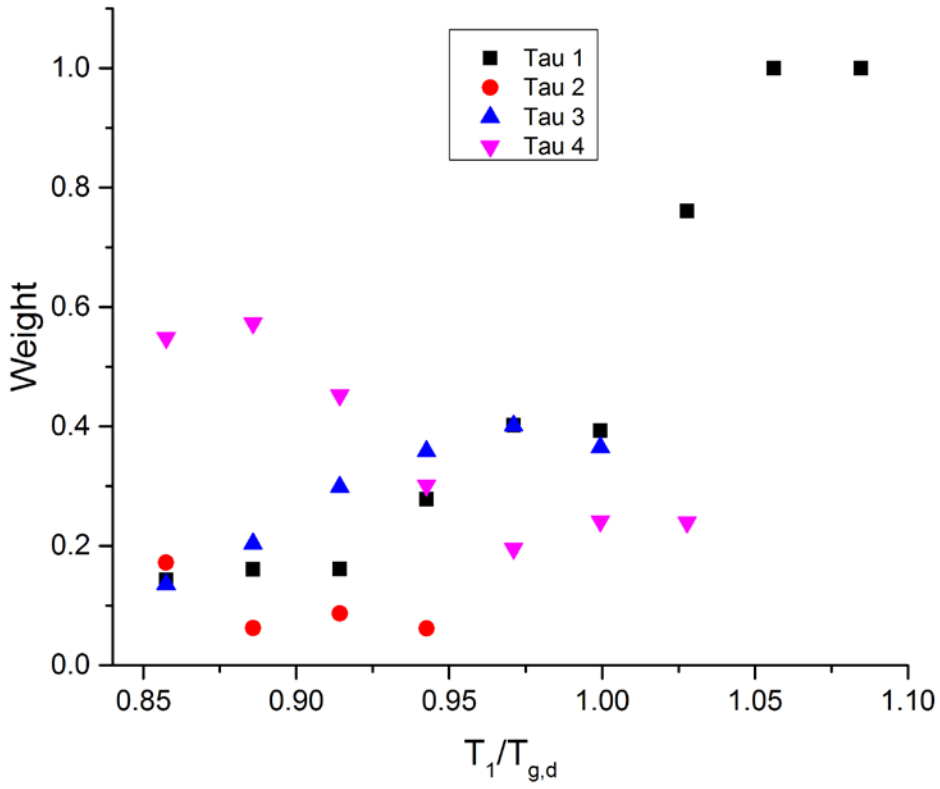

Figure 4.28: Weights versus normalized temperature in $As_{40}Se_{60}$ for ΔT = 10 °C

The weights shown above display a couple of important, though obvious trends. The first and most noticeable is the weight behavior of the peak corresponding to Tau 1. The first peak steadily increases in weight, eventually becoming 100% of the relaxation behavior at the highest temperatures. This trend is predictable without even plotting the weights. The next trends that present themselves are the other three relaxations that show unique behaviors. Weight 2 and 4 both immediately decrease with temperature until they disappear, while weight 3 initially increases until just before $T_{g,d}$ and then begins

decreasing as it remains alone with the first relaxation peak, disappearing soon after, as the shortest time relaxation dominates at high temperatures. In addition to providing some insight as to the order in which relaxations disappear, the weight trends also help ensure that the relaxation time peaks are correctly designated. It would often happen that the correct designation for relaxation peaks would not be self-evident at the outset. For instance, if the relaxation behavior goes from 4 to 3 peaks as temperature increases, it is not always clear from the relaxation time trends which peak it is that ceases to exist. The weight trends help identify which peak is headed towards insignificance more imminently and aid in validating or invalidating theories originally identified from the relaxation time trends.

The Prony weights for the remaining compositions are plotted below in Figure 4.29 and Figure 4.30. Having established the viewpoint from which these are discussed in the $As_{40}Se_{60}$ case, the plots below can be discussed properly.

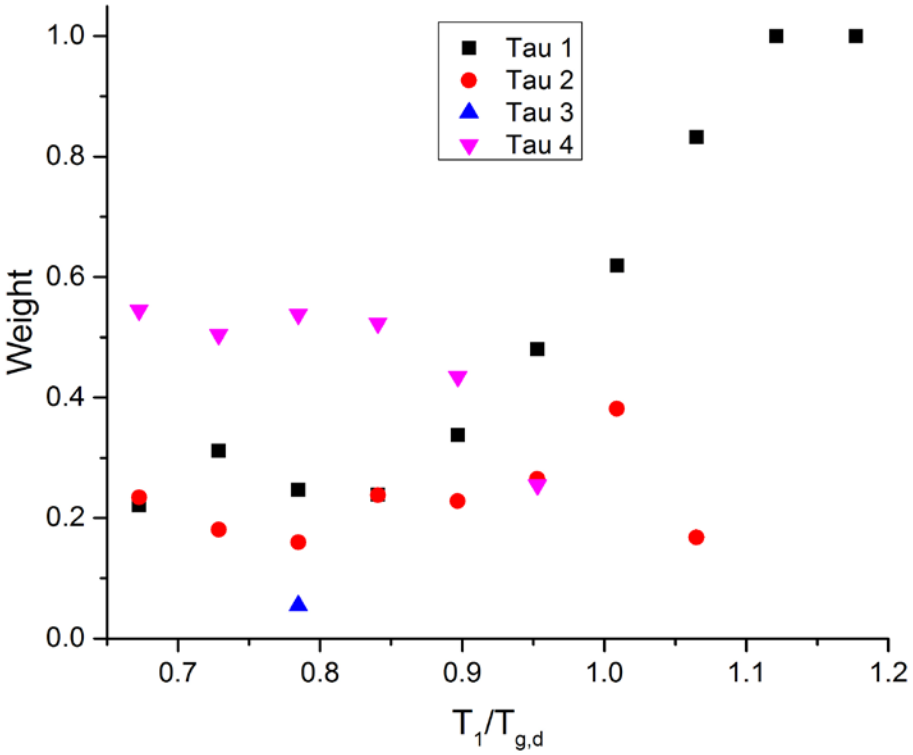

Figure 4.29: Weights versus normalized temperature in $As_{20}Se_{80}$ for ΔT = 10 °C

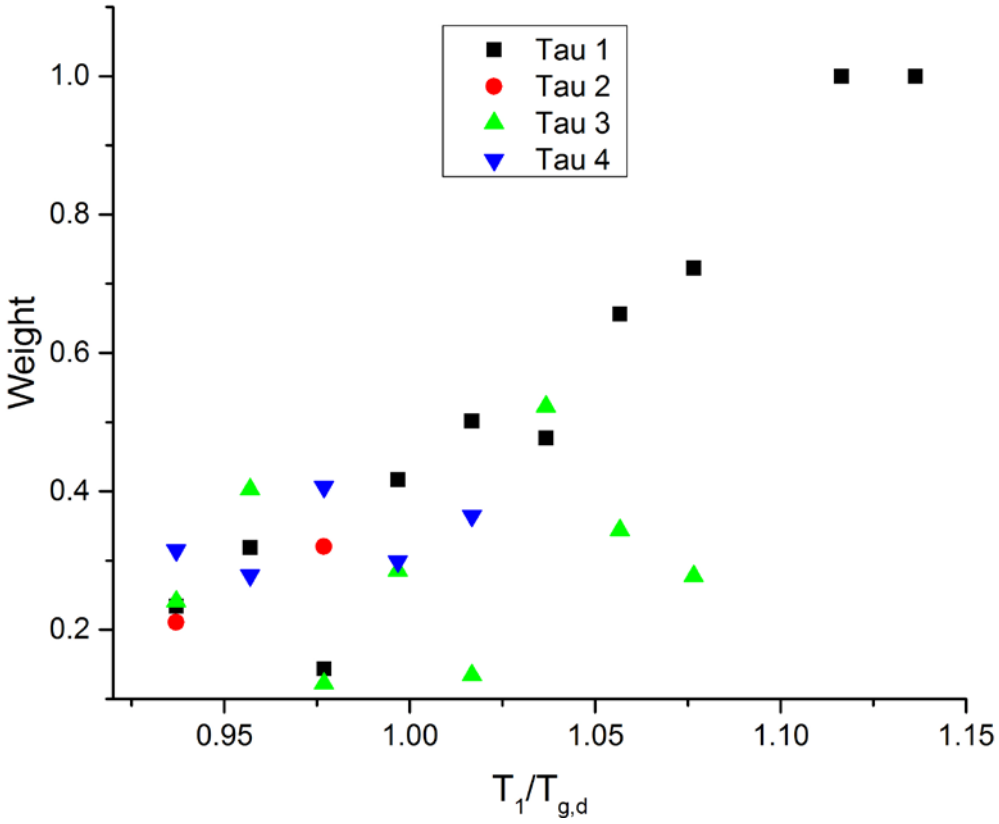

Figure 4.30: Weights versus normalized temperature in $Ge_{17.9}As_{19.7}Se_{62.4}$ for ΔT = 10 °C

The Prony weight and relaxation time trends of this specific glass can be modeled as functions of time and temperature similar to the procedure carried out on N-BK7. The main difference is that many of the trends for this chalcogenide glass are not linear, but as far as re-creating a relaxation "model" it is not crucial to understand what form the changes in weight and relaxation time take. As long as there is a function such as an exponential or polynomial that can fit them and be used to recreate the entire relaxation region of interest, that is enough for modeling. This is a useful result and is the first comprehensive model of volume relaxation developed to predict structural relaxation changes for a specific glass given various inputs such as quench rate and annealing time etc. This is the

engineering outcome of the work done on this topic. There is however, a scientific end in mind and that is the direction we will turn now.

The plot of weight versus temperature trend for $As_{20}Se_{80}$ shows an interesting result (Figure 4.29). The first feature that stands out is the appearance and disappearance of "peak 3". This relaxation appears when $T_1/T_{g,d}$ = 0.785 and then disappears at the next highest temperature. Figure 4.26 shows that the relaxation time associated with this peak lies directly between the relaxation times of peak 2 and peak 4. Using an ELT point of view, it could be said that a specific metabasins corresponds to the lone peak. The disappearance of this MB that specific relaxation cease to exist.

The relaxation weights equate to the relative contribution of each relaxation event to the total relaxation behavior. It is difficult to draw concrete meaning from them when taken by themselves. The fact that they are relative means that an increase in one weight could be the increase in prominence of that relaxation due to the increased number of these structures or increased strength of the structure itself. Conversely an increase in weight could be simply indicative of the disappearance of a different mechanism. So a given weight could increase because the relaxation it describes becomes more prominent or because one or many of the other relaxations become less so. When taking the idea of the Prony series as a description of the material behavior, the weights correspond to the spring behavior in Figure 4.4. The equations describing the relations between the various spring elements are discusses below. The result is that they are all dependent on one another. No specific spring constant values can be derived from the relative weights without knowing at least one of the elements. If you assume the Generalized Maxwell model, physically

shown in Figure 4.4, then Equation 62, is valid, where *F* is the thermodynamic force on the system.

Equation 62

$$F(t) = F(0) * \sum_{i=1}^{N} w_i * e^{-\left(\frac{t}{\tau}\right)}$$

At time = 0, the force on the system is entirely dictated by the spring elements in the Generalized Maxwell model, because the relaxation mechanism (i.e. the dampers/dashpots) have not relaxed at all. Given this fact, the force at time = 0 can be defined as Equation 63, where *x* is the maximum instantaneous displacement of the system away from equilibrium at the moment the temperature of the material is changed, k_i is the spring constant. Although the displacements of each element are independent in time, at the exact moment of initial displacement they all experience the same displacement from equilibrium.

Equation 63

$$F(0) = k_1 * x + k_2 * x + k_3 * x + k_4 * x$$

Given that the weights are the relative amounts of relaxation between any number of relaxation mechanisms, they also define the initial force distribution between the spring elements such that Equation 64 is the case.

Equation 64

$$k_i * x = w_i * F(0)$$

If there exists a system of equations for i = 1-4, and assuming that none of the spring constants are zero, you can, at best reach a ratio of spring constants. For instance, if *i* is one of the spring components, and *j* is one of the spring components but $i \neq j$, then Equation 65 is true.

Equation 65

$$k_i = \frac{w_i}{w_j} * k_j$$

This allows for comparison between spring constants not the direct determination of the values of spring. If one of the effective spring constants was able to be determine, it would be possible to get the rest. This is an area of work that could lead to future scientific gains in understanding relaxation mechanisms.

6.4 Effective enthalpy of relaxation

The relaxation times observed in this experiment have a strong dependence on temperature. If structural relaxation is considered to take place through a process of atomic or molecular motion within a viscous, though super cooled liquid, it should at least loosely resemble the process of diffusion. The speed of a species diffusing through a material, the diffusivity as it is known, is typically described as an exponential function of temperature.

The question then becomes, can relevant information like the activation energy of the mechanisms be used to describe the structure that is relaxing? When analyzing the results of experiments that have not been done before, at least with the same perspective and intent as the experiments detailed here, it is paramount to begin analysis from the most

direct sources. That is to say, to glean as much meaning and base as much of the conclusions as possible on first tier data or data that is directly gained from experiments. An analogy would be, a person would not measure the temperature of a cup of coffee by timing how long it takes for an ice cube to melt in the coffee. That would work but it's much easier to use a thermometer. Likewise, in the case of these relaxation experiments, the parameter that is most directly related to the material being measured is the set of relaxation times. From this we can calculate the activation energy needed for relaxation using the idea of relaxation as a thermally-activated process.

Equation 66 is known as the Eyring equation, it is commonly used to describe the rate of an occurrence of reactions within a material. The Eyring equation is related to the Arrhenias equation and has a similar form. The use of this equation is predicated upon something called Transition State Theory (TST).[111] TST is a statistical mechanically derived expression that relates rates of reactions to activation enthalpy (ΔH), activation entropy (ΔS), as well as Gibbs energy of activation (ΔG). Essentially this means that structural relaxation of these glasses is comprised of a number of Arrhenian or very nearly Arrhenian processes that act at the same time to cause structural relaxation. In this equation $1/\tau$ is the rate of reaction or occurrence in time^{-1}, k_b is the Boltzmann constant (1.381 x 10^{-23} J/K), ΔG is the Gibbs energy of activation of relaxation, R is the universal gas constant (8.314 J/mol*K), h is Planck's constant (6.26 x 10^{-34} J*s) and T is temperature in Kelvin.

Equation 66

$$\frac{1}{\tau} = \frac{k_b T}{h} e^{\left(\frac{-\Delta G}{RT}\right)}$$

Calculation of activation is done by fitting the change in relaxation times with temperature. A convenient feature of Equation 66 is that when the reaction rate multiplied by *1/T* is plotted as a natural log versus *1/T* the relevant energies can be determined with relative ease. Equation 70 shows the form that the plot must take to make the calculations described above. If relaxation time or $1/\tau$ were plotted versus *1/T*, that plot could be fit with an exponential and the parameters extracted in the form of Equation 66. However, exponential fits cannot be applied to a data set with only two points. The Gibbs free energy or the Gibbs energy of activation can be expressed as a combination of temperature, enthalpy and entropy. Equation 67 gives the well-known relation.

Equation 67

$$G(p,T) = H - TS$$

When expressed in terms of a change in Gibbs energy, the enthalpy and entropy become changes also, as in Equation 68.

Equation 68

$$\Delta G = \Delta H - T\Delta S$$

Substituting that expression into Equation 68 yields Equation 69, which upon dividing by *T* and taking the natural log of both sides yields the operative expression for this case, Equation 70 .

Equation 69

$$\frac{1}{\tau} = \frac{k_b T}{h} e^{\left(\frac{-\Delta S}{R}\right)} e^{\left(\frac{-\Delta H}{RT}\right)}$$

Equation 70

$$\ln\frac{1}{\tau * T} = \frac{-\Delta H}{R} * \frac{1}{T} + ln\frac{k_b}{h} + \frac{\Delta S}{R}$$

Plotting the natural log of *1/τ* times *1/T*, versus *1/T* means that any linear fit of the data will lead Equation 70 to be in the form of a standard "*y = mx+b*" format. The slope of any linear fit will be equivalent to Equation 71 and the "y-intercept" will be equal to Equation 72. Performing this operation means that calculation of the activation enthalpy and entropy is fairly straightforward and allows for the calculation from as little as two data points. This is necessary for the case considered here. Figure 4.31 shows the natural log of inverse relaxation times multiplied by inverse temperature determined from the Prony series fit of $As_{40}Se_{60}$ relaxation experiments plotted versus *1/T*, with *T* being in Kelvin.

Equation 71

$$m = \frac{\Delta H}{R}$$

Equation 72

$$b = \ln\left(\frac{k_b}{h}\right) + \frac{\Delta S}{R}$$

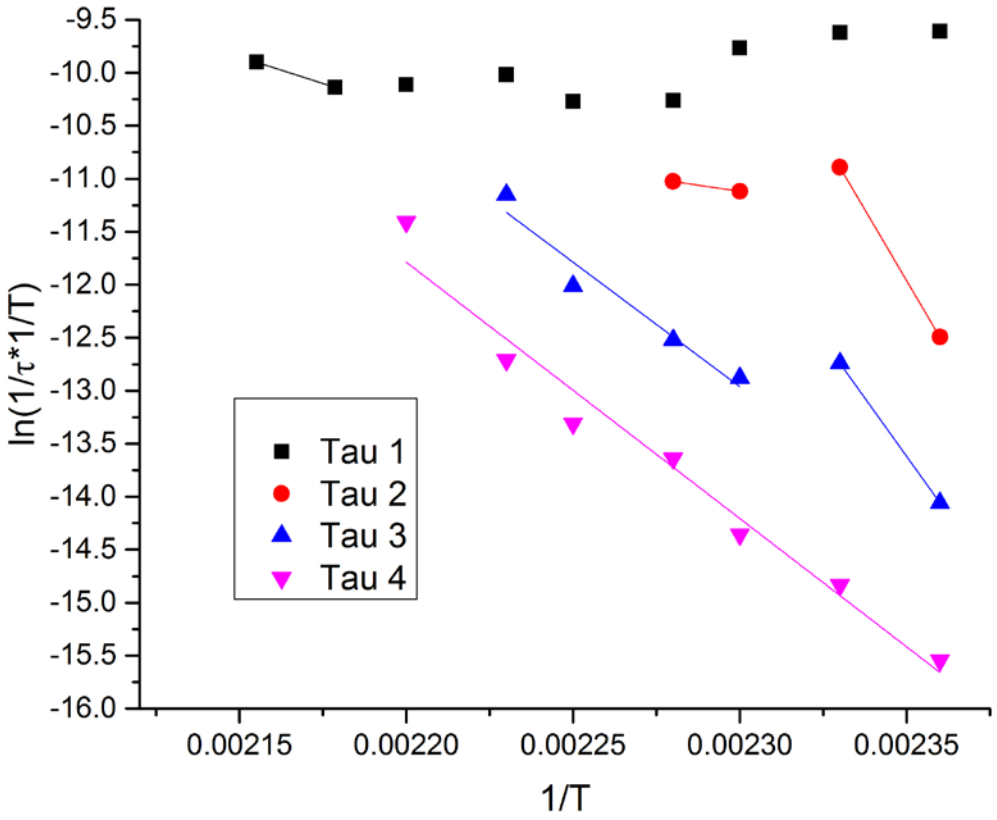

*Figure 4.31: Plot of natural log of 1/τ * 1/T versus 1/T for $As_{40}Se_{60}$ for ΔT = 10 °C with best linear fit lines*

The jog in the relaxation times which is believed to have resulted from a fundamental change in glass structure approaching $T_{g,d}$, means that there is a corresponding jog in Figure 4.31. This means that although a single linear fit may approximate the activation enthalpy and entropy of a given relaxation time trend, different linear fits must be used for the distinct sections in relaxation times, for a characterization of the abrupt change in relaxation time to be accounted for in the energy calculation. Earlier in this chapter the idea that this jog in relaxation times was due to a transition from a dominance of the density change with temperature to the dominance of kinetic movement of atoms and structures that allow one another to more cooperatively rearrange, was put forth. One

of the arguments against such a theory is that, while the 2nd and 3rd set of relaxation times change temperature dependent behavior from $T_1/T_{g,d}$ = 0.96 – 0.98, the 1st and 4th sets do not seem to be affected in the same way. The possible reason that the 1st peak does not fluctuate in an easily discernable way is discussed in Section 6.1 of this chapter. The stability of the slope of the 4th peak with temperature is most likely connected to a completely different phenomenon. One of the assumptions involved in analyzing these varying relaxation times is that the different sets of values correspond to different sizes or length scales within the glass network. A relaxation peak at a longer time should correspond to a larger mechanism or structural unit within the glass. If this is indeed the case, then it would follow that the 4th relaxation peak corresponds to the largest mechanism in the glass. The size of the mechanism connected to the 4th peak may be larger than the others to such an extent as to behave in a different way than the other features. At a larger size the 4th peak operates on perhaps an intermediate range scale where the transition of the material at a localized level may not have an observable effect on the timescale of relaxation. Another possible cause altogether is the fact that in $As_{40}Se_{60}$, evidence has been observed of a flattening out of the pinched "puckered-layer" sheets of As-Se.[50] As temperature increases towards T_g, the puckered layers flatten out, order decreases within each layer, this allows for greater ordering between different layers which can now stack more effectively. If the effects of the long time peak of relaxation are due to a phenomenon such as layer stacking, the fact that the long time peak does not participate in the disjointed behavior of the other peaks could be explained.

A separate issue is the 1st peak trends with temperature. In order to properly calculate an activation energy there must be a reasonably clear trend that appears as the temperature changes. The 1st peak does not display a satisfactorily consistent trend until it is the only peak left to describe relaxation. This is also the case in which the relaxation trend is least effected by any other factors, for this reason the activation enthalpy and entropy of the 1st peak are calculated from the two points that exists in temperature after all other relaxations have ceased to be detectable. Figure 4.32 and Figure 4.33 show the reaction rate plots versus temperature for $As_{20}Se_{80}$ and the Ge-As-Se composition respectively.

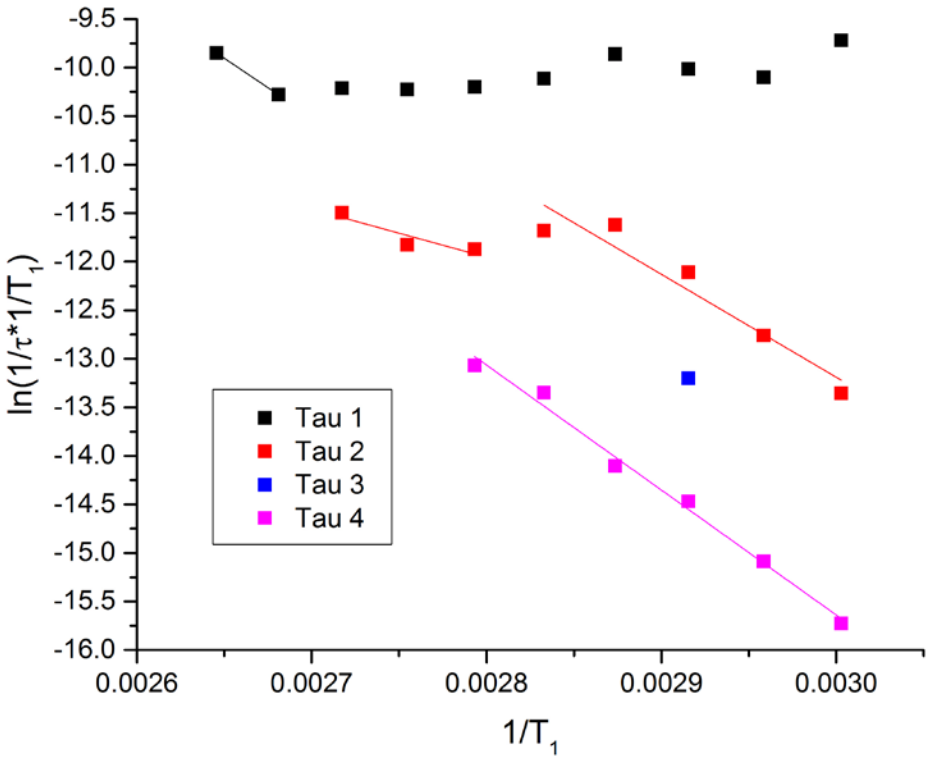

*Figure 4.32: Plot of natural log of 1/τ * 1/T versus 1/T for $As_{20}Se_{80}$ for ΔT = 10 °C with best linear fit lines*

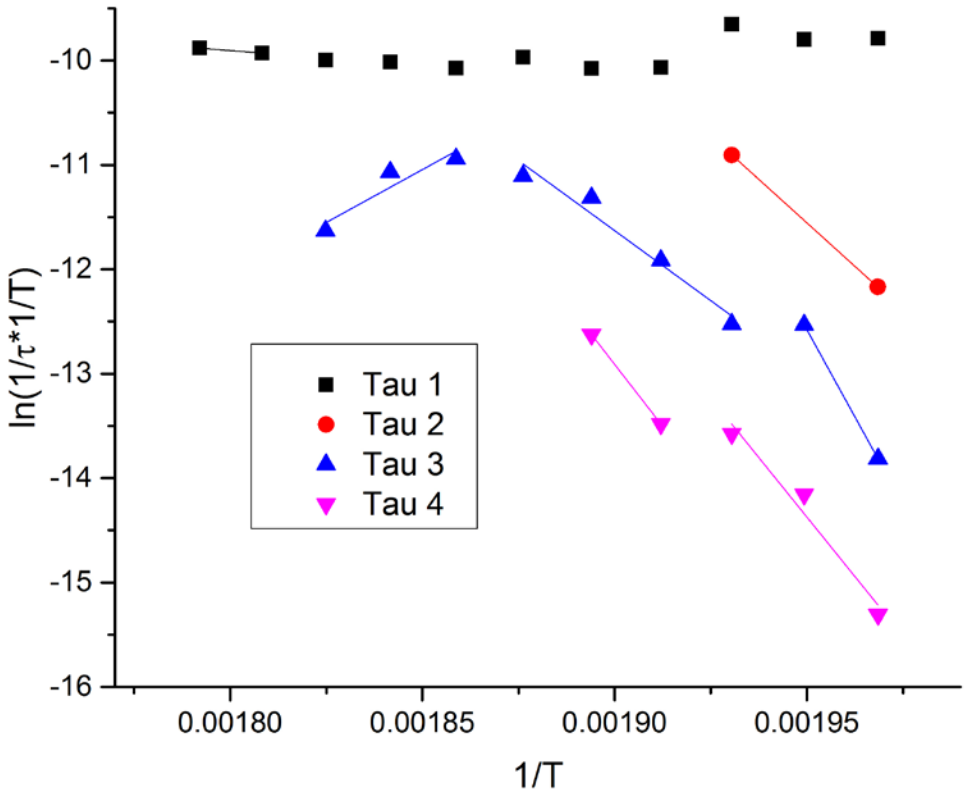

*Figure 4.33: Plot of natural log of 1/τ * 1/T versus 1/T for $Ge_{19.7}As_{17.9}Se_{62.4}$ for ΔT = 10 °C with best linear fit lines*

The same trend observed in Figure 4.25, Figure 4.26, and Figure 4.27 are observed in the plots above. There is a definite jog in the behavior of relaxation times as the glass approaches the transition temperature. All of the glasses experience the beginning of this transition from between .96 and .98 T_1/T_g and exit the transition zone from around .98 to 1.00. Something interesting about the perceived transition is that the feature appears to be "sharpest" or most abrupt in the Ge-As-Se glass and least defined in the $As_{20}Se_{80}$ glass. The nature of this transition appears to follow the general trend of coordination number, with the higher coordinated Ge containing glass experiencing a more abrupt change in

behavior through the transition. $As_{20}Se_{80}$ contains much less rigidly constrained structures and so it appears as if the transition is a more gradual process, most likely due to the presence of Se-Se bonds that have a higher degree of flexibility than As-Se or Ge-Se bonds. The width of this transition is ~ 10 K for Ge-As-Se, ~ 11 K for $As_{40}Se_{60}$ and ~ 18 K for $As_{20}Se_{80}$.

The next step in the calculation of relaxation characteristics is to convert the fitting parameters found from the fits in Figure 4.31, Figure 4.32, and Figure 4.33 to enthalpies and entropies of activation and then to Gibbs energy of activation. This process will be demonstrated for $As_{40}Se_{60}$, the process is the same for all compositions and the results will be shown for each composition. First, the fitting parameters must be converted into useable values. Equation 71 and Equation 72 can be solved for the enthalpy of activation (ΔH) and entropy of activation (ΔS) in order to obtain those values for each fit. Equation 73 and Equation 74 are the result of that solving.

Equation 73

$$\Delta H = m * R$$

Equation 74

$$\Delta S = \left[b - ln\left(\frac{k_b}{h}\right)\right] * R$$

Table 4.4 shows the fitting parameters and fitting errors, note that fitting between two points produces no fitting errors that is why some of the values show no error. The combined error from the relaxation time uncertainty which is ~ 7.5% is incorporated into

the enthalpy and entropy calculations. For plots of the enthalpy and entropy of activation error bars are shown, unless the error is within the size of the data point.

Table 4.4: Activation enthalpy and entropy of $As_{40}Se_{60}$ for ΔT = 10 °C

i	m_i	Fitting Error ±	ΔH (kJ/mol)	Fitting Error ±	b_i	Fitting Error ±	ΔS (kJ/mol*K)	Fitting Error ±
1	-10070.07		83.72		11.80		0.11	
2a	-53460.33		444.47		113.67		0.96	
2b	-4649.00		38.65		-0.43		0.01	
3a	-43892.00		364.92		89.53		0.76	
3b	-23491.33	3849.98	195.31	-16.00	41.07	8.72	0.35	0.04
4	-24193.35	1873.75	201.14	-7.79	41.44	4.27	0.36	0.02

The data from Table 4.4 is then used to calculate the Gibbs energy of activation using Equation 68. The Prony weight terms define the percentage of the total relaxation that is carried out by each mechanism, associated to each relaxation time. If this reasoning is carried further, it can be assumed that for each mole of material, a given relaxation mechanism makes up a fraction of the relaxing species in that mole of material equal to its Prony weight. Using this idea, the amount of enthalpy and entropy for a given relaxation in a mole of material should be equivalent to the enthalpy and entropy of the relaxation mechanism time the Prony weight. This calculation was done for the values from Table 4.4 and using the weights for $As_{40}Se_{60}$ from Figure 4.28. The results of these calculations are plotted below. Figure 4.34 contains the enthalpy of relaxation versus $T_1/T_{g,d}$ for $As_{40}Se_{60}$, Figure 4.35 contains the entropy times temperature versus $T_1/T_{g,d}$, and Figure 4.36 contains the Gibbs activation energy for the same material versus $T_1/T_{g,d}$.

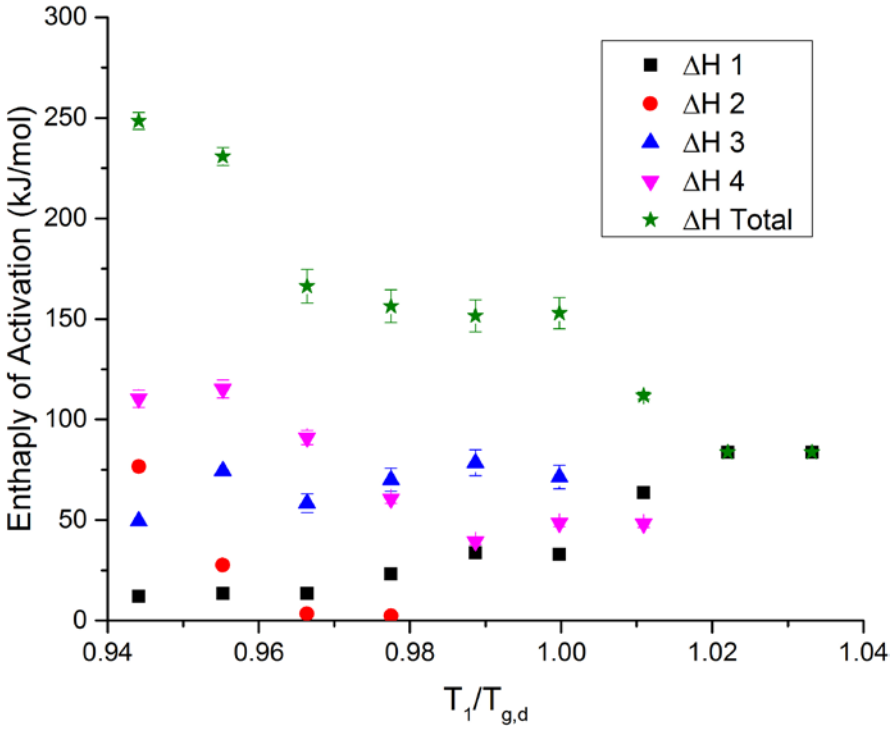

Figure 4.34: Enthalpy of activation vs $T_1/T_{g,d}$ of $As_{40}Se_{60}$ for ΔT = 10 °C

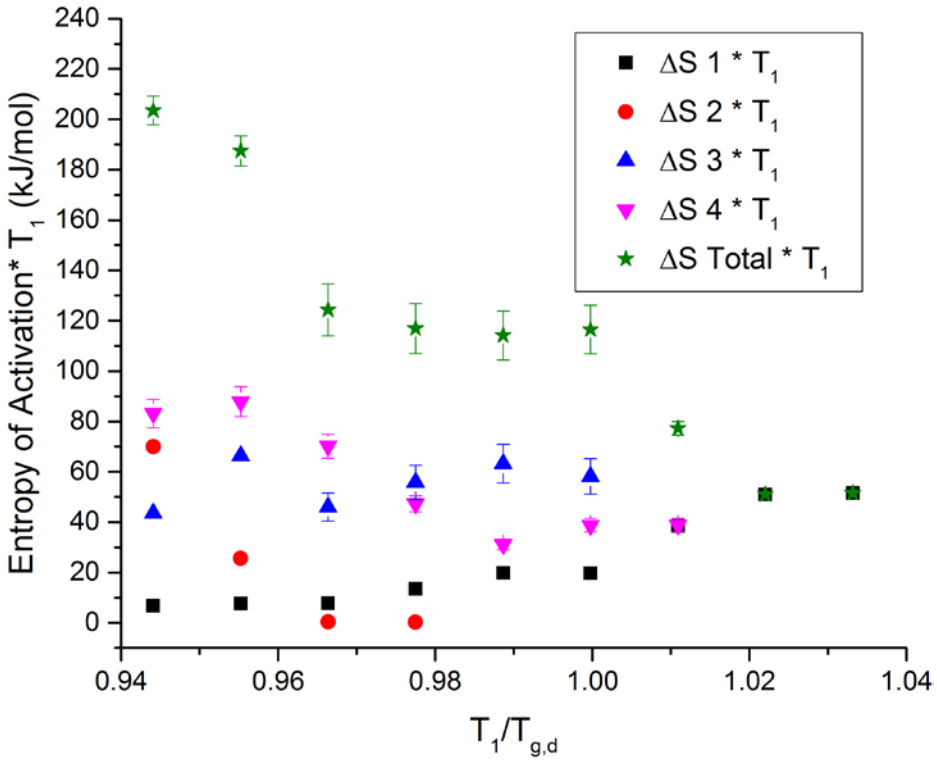

Figure 4.35: Entropy of activation vs $T_1/T_{g,d}$ of $As_{40}Se_{60}$ for ΔT = 10 °C

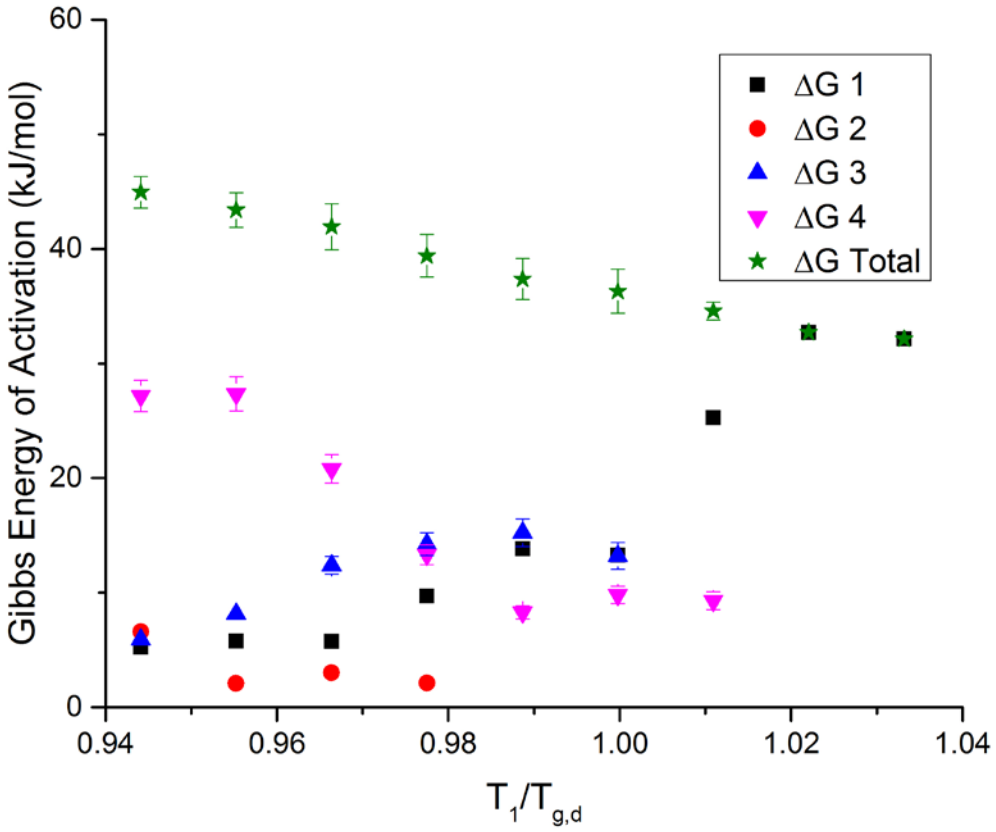

Figure 4.36: Gibbs Energy of activation vs $T_1/T_{g,d}$ of $As_{40}Se_{60}$ for ΔT = 10 °C

What is immediately noticeable for Figure 4.34 and Figure 4.35 is the seeming discontinuity that resembles the jog in relaxation times seen earlier in this chapter. This is related to the change in behavior seen in the material as it passes through the transition region. However, once the entropic component is removed from the enthalpy of activation, the resulting Gibbs energy of activation is smoothed of these discontinuities and results in a more continuous trend through the transition region. Another interesting note is that the maximum enthalpy of activation is a very similar value to the activation energy term calculated in Section 6.1 for $As_{40}Se_{60}$. This reinforces the idea that approximation of activation energy needed for structural relaxation is definable from a number of different

methods using the same set of data. The Gibbs energy of activation is shown below in Figure 4.37 for all the compositions in question.

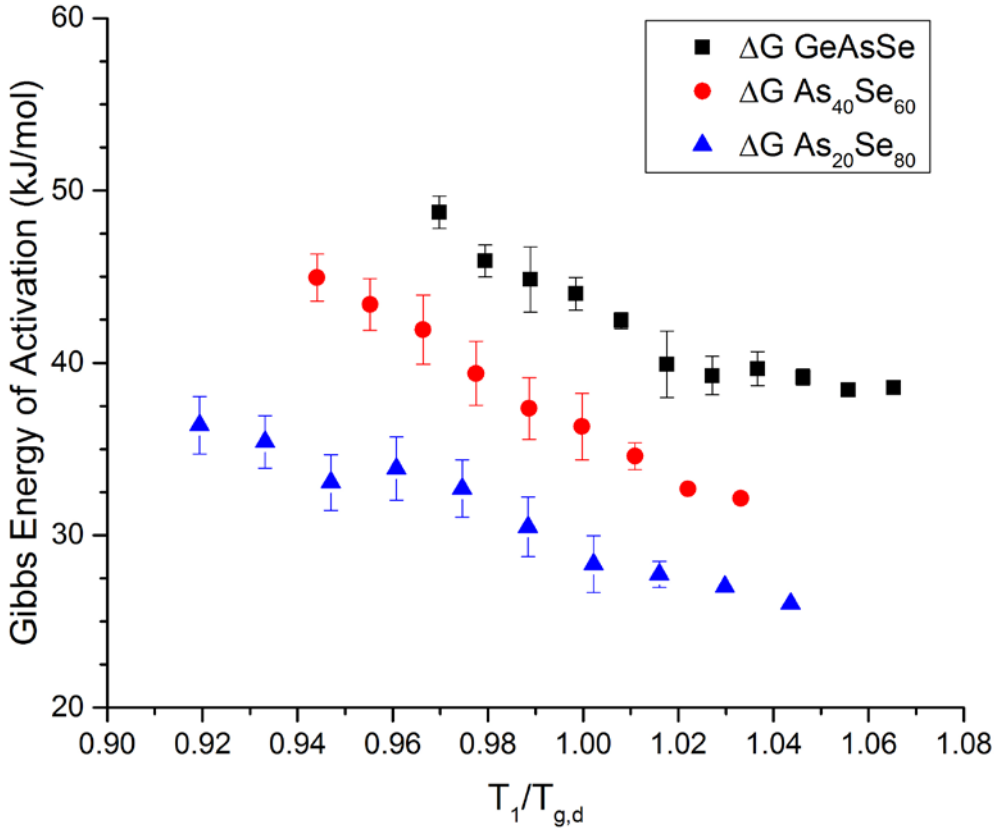

Figure 4.37: Gibbs Energy of activation vs T1/Tg,d of all compositions for ΔT = 10 °C

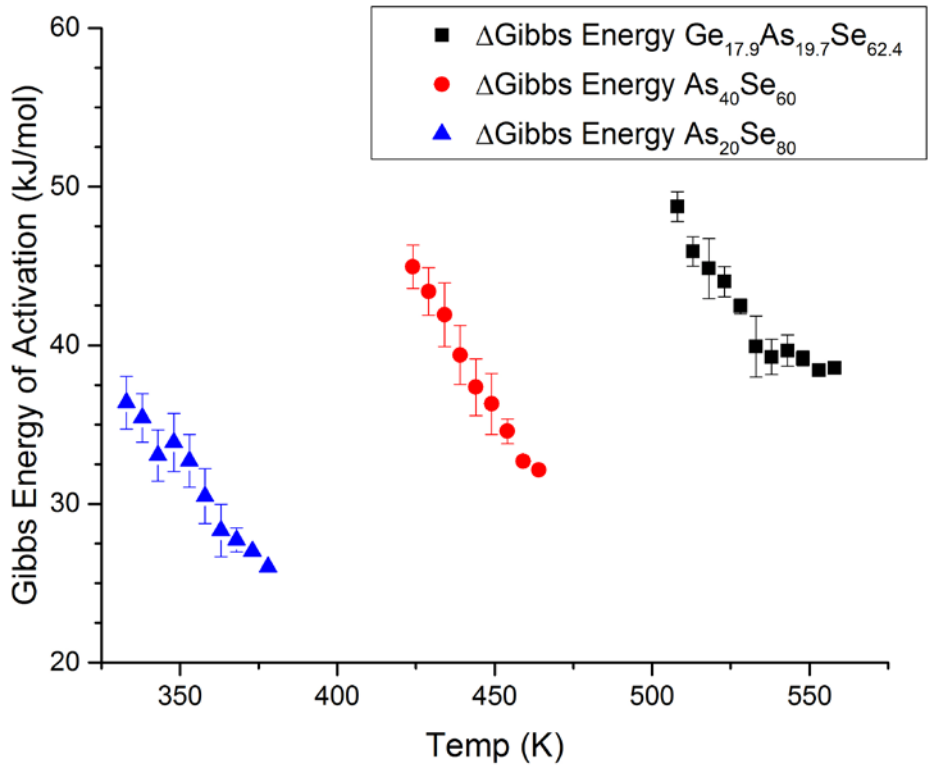

Figure 4.38: Gibbs Energy of activation vs temperature of all compositions for ΔT = 10 °C

The significance of Figure 4.37 is two-fold; first it confirms what is intuitively expected from a coordination number and connectivity argument, that the higher CN glasses have higher activation energies at a given temperature. In addition each composition displays a "jog" in their behavior as temperature increases through $T_{g,d}$. The abrupt change in energy of activation can be seen more clearly in Figure 4.38. This shows a change in the amount of energy per degree of temperature and is analogous to the jog and subsequent transition shown in relaxation times. The increasing energy with decreasing temperature means there will be a point at which the energy needed for relaxation will be

prohibitively high. This relates to the continual reduction in configurational freedom as the temperature is decreased. The significance of this is discussed further in Section 6.5. This could have huge implications for the glass community as far as providing evidence of a real transition whether thermodynamic, kinetic or both in the glass that ensures the glass never obtains intrinsic properties more favorable than the crystal.

6.5 Entropy Change

The Kauzmann Paradox raised the question of whether or not the excess entropy that a glass has at T_g is continuously decreasing with temperature until it goes to an entropy below that of a crystal. Clearly the paradox cannot happen, the question of how this paradox is avoided was treated by many authors and theories detailed in Section 3 of Chapter 3. Kauzmann believed the material crystallized before reaching the paradox.[4] Adam and Gibbs theorized that the decreasing entropy of the glass would limit the number of configurations available to the glass until there was only one configuration left with an entropy at or just above the crystal.[1] This was predicated on the idea of a true second order transition somewhere between T_g and the Kauzmann temperature. Energy or Enthalpy Landscape Theory states that the configuration of the liquid above T_g and the glass below T_g is defined by a hypersurface of potential energy or enthalpy wells that determine the positions of atoms relative to one another.[2] This theory as a description of the glass transition temperature was further advanced by Carmi who defined a percolation temperature at which, when cooled, certain regions of the energy landscape would be rendered completely inaccessible to one another forming metabasins that would grow in either number or size.[3]

The result of all of these theories is a decreasing of the excess entropy with temperature either continuing steadily after a true thermodynamic transition at T_g or continuing steadily until a true thermodynamic transition at T_2 or T_K. This decrease in excess entropy is something that must necessarily happen. However, entropy is not something that can be measured as a direct value, it must be obtained through other means.

The data presented so far in this dissertation is related to how the glasses in question relax from one equilibrium thermodynamic state to another. That being the case, the relaxation times and weights and the properties derived therefrom all contain information on the kinetics of the system and any effects that the viscosity of the material has on the relaxation process. So not only does the data described so far contain information on potential thermodynamic specifics of the system, it contains path information on the transit from one thermodynamic state to another. That is why any information gleaned from the data presented so far cannot be considered purely thermodynamic in nature. There is however, a facet of these TMA experiments which directly samples the thermodynamic state or more correctly the change in thermodynamic state from one temperature to another. That data is the amount of configurational volume change taking place during an entire relaxation. The total change in height of the sample is a product of the difference in thermodynamic states between T_0 and T_1.

The total height change of each structural relaxation measurement, after removing the instantaneous and viscous flow aspects of the measurement, was obtained. These values were normalized by the initial room temperature height of the sample. The configurational change in height, related of course to the change in volume, is directly

proportional to a change in entropy between thermodynamic states. A logical case can be made that a decrease in configurational volume from one thermodynamic state to another will lead to a decrease in entropy. In a closed system, which can be assumed for this essentially solid material, less free volume means less available space for the material components to occupy and less configurations for it to sample. This means a decrease in entropy. The nature of the relation in a non-ideal gas case is not fully known, but the conclusion is reinforced by the ideal gas case. An ideal gas at constant pressure and temperature can be said to adhere to the volume-entropy relationship shown in Equation 75.

Equation 75

$$S_1 - S_0 = -R * \ln\left(\frac{V_0}{V_1}\right)$$

Figure 4.39 shows the change in length between thermodynamic states normalized by the initial sample height at room temperature for all chalcogenide glasses studied. Given that glass is amorphous, it is also considered isotropic, this means that a change in length is considered to be 1/3 the change in volume. The trends indicated by each composition are consistent with one another, they display a downward trend towards low temperature and an upward trend towards high temperature. The Ge-containing composition displays the most noticeable jog in behavior at ~ 1.01 $T_1/T_{g,d}$, this shows a marked shift in the behavior of the length/volume change for a given change in thermodynamic state. As noted in other experiments, the length change and therefore entropy change of the system decreases towards zero as the temperature decreases. The slopes of these trends are steep

enough to ensure, if a continuing linear trend is assumed, that the properties in questions will extend to the theorized T_K and T_2 points that are the subject of so much research.[1,4] Figure 4.40 shows temperature plots of the same data and the linear fits used to calculate the temperature at which the length/volume/entropy change would reach zero. If the lowest temperature linear portions of the curves in Figure 4.39 are fit and extrapolated to a length change of zero they result in the temperatures stated in Table 4.5. In addition, assuming that the point at which they reach or would reach zero if linearly extrapolated, is the T_2 of Bestul and Chang, the $T_{g,d}/T_2$ and T_g/T_2 values are calculated as well. The shape of the curve is displayed versus absolute temperature in Figure 4.40.

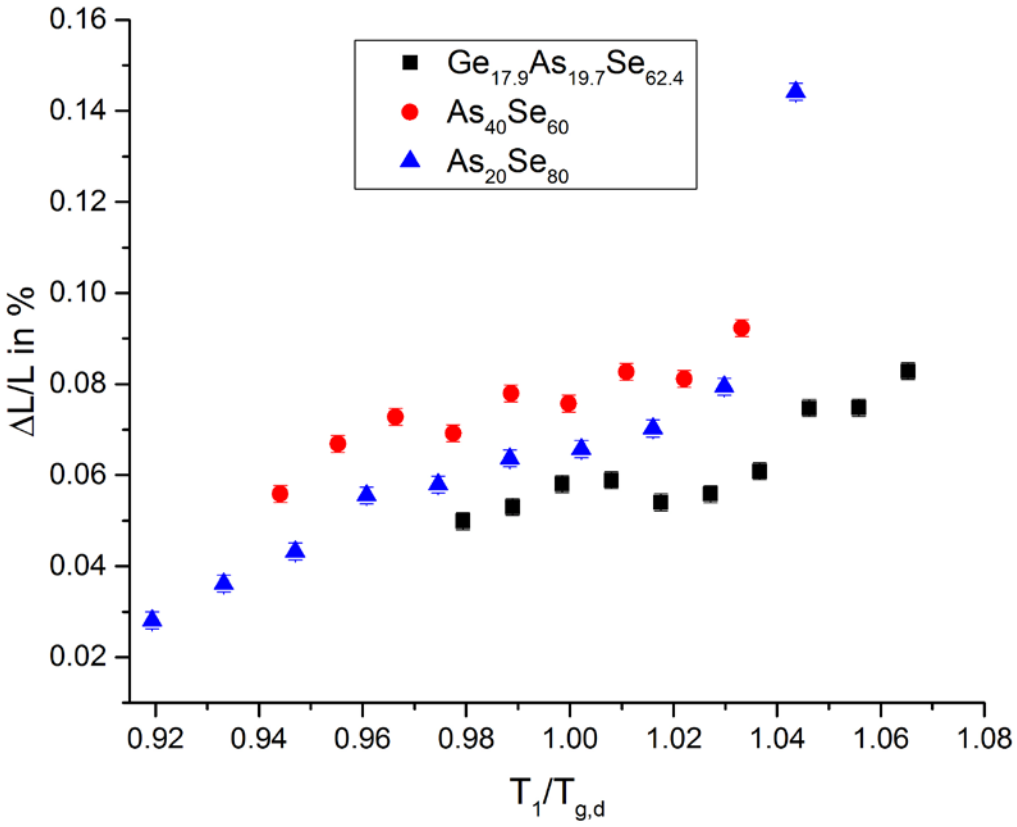

Figure 4.39: Percentage of configurational length change normalized by sample length versus $T_1/T_{g,d}$ of all chalcogenide compositions for ΔT=10°C

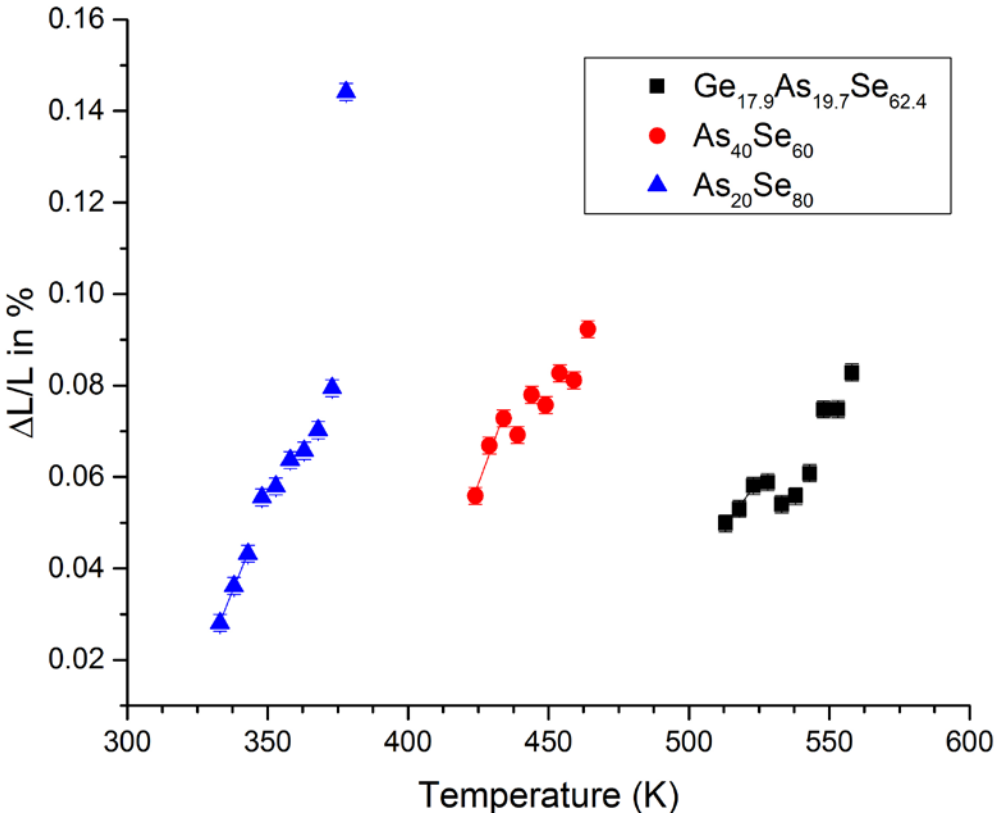

Figure 4.40: Percentage of configurational length change normalized by sample length versus temperature of all chalcogenide compositions for ΔT=10°C

Table 4.5: T2 and Tg/T2 ratios for all chalcogenide glasses studied

Composition	T_2 (K)	$T_{g,d}/T_2$	T_g/T_2	$T_{g,d}$-T_2 (K)
$Ge_{17.9}As_{19.7}Se_{62.4}$	452	1.158	1.205	71
$As_{40}Se_{60}$	391	1.148	1.183	58
$As_{20}Se_{80}$	315	1.149	1.197	47

The results of the T_g/T_2 calculation make sense in light of the arguments presented so far in this dissertation. The ratios listed in Table 4.5 are inversely proportional to the fragility trends of the glasses shown in Table 2.1. The inverse nature of the relationship

between fragility is well documented and commonly used as defined in Equation 76.[17,112,113]

Equation 76

$$m \propto 1 + \frac{c_p^{config}(T_g)}{S_c(T_g)}$$

Assuming a relatively similar rate of entropy loss with temperature, the glass showing the highest fragility and lowest T_g/T_2 value should be the same, which is indeed the case with $As_{40}Se_{60}$. The Ge-containing glass and $As_{20}Se_{80}$ follow T_g/T_2 trends are inversely proportional to their fragility trends.

In addition to having relative values that are reasonable when compared with fragility, the predicted T_g/T_2 values are of the same order of magnitude and in fact in close proximity to the same values calculated by Bestul and Change calorimetrically and by Adam and Gibbs viscometrically.[1,86] This is the first instance of volumetric structural relaxation data being used to calculate the T_g/T_2 ratio as far as this author knows. The configurational changes in volume shed light on changes in the excess entropy as the temperature is decreased.

7 Conclusion

The relaxation measurements carried out in the above sections answer a number of important questions about structural relaxation. The results show that this method does indeed contain relevant information about T_g and structural relaxations that take place near T_g. Clear indications of structural changes in the glass as well as marked transitions from

glassy behavior to liquid were evident. Additionally a two-fold description of structural relaxation extending to temperature well below T_g was obtained and support for current theories was noted. While the few prior studies using dilatometric structural relaxation experiments of this type had only ever been to a 1st order extent to utilize the TNM model. Extensive data analysis has led to insights never before examined or realized by any previous dilatometric studies. The use of a Prony series in the characterization of relaxation is not uncommon, however analysis of the Prony parameters as indicators of configurational change in a glass has not previously been employed to deconvolve structural relaxation data.

This work has shown that the dilatometric characterization method is easily adaptable to a predictive model with reasonable accuracy. From these investigations, the use of this model could be employed in applications that extend from annealing time predictions for bulk glass manufacturers to volume and shape change factors for manufacturing methods such as PGM. Detailed below are specific conclusions related to these findings that make up the unique contribution of this dissertation to our community.

7.1 Predictive models for structural relaxation behavior

The materials engineering goal of this dissertation was to construct a model enabling the prediction of configurational volume change with temperature. That goal was specifically targeted to N-BK7 oxide glass as a proof of concept material. Dilatometric structural relaxation experiments were carried out on N-BK7. Relaxation data from N-BK7 was fit with sets of Prony series as described in Section 3 of this chapter. The

relaxation times extracted from the Prony series fit were nearly constant with temperature, creating a simple model for temperature-dependent relaxation time change. Additionally the Prony weights displayed a linear trend with temperature. The long time relaxations decreased in weight as the temperature increased until only two relaxations out of the original four remained. Upper temperature limitations on the instrument prevented tests at higher temperature which may have produced more insight, and further experiments at high temperature would have enabled a better understanding of the evolution to single exponential relaxation behavior. The curve fits of the Prony weights and the constant relaxation times are shown in Table 4.2. The expression used to model volumetric relaxation from these parameters can be seen in Equation 58.

The resulting model was used to predict the relaxation, in this commercial glass, at a temperature which experimental data had already been obtained for. The plot of normalized configurational height change versus time is shown in Figure 4.13 and a semilog-x plot of the same data can be seen in Figure 4.14. Comparison of predicted and measured curves proved a good match with the Prony series model developed in this dissertation yielding $R^2 = .998663 \pm .000986$. This highlights the accuracy and success possible when using this Prony series representation of configurational length and volume change to predict structural relaxation behavior in N-BK7 oxide glass. The current model is only strictly valid for 10 °C temperature jumps, however, subsequent relaxation measurements show that relaxation magnitude scales directly with the size of the temperature jump.

7.2 Complexity of structural relaxation behavior

A key component of the impetus for this work was to determine if the TNM model of relaxation was descriptive of configurational volumetric changes between thermodynamic states. The TNM model utilized the KWW function in order to describe the evolution of a property. The KWW function is able to characterize a distribution of relaxation times centered on a main relaxation time. However, as this work has shown, the volumetric structural relaxation behavior of these glasses can contain up to four exponentials separated by up to an order of magnitude in time. The KWW function and TNM model are unable to describe the relaxation behaviors presented in this study at the level necessary to characterize the relaxations. The major question of how many relaxation times are needed to describe volumetric configuration change has been answered for both a commercial glass (N-BK7) and multiple homemade multi-component ChG glasses. In all cases, the maximum number of dominant relaxation times observed was four and the minimum was one. The evolution of structural relaxation from a process defined by many, to a process defined by one relaxation time is discussed in Section 7.4.

7.3 Structural relaxation as evidence of a glass transition

One of the goals of the research, has been to use a dilatometric approach to measuring structural relaxation in order to understand something about the structure of the glass as it goes through the glass transition. The glass transition has long been studied in the field of glass science, and a more clear understanding of glass behavior near the glass transition region is a priority for the glass community. The transition region is typically

assumed to be a temperature range in which the behavior the material changes from a solid to a liquid. Below the glass transition temperature, rearrangement of the glass network towards thermodynamic equilibrium is a process that occurs over long time periods (from hours to days). At and above T_g the kinetics change such that the glass network can relax towards equilibrium more quickly. An open question has been whether the glass transition includes some change in thermodynamic state or whether it is simply the changing kinetics state of the glass which leads to the behavior observed in that region.

The trends of Prony relaxation times versus temperature indicate that a transition occurs near $T_{g,d}$ as evidenced by a jog in relaxation times as shown in Figure 4.25, Figure 4.26, and Figure 4.27. This evidence is supportive of a number of possible interpretations. The seeming change in relaxation time behavior may be configurational confirmation of a glass transition temperature. Most intrinsic glass properties show a change in behavior in the glass transition region, however, the change in relaxation time behavior appears more complex than the idea of a *general* glass to liquid transition can account for. The abrupt change in relaxation time behavior points to a possible true transition in the material.

Using $As_{40}Se_{60}$ as an example, Figure 4.25 shows a distinct change in relaxation time behavior versus temperature at ~ 0.96 T_1/T_g, with a similar trend seen in Figure 4.26 and Figure 4.27. This jog appears to mark the onset of a change of glass behavior from structural relaxation dominated by the glass density and free volume, to relaxation increasingly dominated by more liquid-like kinetics. However, the jog is only the *start* of the seeming transition indicated by the relaxation times. The relaxation times show further change in behavior as temperature increases past the jog, where this transition appears to

continue until the relaxation becomes single exponential in nature. This change in behavior is believed to be responsible for many of the property behaviors associated with the glass transition. The dilatometric studies that have been done in the glass transition region typically begin at a common temperature and then ramp down to various test temperatures. The relaxation behavior in other studies is sampled at varying ΔT values. In contrast, the method presented here involves set changes in thermodynamic state. Observing isothermally measured volume-based evidence for structural relations to T_g is a portion of the uniqueness of this work.

7.4 Decreasing structural relaxation complexity with temperature

The question of how many relaxations contribute to a change in structure was answered in Section 7.2. The question remains what occurs in the transition from many to a single relaxation.

The nature of structural relaxations change when going through T_g. This was demonstrated in the section above; however, more significant changes occur than just a relaxation based indication of T_g. As the temperature is increased from low to high temperature, the relaxation times go through a region of significant transition. This transition looks like a recovery after the abrupt change in slope detailed above. The apparent transition, culminates in the disappearance of relaxation times within a fairly small temperature window. The disappearance of longer relaxation times is predicted and modeled by energy landscape theory. This work represents experimental validation of that idea, previously not seen.

Figure 4.25,Figure 4.26, and Figure 4.27, show that after the jog in relaxation times, the number of exponentials describing relaxation quickly decrease. It is known that liquids typically relax in a single exponential manner and that glasses often times contain complex relaxations below T_g. The work in this dissertation captures the transition from many to a single relaxation volumetrically, which has not been previously documented.

The change in behavior dictated by a single relaxation time demonstrates the return of a system to ergodicity. If the glass configuration is viewed as an enthalpy landscape, at low temperatures where configurational change is restricted, energy basins are segregated because transitions between basins become less probable. This forms areas known as metabasins. Configurations within a metabasins can be sampled by the glass, but once within a particular metabasin, there is not a reasonable probability of moving outside of that metabasin. The probabilities associated with atoms moving from one basin to another theoretically allow for jumps, but the probabilistic nature of the process allows for the assumption that inter-metabasin jumps are not made. The breakdown of these metabasins as temperature increases, explains the region between the jog and the disappearance of relaxation times, observed in experimental findings presented in Section 6.2. The reduction to a single relaxation signals a return to ergodicity for the glass network, meaning that, given enough time, any atom can reach any basin within the energy landscape.

The behavior of the glass can be described in another way. Consider that in a given material at a given temperature there is always a certain probability of bonds being broken and reformed. As the temperature increases, the number of bonds that are broken at any given time increases, the amount of time that the average bond remains broken also

increases. The transition region of the glass could then be described as the region in which the number of bonds broken at any given time eclipses some critical value. When this happen the glass loses much of its structural rigidity when viewed as a solid. The behavior of the glass becomes more liquid-like with each degree in temperature. The "break down" of the glass structural rigidity in favor of a liquid behavior could also describe the disappearance of relaxation times seen in this study, with increasing temperature. Structures that exist and relax cooperatively are held together by the bonds that are constantly breaking and reforming. The energy in the system will at some point reach a stage where the bonding that holds a relaxing structure or region together will effectively dissolve. When this happens the relaxation contribution from that mechanism will cease to be measureable as a separate exponential from the rest of the system. This view of the evidence is not at all incompatible with ELT; which defines the glass configuration by a landscape comprised of low energy basins. On the contrary it is a complimentary way of viewing the evolution of the glass network in temperature.

Further evidence of this return to ergodicity is seen in Figure 4.38. All of the (3) homemade ChG compositions studied, showed a change in Gibbs energy of activation within the transition region. It is believed that this temperature dependent change shows a reduced temperature sensitivity for relaxation activation energies. When viewed through the lens of ELT, it is intuitive that the presence of metabasins which limit the freedom of the configuration to change ergodically, lead to a higher energy of activation for structural relaxation. As the metabasins begin to disappear with increasing temperate, the allowable

configurations for relaxation are increased. The more freedom the material has to relax the lower the energy needed for structural relaxation.

7.5 The importance of configurational change between thermodynamic states

Along the course of scientific discovery, there are often questions that are answered before they are even raised. A question which perhaps should have been asked in hindsight is, does the total amount of configurational volume relaxation change as a function of temperature. Isothermal experiments transit between two thermodynamic states, as in this study. So does the glass structure relax the same amount for a 10 °C at low temperatures as it does at higher temperatures? This gets at the heart of the thermodynamic question since the data discussed below is the most pure thermodynamic data gathered in these experiments.

7.5.1 Decreasing volumetric configuration change towards low temperatures

A change in volume at an isothermal condition can be tied to a change in entropy. Glass scientists have been looking for ways to measure whether or not an actual phase transition occurs at T_g, as one indication is a discontinuity in entropy. This suggests that there *is* some thermodynamic transition which takes place in the material that causes the amount of entropy in the system to change instantaneously. Materials display this behavior when they crystallize for instance. A material that goes from liquid to crystal has a discontinuous change in entropy, the material goes from a higher entropy to a more ordered lower entropy system. Tracking the amount of configurational volume change, which relates to entropy, has led, in the present effort, to an interesting result.

The changes in ΔL (and ΔV) for all compositions trend toward zero as the temperature decreases. This result is consistent with experiments that predicted and subsequently showed that the excess entropy a glass contains at T_g should decrease with temperature. Kauzmann predicted from the liquid properties of the glass that the entropy of the glass would decrease below the entropy of the crystal which is, of course, impossible. He and others theorized that the glass undergoes a true second-order thermodynamic transition either just before reaching that temperature (T_2) or at T_g. Still other authors have theorized that T_g was the experimental manifestation of the transition at T_2 and if given infinite time T_g and T_2 would occur at the same temperature. The plots of the change in length between thermodynamic conditions are shown in Figure 4.39 and the calculation of the $T_{g,d}/T_2$ is displayed in Table 4.5. The ratio of $T_{g,d}/T_2$ is in the realm of that measured for other glass forming liquids.[86] Bestul and Chang claimed that the ratio between $T_{g,d}$ and T_2 is actually what defines the glass transition temperature, essentially an amount of excess entropy causes the transition.

7.5.2 Abrupt change in configurational relaxation magnitudes near T_g

The rapid decay of change in length per 10 K jumps would lead to an expectation of a second order transition occurring at or near T_2, however the trends shown in Figure 4.39 make a different outcome possible. In all of the glasses analyzed, but especially in $G_{17.9}As_{19.7}Se_{62.4}$ a definite feature of length change can be seen in the glass transition region. The feature appears as a dip in the length (or volume) change with a given temperature jump. This feature may hold evidence of a possible discontinuity in the change

in volume. The apparent phenomenon that is undergone by the configurational volume change is not incompatible with indication of a phase transition.

A change of state from a liquid to a crystalline solid, results in a large entropy decrease. It is not known whether a thermodynamic transition occurs near T_g. The nature of the glass transition which appears as a much more gradual process, would most likely have a transition that was less abrupt than crystallization for instance. The change of the material from liquid to crystal represents a much larger downward jump in entropy. For this reason it may be difficult to detect small changes in entropy. The evidence presented here provides an interesting extension of the search for a thermodynamic transition. It is certainly not proof of a transition, but indicates the possibility that such a transition exists.

7.6 Summary of conclusions

The conclusions drawn from this dissertation include the development of an isothermal method for measuring and characterizing structural relaxation through length dilatometry which is a materials engineering contribution of note. Along with that the ability to accurately mathematically model the structural relaxation behavior of oxide and chalcogenide glasses for use as a guide to annealing times is significant. The models developed here can be extended further with FEM and used to precisely predict changes in volume during annealing of precision molded lenses or other hot formed optics.

In the realm of material science, this dissertation presents a new volumetric approach to analyzing the glass transition region via structural relaxation. The relaxation is dependent on the configurations that the glass is relaxing from, and towards. The

definition of relaxation times in the form of Prony series parameters has led to a new view of relaxation from multiple events. The relaxation times determined in this study showed a definitive decay with temperature and an evolution towards single exponential relaxations in the glass transition region. This result has previously never before been observed through these type of isothermal volumetric measurements.

The identification of a transition point or region from the relaxation times is also a significant contribution to the field of glass science. The results presented support the interpretations of both the Adam-Gibbs view on relaxation as well as the Energy/Enthalpy Landscape Theory interpretation. The use of a stretched exponential and the TNM model were called into question for this specific measurement, though they remain viable for DSC measurements of other properties.

The quantification of configurational length change with changing thermodynamic condition is tied to entropy change in most materials. The trends presented in this dissertation point to the rapid and seemingly linear decrease of the change in length (or volume) over given thermodynamic intervals. This agrees with a number of theories depicting the excess entropy in a glassy material as decreasing toward some critical temperature (T_2). The evidence presented here supports this idea with volumetric data which has not been previously analyzed or presented.

Finally the appearance of an inflection in the change in length (or volume) versus T_1 curve for these chalcogenide glasses raises questions of whether or not it signifies the existence of an actual thermodynamic transition at T_g. The evidence presented here is far

from enough to confirm the existence of a true thermodynamic transition but it warrants further study of the question. Further study of structural relaxation phenomena through length and/or volume dilatometry would be highly beneficial to glass science and the materials field at large.

An investigation of further compositions along the As-Se binary such as Se-rich and As-rich compositions would allow further testing of the conclusions espoused in this dissertation. The role that germanium plays could be further investigated through glasses in this ternary with varying amounts of Ge. Study is also needed in the areas of nuclear magnetic resonance imaging and x-ray photoelectron spectroscopy. These techniques have the potential to identify relaxing regions through in-situ, high temperature tests or room temperature tests of fast quench glasses. The structural resolution on these techniques is not ideal for linking structures or metabasin configurations with relaxation phenomena, however research is ongoing in these areas.

REFERENCES

1. G. Adam and J. H. Gibbs, 'On the temperature dependence of cooperative relaxation properties in glass-forming liquids,' *J. Chem. Phys.*, 43 [1] 139-146 (1965).

2. F. H. Stillinger and T. A. Weber, 'Dynamics of structural transitions in liquids,' *Phys. Rev. , A*, 28 [4] 2408-2416 (1983).

3. S. Carmi, S. Havlin, C. Song, K. Wang and H. A. Makse, 'Energy-landscape network approach to the glass transition,' *Journal of Physics A: Mathematical and Theoretical*, 42 [10] 105101 (2009).

4. W. Kauzmann, 'The Nature of the Glassy State and the Behavior of Liquids at Low Temperatures.' *Chem. Rev.*, 43 [2] 219-256 (1948).

5. H. E. Bennett and M. J. Soileau, 'FABRICATING INFRARED OPTICS,' *Optical Engineering*, 15 [5] 442-445 (1976).

6. S. Zhu, H. Ma, L. Calvez, X. Zhang, J. Lucas, J. Adam, H. Shang and T. Rouxel, 'Optical and mechanical properties of far infrared transmitting glass-ceramics,' *J. Non Cryst. Solids*, 353 [13-15] 1298-1301 (2007).

7. E. Bormashenko, R. Pogreb, S. Sutovsky, V. Lusternik and A. Voronel, 'Mechanical and thermodynamic properties of infrared transparent low melting chalcogenide glass,' *Infrared Phys. Technol.*, 43 [6] 397-9 (2002).

8. J. Yan, T. Zhou, J. Masuda and T. Kuriyagawa, 'Modeling high-temperature glass molding process by coupling heat transfer and viscous deformation analysis,' *Precis Eng*, 33 [2] 150-159 (2009).

9. J. H. Gibbs and E. A. DiMarzio, 'Nature of the Glass Transition and the Glassy State,' *J. Chem. Phys.*, 28 [3] 373-383 (1958).

10. M. Z. Tidrow and W. R. Dyer, 'Infrared sensors for ballistic missile defense,' *Infrared Phys. Technol.*, 42 [3-5] 333-6 (2001).

11. B. D. O. Richards, A. Jha, G. Jose and X. Jiang, 'Oxide glasses for mid-infrared lasers,', 8039 The Society of Photo-Optical Instrumentation Engineers (SPIE) (2011).

12. X. Zhang, H. Ma, J. Lucas, Y. Guimond and S. Kodjikian, 'Optical fibers and molded optics in infrared transparent glass-ceramic,' *J. Non Cryst. Solids*, 336 [1] 49-52 (2004).

13. R. Golovchak, O. Shpotyuk, A. Kozdras, S. Szymura and M. Shpotyuk, 'Structural relaxation in vitreous arsenic selenide induced by -irradiation,' *Physics and Chemistry of Glasses*, 46 [6] 579-82 (2005).

14. D. A. Drabold, J. Li and D. N. Tafen, 'Simulations of arsenic selenide glasses,' *Journal of Physics Condensed Matter*, 15 [16] S1529-S1536 (2003).

15. B. Bureau, J. Troles, M. LeFloch, F. Smektala, G. Silly and J. Lucas, 'Solid state 77Se NMR investigations on arsenic-selenium glasses and crystals,' *Solid State Sciences*, 5 [1] 219-24 (2003).

16. J. C. Mauro and A. K. Varshneya, 'Multiscale modeling of arsenic selenide glass,' *J. Non Cryst. Solids*, 353 [13-15] 1226-31 (2007).

17. J. D. Musgraves, P. Wachtel, S. Novak, J. Wilkinson and K. Richardson, 'Composition dependence of the viscosity and other physical properties in the arsenic selenide glass system,' *J. Appl. Phys.*, 110 [6] 063503 (2011).

18. J. C. Phillips, 'Topology of covalent non-crystalline solids. I. Short-range order in chalcogenide alloys,' *J. Non Cryst. Solids*, 34 [2] 153-81 (1979).

19. G. Guery, J. D. Musgraves, C. Labrugere, E. Fargin, T. Cardinal and K. Richardson, 'Evolution of glass properties during a substitution of S by Se in Ge 28Sb12S60 -xSex glass network,' *J. Non Cryst. Solids*, 358 [15] 1740-1745 (2012).

20. J. Malek, 'Structural relaxation of As2S3 glass by length dilatometry,' *J. Non Cryst. Solids*, 235-237 527-33 (1998).

21. D. C. Harris, 'Optical Coatings'; pp. 197 1999.

22. V. M. Al'tshuller, S. A. Gerasimov and O. Y. Terent'eva, 'Diamond tool with a rubber binder for fine grinding of optical glass,' *Journal of Optical Technology*, 61 [6] 472-3 (1994).

23. U. Henkel and G. Boswetter, 'Grinding and hole boring of optical glass-a comparison,' *Wissenschaftliche Zeitschrift der Technischen Hochschule Ilmenau*, 30 [2] 125-9 (1984).

24. P. Paul Hed and D. F. Edwards, 'Relationship between subsurface damage depth and surface roughness during grinding of optical glass with diamond tools,' *Appl. Opt.*, 26 [13] 2491 (1987).

25. S. Chatterjee, 'Simple technique for polishing super-smooth optical glass and fused silica substrates,' *Journal of Optics*, 34 [4] 153-63 (2005).

26. J. P. Marioge, 'Theoretical hypothesis on grinding and polishing of optical glass surfaces,' *Nouvelle Revue d'Optique,* 6 [2] 121-6 (1975).

27. J. C. Lambropoulos, S. Xu and T. Fang, 'Loose abrasive lapping hardness of optical glasses and its interpretation,' *Appl. Opt.*, 36 [7] 1501-16 (1997).

28. J. Neauport, J. Destribats, C. Maunier, C. Ambard, P. Cormont, B. Pintault and O. Rondeau, 'Loose abrasive slurries for optical glass lapping,' *Appl. Opt.*, 49 [30] 5736-5745 (2010).

29. B. E. Gillman and S. D. Jacobs, 'Bound-abrasive polishers for optical glass,' *Appl. Opt.*, 37 [16] 3498-505 (1998).

30. Y. D. Filatov, O. Y. Filatov, G. Monteil, U. Heisel and M. Storchak, 'Bound-abrasive grinding and polishing of surfaces of optical materials,' *Optical Engineering*, 50 [6] 063401 (7 pp.) (2011).

31. N. Belkhir, D. Bouzid and V. Herold, 'Wear behavior of the abrasive grains used in optical glass polishing,' *J. Mater. Process. Technol.*, 209 [20] 6140-5 (2009).

32. B. Guo, Q. Zhao and X. Fang, 'Precision grinding of optical glass with laser micro-structured coarse-grained diamond wheels,' *J. Mater. Process. Technol.*, 214 [5] 1045-1051 (2014).

33. W. Kordonski and S. Gorodkin, 'Material removal in magnetorheological finishing of optics,' *Appl. Opt.*, 50 [14] 1984-1994 (2011).

34. A. B. Shorey, S. D. Jacobs, W. I. Kordonski and R. F. Gans, 'Experiments and observations regarding the mechanisms of glass removal in magnetorheological finishing,' *Appl. Opt.*, 40 [1] 20-33 (2001).

35. J. A. Menapace, 'Developing magnetorheological finishing (MRF) technology for the manufacture of large-aperture optics in megajoule class laser systems,', 7842 Lawrence Livermore National Laboratory; Pacific Northwest National Lab.; Spica Technologies, Inc.; Office of Naval Research (2010).

36. T. P. Leung, W. B. Lee and X. M. Lu, 'Diamond turning of silicon substrates in ductile-regime,' *J. Mater. Process. Technol.*, 73 [1-3] 42-48 (1998).

37. K. E. Puttick, M. R. Rudman, K. J. Smith, A. Franks and K. Lindsey, 'Single-point diamond machining of glasses,' *Proceedings of the Royal Society of London, Series A (Mathematical and Physical Sciences)*, 426 [1870] 19-30 (1989).

38. E. Koontz, V. Blouin, P. Wachtel, J. D. Musgraves and K. Richardson, 'Prony series spectra of structural relaxation in N-BK7 for finite element modeling,' *Journal of Physical Chemistry A*, 116 [50] 12198-12205 (2012).

39. A. Y. Yi and A. Jain, 'Compression molding of aspherical glass lenses - A combined experimental and numerical analysis,' *J Am Ceram Soc*, 88 [3] 579-586 (2005).

40. B. Gleason, P. Wachtel, J. D. Musgraves and K. Richardson, 'Using Design of Experiments to Improve Precision Glass Molding,' *Int. J. of Experimental Design and Process Optimization*, Accepted, In Press (2013).

41. B. Gleason, P. Wachtel, J. D. Musgraves, R. Steinkopf, R. Eberhardt and K. Richardson, 'Chalcogenide - Mold interactions during Precision Glass Molding (PGM) of GeAsSe glasses,', 8884 The Society of Photo-Optical Instrumentation Engineers (SPIE); The American Precision Optics Manufacturers Association (2013).

42. E. Koontz, P. Wachtel, J. D. Musgraves, K. Richardson, S. Mourad, M. Huber, A. Kunz and M. Forrer, 'Interaction of N-FK5 and L-BAL35 optical glass with various carbide and other precision glass mold tooling,' *Proceedings of the SPIE - The International Society for Optical Engineering*, 8884 88841Y (5 pp.) (2013).

43. F. Klocke, K. Georgiadis, O. Dambon, K. -. Bouzakis, S. Gerardis and G. Skordaris, 'A complete qualification methodology for coatings of precision glass molding tools,', 8126 The Society of Photo-Optical Instrumentation Engineers (SPIE) (2011).

44. F. Klocke, O. Dambon and K. Georgiadis, 'Comparison of nitride and noble metal coatings for precision glass molding tools,', 438 9-16 (2010).

45. D. J. Sugg, 'Coated tooling can improve glass-forming operations,' *Glass Ind*, 71 [5] 40-41 (1990).

46. D. G. Georgiev, P. Boolchand and M. Micoulaut, 'Rigidity transitions and molecular structure of AsxSe1-x glasses,' *Physical Review B (Condensed Matter)*, 62 [14] 9228-31 (2000).

47. C. Rivero, A. Schulte and K. Richardson, 'Structure-property relationships in As-S-Se glasses for waveguide applications probed by near-infrared Raman spectroscopy'; pp. 79-85 in Optoelectronic Materials and Technology in the Information Age. The American Ceramic Society 2006.

48. Y. Wang, P. Boolchand and M. Micoulaut, 'Glass structure, rigidity transitions and the intermediate phase in the Ge-As-Se ternary,' *Europhys. Lett.*, 52 [6] 633-9 (2000).

49. R. Golovchak, A. Kovalskiy, A. C. Miller, H. Jain and O. Shpotyuk, 'Structure of Se-rich As-Se glasses by high-resolution X-ray photoelectron spectroscopy,' *Physical Review B (Condensed Matter and Materials Physics)*, 76 [12] 1-7 (2007).

50. L. E. Busse, 'Temperature dependence of the structures of As2Se3 and AsxS1-x glasses near the glass transition,' *Physical Review B (Condensed Matter)*, 29 [6] 3639-51 (1984).

51. D. C. Kaseman, I. Hung, Z. Gan, B. Aitken, S. Currie and S. Sen, 'Structural and topological control on physical properties of arsenic selenide glasses,' *J Phys Chem B*, 118 [8] 2284-2293 (2014).

52. K. Tanaka, 'Structural phase transitions in chalcogenide glasses,' *Physical Review B (Condensed Matter)*, 39 [2] 1270-9 (1989).

53. M. J. O'Neill, 'The analysis of a temperature-controlled scanning calorimeter,' *Anal. Chem.*, 36 [7] 1238-1245 (1964).

54. G. A. Hinze, D. D. Brace, S. D. Gottke and M. D. Fayer, 'A detailed test of mode-coupling theory on all time scales: Time domain studies of structural relaxation in a supercooled liquid,' *J. Chem. Phys.*, 113 [9] 3723-33 (2000).

55. J. Bisquert, F. Henn and J. -. Giuntini, 'A simple model of entropy relaxation for explaining effective activation energy behavior below the glass transition temperature,' *J. Chem. Phys.*, 122 [9] 94507-1 (2005).

56. M. Tokuyama, 'A statistical-mechanical theory of self-diffusion in glass-forming liquids,' *Physica A: Statistical Mechanics and its Applications*, 387 [21] 5003-5011 (2008).

57. M. Fuchs, W. Gotze, S. Hildebrand and A. Latz, 'A theory for the -relaxation process near the liquid-to-glass crossover,' *Journal of Physics: Condensed Matter*, 4 [38] 7709-44 (1992).

58. L. -. Martinez and C. A. Angell, 'A thermodynamic connection to the fragility of glass-forming liquids,' *Nature*, 410 [6829] 663-667 (2001).

59. R. Svoboda, P. Honcova and J. Malek, 'Apparent activation energy of structural relaxation for Se70Te30 glass,' *J. Non Cryst. Solids*, 356 [3] 165-168 (2010).

60. S. Gaylord, 'Thermal and Structural Properties of Candidate Moldable Glass Types,' (2008).

61. 'Test Method for Measurement of Viscosity of Glass Between Softening Point and Annealing Range (Approximately 108 Pas to Approximately 1013 Pas) by Beam Bending (Metric),' (2013).

62. C. A. Angell, 'Formation of glasses from liquids and biopolymers,' *Science*, 267 [5206] 1924-1924 (1995).

63. Z. Cernosek, J. Holubova, E. Cernoskova and M. Liska, 'Enthalpic Relaxation and the Glass Transition,' *Journal of Optoelectronics and Advanced Materials*, 4 [3] 489-489-503 (2002).

64. R. Golovchak, J. Oelgoetz, M. Vlcek, A. Esposito, A. Saiter, J. -. Saiter and H. Jain, 'Complex structural rearrangements in As-Se glasses,' *J. Chem. Phys.*, 140 [5] 054505 (8 pp.) (2014).

65. P. Lucas, 'Energy landscape and photoinduced structural changes in chalcogenide glasses,' *Journal of Physics: Condensed Matter*, 18 [24] 5629-38 (2006).

66. J. C. Mauro, R. J. Loucks and P. K. Gupta, 'Fictive temperature and the glassy state,' *J Am Ceram Soc*, 92 [1] 75-86 (2009).

67. R. Golovchak, O. Shpotyuk, A. Kozdras, M. Vlcek, B. Bureau, A. Kovalskiy and H. Jain, 'Long-term physical ageing in As-Se glasses with short chalcogen chains,' *Journal of Physics: Condensed Matter*, 20 [24] 245101 (7 pp.) (2008).

68. A. Q. Tool, 'Viscosity and extraordinary heat effects in glass,' *United States Bureau of Standards -- Journal of Research*, 37 [2] 73-90 (1946).

69. S. Spinner and A. Napolitano, 'Relation between refractive index and elastic moduli of borosilicate glass after heat-treatment,' *American Ceramic Society -- Journal*, 39 [11] 390-394 (1956).

70. S. Spinner and A. Napolitano, 'Further studies in annealing of borosilicate glass,' *United States Bureau of Standards, Journal of Research -- Physics and Chemistry*, 70A [1] 147-152 (1966).

71. H. N. Ritland, 'Relation between refractive index and density of glass at constant temperature,' *American Ceramic Society -- Journal*, 38 [2] 86-88 (1955).

72. L. BOESCH, A. NAPOLITANO and P. B. MACEDO, 'SPECTRUM OF VOLUME RELAXATION TIMES IN B2O3,' *J Am Ceram Soc*, 53 [3] 148-153 (1970).

73. O. S. Narayanaswamy, 'Thermorheological simplicity in the glass transition,' *J Am Ceram Soc*, 71 [10] 900-4 (1988).

74. R. Loucks, 'Relaxation Course, TNM Lectures,', Lectures 13-16 (2010).

75. A. V. Milovanov, J. J. Rasmussen and K. Rypdal, 'Stretched-exponential decay functions from a self-consistent model of dielectric relaxation,' *Physics Letters A*, 372 [13] 2148-54 (2008).

76. J. C. Phillips, 'Stretched exponential relaxation in molecular and electronic glasses,' *Reports on Progress in Physics*, 59 [9] 1133-207 (1996).

77. M. Potuzak, R. C. Welch and J. C. Mauro, 'Topological origin of stretched exponential relaxation in glass,' *J. Chem. Phys.*, 135 [21] 214502 (7 pp.) (2011).

78. C. T. Moynihan, S. N. Crichton and S. M. Opalka, 'Linear and nonlinear structural relaxation,' *J. Non Cryst. Solids*, 131 [2] 420-34 (1991).

79. C. T. Moynihan, A. J. Easteal, M. A. DeBolt and J. Tucker, 'Dependence of the fictive temperature of glass on cooling rate,' *J Am Ceram Soc*, 59 [1-2] 12-16 (1976).

80. C. T. Moynihan and J. Schroeder, 'Non-exponential structural relaxation, anomalous light scattering and nanoscale inhomogeneities in glass-forming liquids,' *J. Non Cryst. Solids*, 160 [1-2] 52-9 (1993).

81. J. Malek, R. Svoboda, P. Pustkova and P. Cicmanec, 'Volume and enthalpy relaxation of a-Se in the glass transition region,' *J. Non Cryst. Solids*, 355 [4-5] 264-272 (2009).

82. C. A. ANGELL, D. R. MACFARLANE and M. OGUNI, 'The Kauzmann Paradox, Metastable Liquids, and Ideal Glasses: A Summary,' *Ann. N. Y. Acad. Sci.*, 484 [1] 241-247 (1986).

83. J. C. Mauro, R. J. Loucks, A. K. Varshneya and P. K. Gupta, 'Enthalpy landscapes and the glass transition,', 68 LNCSE 241-281 (2009).

84. R. J. Speedy, 'Kauzmann's paradox and the glass transition,' *Biophys. Chem.*, 105 [2–3] 411-420 (2003).

85. A. B. Bestul and S. S. Chang, 'Excess Entropy at Glass Transformation,' *J. Chem. Phys.*, 40 [12] 3731-3733 (1964).

86. M. Goldstein, 'Some Thermodynamic Aspects of the Glass Transition: Free Volume, Entropy, and Enthalpy Theories,' *J. Chem. Phys.*, 39 [12] 3369-3374 (1963).

87. C. P. Massen and J. P. K. Doye, 'Power-law distributions for the areas of the basins of attraction on a potential energy landscape,' *Phys Rev E.*, 75 [3] 037101 (2007).

88. T. S. Grigera, A. Cavagna, I. Giardina and G. Parisi, 'Geometric Approach to the Dynamic Glass Transition,' *Phys. Rev. Lett.*, 88 [5] 055502 (2002).

89. J. C. Sharma and J. Shanker, 'Theory of strain derivatives of electronic and static dielectric constants of alkali halides and alkaline-earth fluorides,' *Phys.Rev.B*, 19 [12] 6604-6609 (1979).

90. J. E. Shelby, 'Introduction to Glass Science and Technology'. The Royal Society of Chemistry, Cambridge, UK, 2005.

91. S. Gaylord, B. Ananthasayanam, B. Tincher, L. Petit, C. Cox, U. Fotheringham, P. Joseph and K. Richardson, 'Thermal and structural property characterization of commercially moldable glasses,' *J Am Ceram Soc*, 93 [8] 2207-2214 (2010).

92. U. Fotheringham, A. Baltes, R. Muller and R. Conradt, 'The residual configurational entropy below the glass transition: Determination for two commercial optical glasses,' *J. Non Cryst. Solids*, 355 [10-12] 642-52 (2009).

93. U. Fotheringham, R. Muller, K. Erb, A. Baltes, F. Siebers, E. Wei and R. Dudek, 'Evaluation of the calorimetric glass transition of glasses and glass ceramics with respect to structural relaxation and dimensional stability,' *Thermochimica Acta*, 461 [1-2] 72-81 (2007).

94. S. M. Rekhson, 'Modelling of viscoelastic and structural relaxation in glass,' *J. Non Cryst. Solids*, 73 [1-3] 151-64 (1985).

95. B. Ananthasayanam, 'Computational Modeling of Precision Molding of Aspheric Glass Optics,' (2008).

96. P. K. Gupta, 'Fictive pressure effects in structural relaxation,' *J. Non Cryst. Solids*, 102 [1-3] 231-9 (1988).

97. N. W. Tschoegl, 'Representation by Series-Parallel Models'; pp. 136-145 in The Phenomonological Theory of Linear Viscoelastic Behavior: An Introduction. Springer-Verlag, Berlin, Heidelberg, New York, London, Paris, Tokyo, 1989.

98. G. Vallet, 'Stress Relaxation of a Glass Using a Parallel Plate Viscometer,' (2011).

99. H. C. Kadali, 'Experimental Characterization of Stress Relaxation in Glass,' (2009).

100. R. Golovchak, A. Kozdras, O. Shpotyuk, C. Gorecki, A. Kovalskiy and H. Jain, 'Temperature-dependent structural relaxation in As40Se60 glass,' *Physics Letters A*, 375 [33] 3032-6 (2011).

101. M. M. Smedskjaer, J. C. Mauro and Y. Yue, 'Prediction of glass hardness using temperature-dependent constraint theory,' *Phys. Rev. Lett.*, 105 [11] (2010).

102. S. A. Brawer, 'Theory of relaxation in viscous liquids and glasses,' *J. Chem. Phys.*, 81 [2] 954-75 (1984).

103. G. Carini, M. Cutroni, G. Galli, P. Migliardo and F. Wanderlingh, 'Raman scattering in a-Se bulk near Tg,' *Solid State Commun.*, 33 [11] 1139-1141 (1980).

104. A. Patkowski, E. W. Fischer, H. Glaser, G. Meier, H. Nilgens and W. Steffen, 'Light scattering studies of a glass forming liquid near Tg'; pp. 35-38 in 27th Europhysics Conference on Macromolecular Physics, September 23, 1991 - September 27, 1991, Vol. 91. Publ by Dr. Dietrich Steinkopff Verlag, Crete, Greece, 1993.

105. C. T. Moynihan and J. -. Whang, 'Fluctuation model for structural relaxation and the glass transition,' 133-9 (1997).

106. S. V. Nemilov, 'Maxwell equation and classical theories of glass transition as a basis for direct calculation of viscosity at glass transition temperture,' *Glass Physics and Chemistry*, 39 [6] 609-623 (2013).

107. G. Yang, O. Gulbiten, Y. Gueguen, B. Bureau, J. -. Sangleboeuf, C. Roiland, E. A. King and P. Lucas, 'Fragile-strong behavior in the AsxSe1-x glass forming system in relation to structural dimensionality,' *Physical Review B (Condensed Matter and Materials Physics)*, 85 [14] 144107 (2012).

108. J. C. Mauro and A. K. Varshneya, 'Modeling of rigidity percolation and incipient plasticity in germanium-selenium classes,' *J Am Ceram Soc*, 90 [1] 192-198 (2007).

109. R. M. C. V. Reis, J. C. Mauro, K. L. Geisinger, M. Potuzak, M. M. Smedskjaer, X. Guo and D. C. Allan, 'Relationship between viscous dynamics and the configurational thermal expansion coefficient of glass-forming liquids,' *J. Non Cryst. Solids*, 358 [3] 648-51 (2012).

110. M. Goldstein, 'Viscous liquids and the glass transition: a potential energy barrier picture,' *J. Chem. Phys.*, 51 [9] 3728-39 (1969).

111. E. Gjersing, S. Sen and B. Aitken, 'Structure, Connectivity, and Configurational Entropy of Ge x Se100− x Glasses: Results from 77Se MAS NMR Spectroscopy,' *The Journal of Physical Chemistry C*, 114 [18] 8601-8608 (2010).

112. M. J. Toplis, D. B. Dingwell, K. Hess and T. Lenci, 'Viscosity, fragility, and configurational entropy of melts along the join SiO~ 2-NaAlSiO~ 4,' *Am. Mineral.*, 82 [9] 979-990 (1997).

APPENDIX A

1 Relaxation data processing code

Example Matlab code for relaxation data processing

```
%% Clear all values, close all windows, wipe command window

% clear all;
% close all;
% clc;

%% Inputs
% filename = input('Enter Data File Name:\n','s');
filename = 'aGe17.9As19.7Se_TMA_150g01a_280-275.txt';
Tempdiff = 5;
CTEcalc = 18.07*10^-6;
thermoeqtime = 36;



            tbegin = 3240;

            t1 = tbegin + thermoeqtime;

            t2 = 3550;

            td1a =3500;
```

```
                td1b = 3525;

                td2a = 3525;

                td2b = 3550;


    %% Skip all characters in data file until data and then read in
data

    fid = fopen(filename,'r');
    done = 0;
    counter = 0;
    store = [];
    while ~done
        tline = fgetl(fid);
        counter = counter+1;
         if counter == 7
            samplelength  =  str2num(tline(5:12));   %  Initial  Sample
length in mm
                                                    % as measured by the
TMA
        end

        if ~ischar(tline)
            done = 1;
        else
            if counter > 26
                store = [store;str2num(tline)];
            end
        end
    end
```

```
      %% Convert initial sample length to micrometer and calculate CTE

      samplelength = samplelength*1000;   % Sample length is converted to
um

      %expansionrate = .5216;               % Rate of expansion from TMA
CTE measurements in (um/degC)

      %CTEsamplelength = 23506 ;          % Sample length of CTE measured
sample in um

      out  =  sprintf('Initial  sample  lengths  in  micrometers  is:\n%d
micrometers\n',samplelength);
      disp(out)

      %% Calculate the thermal expansion of the material

      alpha = CTEcalc

      expansion = alpha*Tempdiff*(samplelength/1000000);  % Expansion in
meters
      expansion = expansion*1000000;                      % Expansion in
um

      expansionpertime = expansion/thermoeqtime;         % Expansion per
test time

      %% Create an individual matrix for each set of data

      time(1:size(store),1)=store(1:size(store),1);
```

```
% Change time from minutes to seconds
time=(time*60);
temp(1:size(store),1)=store (1:size(store),2);
% deltal(1:size(store),1)=(store (1:size(store),3))/samplelength;
deltal(1:size(store),1)=(store (1:size(store),3));
forceprobe(1:size(store),1)=store(1:size(store),4);
%
%        figure('Name','Change        in        Length        vs.
Temperature','NumberTitle','off')
% plot(temp,deltal,'-')
% ylabel('Change in Length')
% xlabel('Temperature')



%% Display Temp vs. Time and Delta length vs. Time

figure('Name','Temp vs. Time','NumberTitle','off')
plot(time,temp,'.')
ylabel('Temperature')
xlabel('Time (seconds)')

figure('Name','Change in length vs. Time','NumberTitle','off')
plot(time,deltal,'.')
ylabel('Change in Length')
xlabel('Time (seconds)')



%% Loop to ask for appropriate inputs for the bounding limits of
```

```
      %  the curves in question.  Loop will either do a specific one or
all
      %  of them.  (Would like to be able to pick combinations later)




      %  Find the indices in the time matrix which correspond to the
      %  limits of the section of data in question which were chosen
      %  and entered above (1st curve)

                  store_AA = find(time>=t1&time<=t2);


                  tfunc1                                                =
(time(store_AA(1,1):store_AA(size(store_AA),1))-time(store_AA(1,1));
                  tfunc01                                               =
(time(store_AA(1,1):store_AA(size(store_AA),1))-time(store_AA(1,1));


                  deltalfunc01                                          =
deltal(store_AA(1,1):store_AA(size(store_AA),1),1)-
deltal(store_AA(1,1));
                  deltalfunc1                                           =
deltal(store_AA(1,1):store_AA(size(store_AA),1),1)-
deltal(store_AA(1,1));


      %           Calculate the slope of the linear section of the curve
in question and
      %              display the slope.  This is done by taking points
flanking
      %            two line segments, averaging the data in that segment
and
      %               using those averages as the points with which to
calculate
      %             slope.  The time at the center of each section will
be used
      %             for the "run" calculation.
```

```
store_BB = find(time>=td1a&time<=td1b);

store_CC = find(time>=td2a&time<=td2b);

mean_BB                                                    =
mean(deltal(store_BB(1,1):store_BB(size(store_BB))));
mean_CC                                                    =
mean(deltal(store_CC(1,1):store_CC(size(store_CC))));

slopefunc1 = zeros(1,1);

slopefunc1    =    (mean_CC-mean_BB)/(((td2b+td2a)/2)-
(td1b+td1a)/2);



%% Adjust given data set by accounting for slope

% First create a matrix out of the slope coeffiecient
which is
% slopefunc1 then multiply that


modify = slopefunc1(1,1)*tfunc1;
deltalfunc1 = deltalfunc01- modify;



%% Remove instantaneous (time-dependant) component of
thermal
%  expansion
```

```
                storelimitbegin = find(time>=tbegin);


                timebegin = time(storelimitbegin(1));


    %                                limit   =   find((tfunc1>=(99-(t1-
timebegin)))&(tfunc1<=(100-(t1-timebegin))));
                limit      =      find((tfunc1>=((thermoeqtime-1)-(t1-
timebegin)))&(tfunc1<=(thermoeqtime-(t1-timebegin))));



                done = 0;
                i = 0;


                while ~done


                    i = i+1;
                    if i<=limit
                        deltalfunc1(i)                                  =
deltalfunc1(i)+(expansionpertime*(tfunc1(i)+(t1-timebegin)));
                    else
                        if i<=numel(deltalfunc1)
                               deltalfunc1(i)   =   deltalfunc1(i)   +
(expansionpertime*thermoeqtime);
                        else
                            done = 1;
                        end


                     end


                end
```

```
                %% Adjust minimum of curve to zero and cut curve at
minimum



                k = sqrt((min(deltalfunc1))^2);
                deltalfunc1 = deltalfunc1+k;

                z = find(deltalfunc1==0);
                deltalfunc1 = deltalfunc1(1:z);
                tfunc1 = tfunc1(1:z);

                strainfunc1 = deltalfunc1/samplelength;



                End = tfunc1(numel(tfunc1))+50;

      %Set the end condition for the analyze program

                %% Plot strain function

      %             figure('Name','Zoomed change in Strain vs. Time (1st
curve)','NumberTitle','off')
      %             plot(tfunc1,strainfunc1,'r-');
      %             ylabel('Strain (%)')
      %             xlabel('Time (seconds)')
```

```
%             title('Strain vs. Time')
%             grid on
%             hold off



                %% Calculate viscosity via downslope of relaxation
curves

                done = 1;

                slopefunc = slopefunc1;

                Force = 5000;
                dhdt = (-1)*(slopefunc/10000);
                V = .3*.3*(samplelength/10000);
                h = samplelength/10000;

                visc                                                =
(2*pi*Force*(h^5))/((3*V)*(dhdt)*((2*pi*(h^3))+V));

                visc = visc/10;

                visc = log10(visc);



                out = sprintf('Empirical Viscosity @ 547a degC:\n%d
Pa*s\n',visc);
                disp(out)
```

```
                %% Reset time to the value of tfunc1


                time = tfunc1;


            %% Calculate total relaxation height and pass on


                holder              =              deltalfunc1(1)-
deltalfunc1(numel(deltalfunc1));
                CTEsep     =     deltal(storelimitbegin(1,1))     -
deltal(store_AA(1,1)) - expansion ;


                reheight             =             (deltalfunc1(1)-
deltalfunc1(numel(deltalfunc1))+ CTEsep)/samplelength
```

2 Relaxation data fitting

```
    close all
clear all
clc



%% This program will run the curvefit program for a variety of
curves,
%  capture the data and plot graphs comparing different spectra


% Tell program what curve to analyze, if 0 is entered the program
% will ask for an input
```

```
%% Analyze Curve 1



Run = 'aGeAsSe_280_275_150g01a';
section = 1;
tmp = 275;
Step = 0;
Rstep = 50;
% End = 350;

run aGeAsSe_280_275_150g01a_DataAnalyze

% Feed the program the Prony times to start with

times = [38.1];
% times = [.1:Step:60,60:Rstep:End];
% times = [.1:Step:End];



run Curvefit_Clust;

run Curvefit_KWW

% Save Spectra figure
filename = sprintf('Spectra_%s_%d.fig',Run,Step);

% hgsave(weights,filename);      %Saves the weights vs. Tau figure
generated
                                    % in Curvefit_Clust.m
```

```
% Set data for file output row 1 and 2 are F and solve time, then
% data[times,X] begins

spectra1(3:(length(Xprony)+2),2) = Xprony;
spectra1(3:(length(times)+2),1) = times;
spectra1(1,1) = F;
spectra1(2,1) = elapsedtimeprony;
spectra1(1,3) = X(1);
spectra1(1,4) = X(2);

filename = sprintf('Spectra_%s_%d.txt',Run,Step);
dlmwrite(filename,spectra1,'\t');



%% Save data from semilog plot of curve fit

fit1(1:length(time),1) = time;
fit1(1:length(time),2) = deltalnorm;
fit1(1:length(time),3) = pronyseries;
fit1(1,5) = reheight;

for i = 1:length(time)
fit1(i,4) = exp(-(time(i)/X(1))^X(2));
end
filenamefit = sprintf('PronyFit_%s_%d.txt',Run,Step);
dlmwrite(filenamefit,fit1,'\t');
```

2.1 Curvefit program

```
      % clear all
% close all
% clc

%% Open TMA_Data_Analyze.m and run which will run Curfit.m as well

% run R3_TMA_Data_Analyze;




%% This program will be run from TMA_Data_Analyze.m

%% Need to ask which curve segment will be used for the curve fit

N = section;

%% Cut out bad part of selection




%% This loop takes the curve number entered and assigns that curve's
%  data to the time and deltal matrices for this program

done = 0;

while~done
    if N == 1
```

```
        g = find(strainfunc1==0);
        time = tfunc1(1:g);
        deltal = strainfunc1(1:g);
        done = 1;
    else
        if N==2
            g = find(strainfunc2==0);
            time = tfunc2(1:g);
            deltal = strainfunc2(1:g);
            done = 1;
        else
            if N == 3
                time = tfunc3;
                deltal = strainfunc3;
                done = 1;
            else
                if N == 4;
                    time = tfunc4;
                    deltal = strainfunc4;
                    done = 1;
                else
                    if N == 0;
                        done = 1;
                    end
                end
            end
        end

    end
end
```

```
clear min1 max1 deltalnorm
% deltal = strainfunc1;
% time = tfunc1;
% Normalize function between 0 and 1
min1 = min(deltal);
max1 = max(deltal);
% max1 = drop(1);
deltalnorm = (deltal-min1)/(max1-min1);









tic;



% Number of terms of Prony Series
%                                 times                                 =
[.001:10:15,15:.1:30,30:100:190,190:.1:230,230:100:850,850:.1:940,940:2
00:10300,10350:1:10800];
% times = 10.^[-8:.001:4.2];
% times = [23,209,895,10553];
np = length(times);
X0 = 0.1*ones(1,np);
LB = zeros(1,np);
UB = ones(1,np);
params = [np;times';time;deltalnorm];
% X = FMINCON(FUN,X0,A,B,Aeq,Beq,LB,UB,NONLCON,OPTIONS)
[X,F] = fmincon('objfun',X0,[],[],[],[],LB,UB,'confun',[],params);
[times',X'];
```

```
F


Xprony = X;
clear X



% Construct optimum Prony series
for j=1:length(time);
    pronyseries(j) = 0;
    for i=1:np
        pronyseries(j)   =   pronyseries(j)   +   Xprony(i)*exp(-
time(j)/times(i));
    end
end




elapsedtimeprony = toc;
elapsedtimeprony

figure('Name','Curve fit of relaxation data ','NumberTitle','off')
plot(time,deltalnorm,'b')
hold on
plot(time,pronyseries,'r')
legend('Data','Prony Fit')
ylabel('Normalized relative change in height')
xlabel('Time (seconds)')
title('Curve fit of relaxation data')

figure('Name','Semilog plot of curve fit','NumberTitle','off')
semilogx(time,deltalnorm,'b')
```

```
hold on
semilogx(time,pronyseries,'r')
legend('Data','Prony Fit')
title('Semilog plot of curve fit')

weights = figure('Name','Weights vs. Times ','NumberTitle','off');
plot(times,Xprony,'r')
ylabel('Weights')
xlabel('Times (seconds)')
title('Weights vs. Times')
```

2.2 fmincon objfun

```
 function y = objfun(x,params)

np = params(1);
times = params(2:np+1)';
time = params(np+2:(length(params)-np-1)/2+np+1);
deltal = params((length(params)-np-1)/2+np+2:length(params));

y = 0;
for j=1:length(time)
    pronyseries = 0;

    for i=1:np
        pronyseries = pronyseries + x(i)*exp(-time(j)/times(i));

    end
    y = y + (pronyseries-deltal(j))^2;
```

```
end
y = sqrt(y);
```

2.3 fmincon confun

```
function [C,Ceq] = confun(x,params)

sum1 = sum(x);
C = [
    sum1-1.00
    0.99-sum1
    ];

Ceq = [];
```